AD-A144 149 FRACTO-EMISSION FROM POLYMERS(U) WASHINGTON STATE UNIV 1/2
PULLMAN DEPT OF PHYSICS J T DICKINSON 15 JUL 84
N00014-80-C-0213

UNCLASSIFIED F/G 11/9 NL

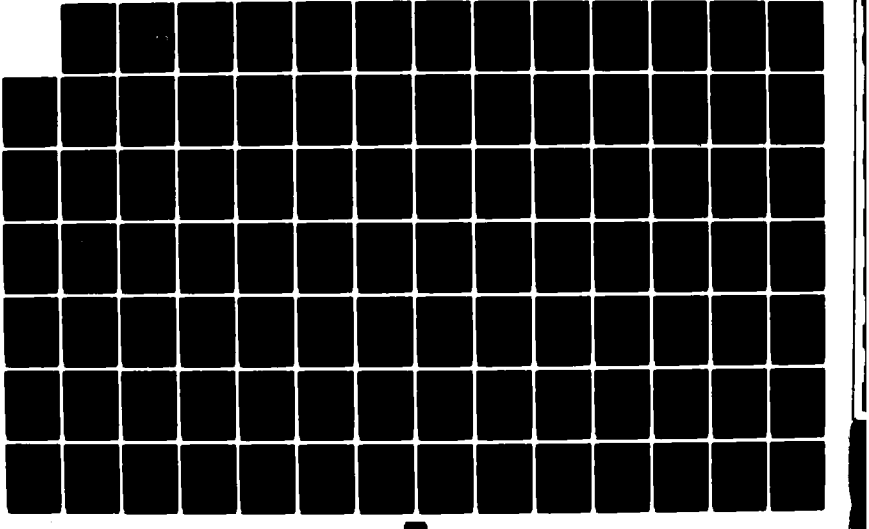

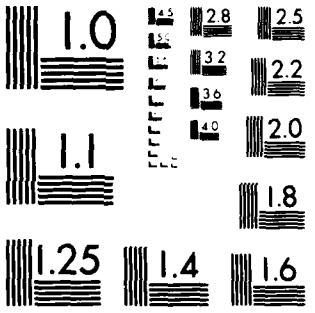

(12)

SECURITY CLASSIFICATION OF THIS PAGE (When Data Entered)

REPORT DOCUMENTATION PAGE		READ INSTRUCTIONS BEFORE COMPLETING FORM
1. REPORT NUMBER	2. GOVT ACCESSION NO.	3. RECIPIENT'S CATALOG NUMBER
4. TITLE (and Subtitle) Fracto-Emission From Polymers		5. TYPE OF REPORT & PERIOD COVERED Annual Technical Report June, 1983 - June 1984 6. PERFORMING ORG. REPORT NUMBER
7. AUTHOR(s) J. Thomas Dickinson		8. CONTRACT OR GRANT NUMBER(s) N00014-80-C-0213
9. PERFORMING ORGANIZATION NAME AND ADDRESS Department of Physics Washington State University Pullman, WA 99164-2814		10. PROGRAM ELEMENT, PROJECT, TASK AREA & WORK UNIT NUMBERS
11. CONTROLLING OFFICE NAME AND ADDRESS Office of Naval Research Propulsion and Energetics Program Arlington, VA 22217		12. REPORT DATE July 15, 1984 13. NUMBER OF PAGES
14. MONITORING AGENCY NAME & ADDRESS(if different from Controlling Office)		15. SECURITY CLASS. (of this report) Unclassified 15a. DECLASSIFICATION/ DOWNGRADING SCHEDULE
16. DISTRIBUTION STATEMENT (of this Report) Approved for public release; distribution unlimited		
17. DISTRIBUTION STATEMENT (of the abstract entered in Block 20, if different from Report)		
18. SUPPLEMENTARY NOTES		

19. KEY WORDS (Continue on reverse side if necessary and identify by block number) fracture, crack propagation, fracture surfaces, interfacial failure, exo-emission, electron emission, positive ion emission, photon emission, tribo-luminescence, radio-wave emission, fracto-emission, surface charging, fracture-induced breakdown, gaseous discharges, electrical breakdown fracture of: Polymers, polybutadiene, elastomers, rubber, and PETN. Electron beam damage, induced fracture.

20. ABSTRACT (Continue on reverse side if necessary and identify by block number) Progress in the investigation of fracto-emission (FE) from polymers is reported. Measurements characterizing the FE, experiments concerning FE mechanisms, and studies of factors influencing FE are discussed. This work includes: experimental evidence for and presentation of a conceptual model for the charged particle emission mechanisms, studies of electron and positive ion emission from single crystals of PETN and the production of electrical breakdown by fracture. Also, the phenomenon of electron beam induced fracture is presented.

DD FORM 1 JAN 73 1473 EDITION OF 1 NOV 65 IS OBSOLETE

SECURITY CLASSIFICATION OF THIS PAGE (When Data Entered)

OFFICE OF NAVAL RESEARCH
Contract N00014-80-C-0213
Project NR 092-558

Annual Technical Report
~~June~~ July 15, 1984

FRACTO-EMISSION FROM POLYMERS

J. Thomas Dickinson

Department of Physics
Washington State University
Pullman, Washington 99164-2814

TABLE OF CONTENTS

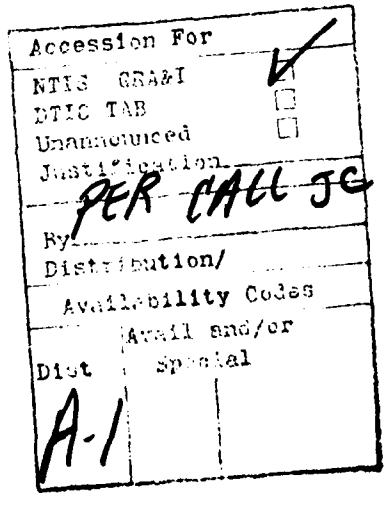

I. TECHNICAL SUMMARY

Crack propagation through an insulating material or at an interface produces regions of high electronic and chemical activity on the freshly-created surfaces. This activity causes the emission of particles, i.e. electrons, ions, and neutral species, as well as photons, from the surfaces both during and after crack propagation. This emission is called fracto-emission (FE), and in many ways serves as a probe of the electronic and chemical activity of the fracture surfaces. The work described in this report represents the results of our research activity from June 1, 1983 to May 31, 1984. Our primary goals have been to further characterize FE from polymers, to further our understanding of the FE mechanisms, and to examine the dependence of FE on the nature of the fracture event and material properties. In this report we include work on filled and unfilled polybutadiene where we have examined in detail the role of charge separation produced by fracture in causing high energy phenomena at the fracture surfaces. Evidence of a microdischarge occurring during fracture is presented. Furthermore, we compare the consequences of electron bombarding surfaces of polybutadiene with the consequences of fracture and show that similar emission results. Details of the electron and positive ion emission following fracture are explored using thermal stimulation techniques.

A study of the FE accompanying fracture of single crystal PETN is also presented, showing that cleavage type fracture does not lead to detectable FE, whereas compressional loading yields

FE. When such crystals are impact loaded, the emission intensities are considerably higher.

We also include a study of fracturing materials known to be strong charged particle emitters in the vicinity of a high voltage gap (in air) and show that there is sufficient electrical activity to cause electrical breakdown.

Finally, our preliminary results on inducing crack growth in polymers with the combination of stress and electron bombardment are presented. Here we show that at stresses below critical crack growth, an electron beam focused into the crack tip of a polymer can cause the crack to move forward. We present experiments which show the effect and attempt to uncover the mechanisms.

II. INTRODUCTION

Fracto-emission (FE) is the emission of particles (e.g. electrons (EE), positive ions (PIE), ground state neutrals (NE), excited state neutrals (NE*), and photons (phE)) during and following fracture. In Sections III - VI of this report we present recent studies of the characteristics of FE, FE mechanisms, and the dependence of FE on material and fracture parameters. These studies deal with fracture of filled and unfilled elastomers, explosive molecular crystals (PETN), and the consequences of fracturing materials near high voltage gaps. Furthermore, we present new results concerning the effect of combining stress and electron bombardment on polymers. We refer these consequences as electron beam induced fracture.

A summary of these results are presented below:

Section III: FRACTO-EMISSION FROM FILLED AND UNFILLED POLYBUTADIENE

(Submitted to J. Poly. Sci.: Physics Edition)

Further studies of EE and PIE mechanisms have been pursued, where experimental evidence in support of a previously presented model that explains the intense, long-lasting emission observed in polybutadiene (BR) filled with glass beads. This model is consistent with a number of other characteristics of FE previously observed. The measurements supporting this model are presented, involving the simultaneous measurements of EE, RE (radiowave emission), and phE (photon emission) versus time for the fracture in vacuum of filled and unfilled BR. These results show

that during fracture there are radio waves and accompanying visible photons due to an electrical discharge caused by charge separation and the desorption of volatiles and/or fracture fragments into the crack tip. This discharge only occurs during crack growth and ceases as soon as the surfaces separate. Thus the RE and the phE rise and fall during and immediately following fracture.

The EE rises with these emissions but then decays with a long tail. Careful measurements of phE from the filled BR showed that it also had a long lasting decay curve. Because such emission is most evident where charge separation is strong and a discharge is more likely to occur, we hypothesized that during the discharge the fracture surfaces are bombarded by electrons and ions with relatively high energies. It is this bombardment which is the key stimulus for the EE, PIE and phE which <u>follows</u> fracture. Calculations of emission kinetics are presented using a simple trap model and used to predict the effect of increasing the sample temperature <u>after</u> fracture. We conclude that both filled and unfilled polybutadiene are experiencing the same excitations except at a considerably reduced intensity for the unfilled material.

Section IV: FRACTO-EMISSION FROM SINGLE CRYSTAL PENTAERYTHRITOL TETRANITRATE (PETN). (To be submitted to J. Appl. Phys.).

A limited number of small single crystals of PETN were fractured in three modes: three-point bending (which yielded cleavage like fracture), slow compression, and fast compression (impact). The latter modes of loading led to considerable

pulverization, accompanied by shear and frictional grinding of the crystal fragments. Three-point bending yielded no detectable FE. The compressional modes yielded easily detected EE and PIE, as shown previously. The impact loaded PETN provided evidence of a microdischarge (electrical breakdown) during impact in the form of phE and RE. We also examine the effect of abrading single crystal PETN with a sharp metal point. We conclude that high deformation rates and frictional effects seem to be the major cause of intense FE.

Section V: ELECTRICAL BREAKDOWN INDUCED BY FRACTO-EMISSION (Submitted to IEEE Transactions on Electrical Insulation).

Assuming that EE and PIE would occur in the presence of a gas (e.g., air), we predicted that we could fracture materials in the vicinity of a high voltage gap and thereby induce electrical breakdown. This in fact was observed for a wide range of known intense FE emitters such as filled BR, quartz and other ceramics, and filled epoxy. The breakdown appeared to nearly coincident with breakdown for the most intense emitters, but required short times on the order of milliseconds for the weaker emitters.

Section VI: ELECTRON BEAM INDUCED FRACTURE OF POLYMERS (To be submitted to J. Appl. Phys.)

In this section we explore the consequences of combining the application of stress and electron bombardment to a notched crack in a polymer. We present evidence of electron beam induced crack growth in polyisoprene, BAMO/THF, and polyethylene. We have modeled the energy deposition and thermal conduction occurring during bombardment and concluded that the effects we are observing are not thermal. We hypothesize that bond scissions due to electronic interactions are the dominant effect leading to crack growth.

III. FRACTO-EMISSION FROM FILLED AND UNFILLED POLYBUTADIENE

J. T. Dickinson and L. C. Jensen
Department of Physics
Washington State University
Pullman, WA 99164-2814

ABSTRACT

We further examine the mechanisms involved in the emission of electrons and positive ions from polybutadiene accompanying fracture. Experimental evidence is given in support of a previously presented model[1-4] involving a micro-discharge accompanying fracture which excites the fracture surfaces by particle bombardment. Calculations of the time dependence for the emission from such excitations for both isothermal and thermal stimulation from a simple trap model are presented. We conclude that both filled and unfilled polybutadiene are experiencing the same excitations except at a considerably reduced intensity for the unfilled material.

I. INTRODUCTION

When materials are put under stress, emission of various types can occur; this emission is particularly apparent when new free surfaces are being formed. The types of emission observed include the release of electrons, ions, neutral molecules, and photons. We call such emission "fracto-emission" (FE) to emphasize the fact that some form of crack growth appears to be a requirement for its occurrence.

In recent papers[1-4] we have outlined a physical model for the emission of charged particles following fracture of solids in vacuum, particularly in cases where a high degree of charge separation occurs. For example, when a polymer such as polybutadiene (BR), initially adhering to a glass surface (either in the form of a macroscopic, planar glass surface or small spherical filler particles), is separated in vacuum from the glass, intense long lasting electron emission (EE) and positive ion emission (PIE) are observed.[5] In such instances we also observe easily detectable photon emission (phE) and long wavelength electromagnetic radiation (RE -- for radiowave emisson) during fracture indicating the occurrence of a micro-discharge in the crack tip. The necessary gas in the region where breakdown is occurring consists of molecules evolving as the fracture occurs.[6] These gases either come from occluded volatiles or from actual fracture fragments produced by bond scissions. The presence of these gases and the electric field due to charge separation results in breakdown during fracture.

This micro-discharge causes ionization of the gases in the crack-tip yielding high concentrations of electrons and positive ions which are attracted to and strike the crack walls. Bombardment of the fresh crack walls creates primary excitations, usually explained in insulators in terms of electron-hole production, raising electrons into traps near conduction band energy levels. The recombination of electrons and "holes" is a thermally stimulated process and can yield an emitted electron (thermally stimulated electron emission (TSEE)),[7] via an Auger Process,[8] or a photon, e.g., thermally stimulated luminescence (TSL)[9] (we place quotation marks around hole because at present we do not know the nature of this recombination center in polybutadiene; it may be simply a positive ion in the polymer, as suggested by Partridge[10] and Bohm[11]). Furthermore, a portion of the electron emission may be attracted back to the fracture surface due to variations in the density and sign of the charge distributions (i.e. charge patches) striking the surface and producing PIE via an electron stimulated desorption (ESD) mechanism.[12] In addition, the positive ions can be neutralized as they escape from the fracture surface[13] and leave in an excited state (e.g., a metastable molecule), forming a component of FE which we call excited neutral emission (NE^*).

In this paper we present further support for this model with regard to fracture of filled and unfilled polybutadiene (BR). The results presented here focus on a comparison of the following:

a) the FE behavior of filled vs unfilled BR

b) the EE and PIE induced by electron bombardment of BR

c) the predictions of a simple trap model (based on TSL work) with isothermal and thermally stimulated EE following fracture and electron bombardment.

d) the EE and phE following fracture of filled BR

e) the effects of thermal stimulation of electron bombarded BR and fractured BR (filled and unfilled).

These comparisons confirm a number of features of the FE model previously presented and also suggest that the emission following cohesive fracture of BR is of the same basic origin as the EE from the filled material, i.e., where interfacial or adhesive failure leads to intense emission.

II. EXPERIMENTAL

The fracture experiments were performed on polybutadiene (BR) samples consisting of Diene 35 NFA, Firestone Tire and Rubber Co., mixed with 0.05% dicumyl peroxide, heated for 2 hours at 150 C to provide a moderately cross-linked material. Some of the BR was filled to 34% by volume with small untreated glass beads, 30-95 um in diameter. The filled and unfilled samples were cut into strips 2 x 5 x 20 mm and pulled in tension in a vacuum system at a pressure of 1×10^{-5} Pa.

The charged particles were detected with channeltron electron multipliers (CEM) which produce fast (10ns) pulses with approximately 90% absolute detection efficiency for electrons and

nearly 100% efficiency for positive ions. The gains of the CEM's used were typically 10^6 -10^8 electrons/incident particle. Background noise counts ranged from one to ten counts/second. Standard nuclear physics data acquisition techniques were used to count and store the pulses as a function of time.

A Bendix 754A Photon Counter Tube with an S-20 photosensitive surface and background count rate of 10-20 counts/second was used to detect the visible photons. The detector was placed within a centimeter of the sample. One serious problem with this detector involved its extremely small photosensitive surface (0.8 mm^2); getting the photocathode aligned with the precise region where the crack was propagating proved extremely difficult because the crack moved slightly due to elongation of the elastomer. By anticipating this motion, we were able to obtain sufficient photon emission for the purposes of the measurements.

The electromagnetic waves (RE) were detected with a 20,000 turn solenoid of No. 30 magnet wire placed 2 mm from the sample. Such an antenna couples to a changing B field. It should be emphasized that this arrangement is detecting the near-field electromagnetic emission because of the close proximity of the solenoid to the source. The intensity of these oscillating fields is so weak that we would not be able to detect them at distances of several wavelengths. Such measurements would have to be made to assure absolutely that a true radiation field existed. Our major interest here is finding evidence of a micro-discharge during fracture and we attribute the changing B fields accompanying fracture to such a breakdown. The accompanying burst

of photons reinforces this interpretation.[1] The coil was connected to the input of a wide-band differential amplifier with high common mode rejection to minimize pick-up noise and then amplified with a tuned amplifier set to the characteristic ringing frequency of the coil-amplifier circuit (8 KHz). The signal was digitized once every 50 us and stored on a computer over the duration of the experiment (approximately 100 ms). The digitized waveform was squared, averaged, and the background subtracted. The appearance of a positive rise thus provided a sensitive probe of the occurrence of RE and the initial rise of the RE signal can be correlated in time with the EE.

The electron beam experiments were performed on pure 35NFA polybutadiene. A thin film approximately 0.2 mm thick was formed on a thin Ni backing by dissolving the polymer in acetone and allowing it to evaporate on the Ni sheet. The 1 cm^2 sample was electron bombarded with an electron gun at currents of 10^{-9} amps to 10^{-6} amps with a 2 mm^2 electron beam in vacuum at a pressure of 1×10^{-7} Pa.

The sample was heated by spot welding 0.7 mm diameter tungsten wires to each side of the Ni sheet and passing a current directly through the Ni sheet. A Chromel-Alumel thermocouple was spot welded to the back of the Ni sheet to measure the temperature. The EE and PIE from the sample were detected with a CEM, appropriately biased, approximately 3 cm from the sample.

To determine the response of the fracture surface to thermal stimulation, the filled and unfilled BR samples were heated by placing 0.7 mm diameter tungsten wires in contact with each side

of the sample. A Chromel-Alumel thermocouple was placed in the sample between the two heating wires to measure the temperature of the BR. The sample was notched about 2 mm from the heating wires so the crack would propagate near and parallel to the heater.

In both heating experiments (the fracture surface and the electron bombarded surface) there was small but unavoidable background electron and ion emission, presumably from the hot heater wires. The response of the excited surfaces to thermal stimulation was several times larger than this background emission so the basic features due to the heating of these surfaces were observable.

III. RESULTS AND DISCUSSION.

To differentiate between different time domains relative to fracture we have adopted the following notation:[5] FE_1 represents emission prior to fracture -- usually due to micro-cracking, crack formation, etc.; FE_2 represents emission <u>during</u> fracture; and FE_3 represents emission <u>after</u> separation of the surfaces. FE_3 is sometimes referred to as "after-emission." Earlier measurements of the EE and PIE from the fracture of filled and unfilled BR showed that they had orders of magnitude different FE intensities but similar decay curves. A more careful comparison shows that the decay curves are essentially the same.

In Figure 1 we show two superimposed decay curves (i.e., EE_3--corresponding to <u>after</u> separation) for the filled and unfilled BR, normalized at a single point, the solid line

representing the much more intense emission from the filled material. The filled material is over a factor of 10^6 more intense. From the agreement shown we see that the kinetics for these two curves are identical. Furthermore, from work on other polymer/glass interfaces,[5] we expect, for the filled material, that the glass surfaces contribute little to this long lasting emission--i.e. the polymer is the emitting surface. Thus the similarities in these emission curves indicate that the polymer fracture surfaces have undergone identical excitation and relaxation processes. The differences in intensity are presumably due to the differences in the extent of excitation of the fracture surface between the two types of fracture (cohesive vs interfacial).

The next question to be addressed concerns the excitation step of the BR fracture surface in the case of fracture of the unfilled polymer. Could a gaseous discharge be occurring even in the case of cohesive failure in such an amorphous material? Because the EE intensity for the unfilled BR was relatively small, we expected our probes of such a discharge, namely RE and phE during fracture, to be significantly smaller, which was indeed the case. To obtain correlations of RE and phE with the charged particle emission it was necessary to place our detectors/antenna very close to the sample to maximize signal-to-noise. Instead of detecting all three emissions simultaneously (as for the filled material[1]) we were limited to detecting RE-EE or phE-EE separately.

Figures 2 and 3 show the results for two different BR

samples. The time scale chosen represents the time during which the sample was being strained. The small burst of EE and RE at about 5 ms was due to the detachment of the two surfaces of the notch which had self-adhered (We have seen this quite often in the EE from BR and polyurethane but have not reported it previously). Note the RE response after the small rise is due to the ringing of the poorly damped LC circuit mentioned earlier and has no significance in terms of the duration of the RE. The much larger growth in EE starting at about 11 ms represents the emission during crack growth (i.e. EE_2) as the crack accelerates, finally separating near the asterisk. In the case of RE we see the burst of RE with its highest response near the instant of separation (followed by the ringing of the circuit). We propose that this RE is indeed produced by a micro-discharge induced by the fracture. For the measurements shown here and those presented earlier,[1,4] our sensitivity is not yet high enough to determine the RE time dependence during the time of crack propagation.

Figure 3 shows similar results for the phE-EE where we see a small burst of photons during the growth in EE which occurs during crack growth (i.e. EE_2). We believe that the source of these photons is principally the excitation of the gases and/or fracture surfaces by the discharge. Because of the considerable extension of the BR samples, the crack actually swept past the photocathode (only 1 mm in diameter) during the fracture. Thus the EE_2 and phE_2 peaks were not quite as well aligned as expected. (A larger photo tube with a 5 cm diameter cathode has been acquired to repeat these measurements in the near future.)

Nevertheless, during the time interval when the crack was propagating (15 to 25 ms) we indeed observed phE.

The FE_2 observed during fracture is expected to be due to two sources:

A) the discharge products (electrons, ions, photons, radio-waves) that can escape the region of the crack and be detected, and

B) the fracture surfaces which are excited by the discharge and can immediately emit electrons, ions, and photons.

Because the discharge producing A) extinguishes immediately upon separation of the two crack walls, this component would decay very quickly. Component B), however, is rate limited by thermally stimulated processes and thus can often last long after fracture and is the after-emission, FE_3, spoken of earlier.

As we shall show, the mechanism of stimulating electron-"hole" recombination, limited by the activated transport of charge, can explain the decay of EE_3 observed. It also predicts a parallel process, namely <u>radiative</u> recombination which should lead to a decaying phE_3. The role of the discharge in exciting the fracture surfaces for type B) or FE_3 processes is believed to be particle bombardment of the surfaces from the discharge. To further investigate this process, we bombarded the thin film of BR with 500 eV electrons for a few seconds, after which the electron beam was turned off, and an electron detector immediately turned on. The resulting EE from the surface in response to this bombardment is shown in Fig. 4. The resulting BR "exo-emission"

showed a decay curve much like the EE_3 from fracture. In fact, the solid curve in Fig. 4a is an EE_3 curve following the fracture of filled BR (normalized to the electron beam induced EE at a single point), showing the similar decay.

One can also observe the emission of positive ions <u>during</u> electron bombardment of the BR (see Fig. 4b). In this case the ESD mechanism, mentioned earlier,[12] requires that electrons strike the surface, exciting electronic states of the molecules involved which can then decay via non-radiative transitions, ejecting positive ions from the surface. The times for such processes are $<< 10^{-6}$s. Thus, when we turn off the incident electron beam, the PIE from the surface should disappear, as it does in Fig. 4b. In the case of fracture, the PIE_3 follows exactly the same decay kinetics as the EE_3[14] and in fact we have detected a <u>coincidence</u>[14,15] between the EE_3 and PIE_3. These facts suggest that the PIE_3 is produced by ESD where the (primary) responsible electrons are emitted from the surface and attracted back by electric fields due to charge patches on the surface. This "self-flagellation" would obviously occur at a rate directly proportional to the EE_3 (which consists of the electrons which have escaped from the surface), and thus produce identical EE_3 and PIE_3 kinetics. The coincidence observed between EE_3 and PIE_3 is presumably due to accompanying Auger electrons from the ESD process[12] or possibly inelastically scattered primary electrons. Either type of process would produce electrons in coincidence with positive ions.

The above explanation of PIE allows us to make an

approximate calculation of the total electron emission from the surface. From Fig. 4b we can convert the observed ion count rate to a current, about 3×10^{-15} A. For 500 eV electrons this implies a yield, Y, of 1.5×10^{-4} ions/electron. In the case of fracture, we do not know the energy distribution of the electrons striking the surface which can affect the yield due to the energy dependence of the excitation cross-sections. However, as a first approximation if we assume Y is the value given above, then a measure of the PIE total counts allows us to calculate the incident electron dose. From filled BR we measure a total PIE of approximately 10^8 ions/cm^2 (actually we believe this to be low due to imperfect collection efficiency). The resulting incident electron dose is then 10^{12} electrons/cm^2. Noting that the total EE observed is also on the order of 10^8 electrons/cm^2, this implies that we are observing only about 1 electron in 10^4 emitted. By far, most of the emitted electrons are returning to and striking the surface.

Modeling EE_3. Studies of irradiated inorganic dielectrics have shown that a simple trap model can describe the basic features of the TSL following exposure.[9] Since we expect the EE_3 and phE_3 to share common rate limiting steps we decided to explore the rate equations used for TSL. Our goal here was not to determine unique values of the parameters; without additional independent measurements of relevant variables it would be very difficult to determine a unique set of constants from just a "good fit" of our data. We are more interested in showing that the overall behavior of the emission is indeed consistent with such

equations.

Halperin and Braner[16] have described the process of TSL in a manner similar to what follows:

A simplified picture of the energy level diagram of a polymer is shown in Fig. 5 where irradiation, fracture, or particle bombardment produces electrons in high lying traps separated from recombination centers near or in the valance band of the material. The thermal stimulation of this solid, which is a departure from equilibrium, leads to electrons being transported through the material recombining with the "hole," yielding an electron via non-radiative Auger processes or a photon via radiative decay. The equations describing these events are:

$$\text{(i)} \quad -dm/dt = A\, m n_f$$

$$\text{(ii)} \quad -dn/dt = B\, n\, e^{-E_A/kT} - C(N - n_f) n_f]$$

$$\text{(iii)} \quad dn_f/dt = dm/dt - dn/dt$$

where: m = concentration of recombination sites

n = concentration of electrons in traps

N = concentration of traps

n_f = concentration of "free" electrons (in a crystalline material, these would be the electrons in the conduction band).

Equation (i) represents the rate of electron-"hole" recombination where A is the appropriate rate constant. We

assume $|dm/dt|$ is directly proportional to the electron emission rate. Equation (ii) represents the thermally activated emptying of the filled electron traps (first term) and refilling or retrapping (second term), with B and C representing the appropriate rate constants. Equation (iii) provides for the conservation of electrons. To reduce the number of adjustable parameters we assume the initial values n_o and m_o are both equal to the total number of detected electrons. The latter was obtained by extrapolating the experimental emission curve to very long times and integrating from the time of fracture.

Numerical methods similar to those developed by Shenker and Chen[17] were used to integrate these equations and produce predicted emission curves for various values of the adjustable constants and initial values. Adjustments were made in a stepwise fashion and compared with the experimental data. Two types of emission curves were calculated: a) the isothermal curves, which we compared with EE_3, and b) the response of the emission to a linear rise in temperature, which we can also compare with experimental data produced by heating the sample either after fracture or after electron bombardment.

Predicted isothermal emission curves (sample temperature: 300 K) for various activation energies, E_A, are shown in Fig. 6, plotted on a log scale. The constants and initial values, given in the figure caption, were chosen to come close to the behavior observed experimentally. The curve shown for an E_A of 0.56 eV matches typical experimental isothermal decay curves fairly well and thus the characteristic form of the decay curve can be

generated with such a model. Variations of the parameters show that for given initial conditions, the values of trap concentrations and retrapping rates strongly influence departure from simple first order decay, which would be a straight line on a log plot. Again, we emphasize that the parameters and initial values chosen are not unique. However, variation of these values indicate that the activation energy appears to remain within a limited range, which we indicate below when we consider thermal stimulation.

As mentioned earlier, this description of EE_3 should also lead to parallel radiative recombination. In the case of the filled BR with careful placement of the photon detector relative to the fracture surfaces we obtained sufficient phE intensity to detect after-emission (phE_3) shown in Fig. 7. The solid curve superimposed on the phE is an experimental EE_3 curve (from another sample) normalized to the phE_3 at a single point. This comparison shows that there is indeed a parallel process occurring for EE_3 and phE_3 and further supports the concept of EE_3 being produced by electron-"hole" recombination, the commonly accepted model for TSL. (We have been able to make a similar comparison between the EE_3 and phE_3 from single crystal SiO_2.)

Thermal stimulation (e.g., a linear temperature increase from 300 K) of a system obeying the above equations should yield a rise and fall of emission intensity, similar to a glow curve in TSL. Fig. 8a shows the predicted behavior on a log scale for an activation energy of 0.56 eV and a heating rate of 3.2 K/s, starting at the time indicated by the arrow. The initial part of

the curve consists of the isothermal decay previously discussed. At the arrow, as the temperature increases, the emission rises to a peak and then falls due to the competition between increasing excitation of trapped electrons vs loss of electrons to recombination centers. Figure 8b shows the same data on a linear scale emphasizing just the predicted "glow curve". Figures 9 and 10 show the experimentally measured response to this thermal stimulation for both the fracture surface and the electron bombarded surface. In both figures, (a) represents the initial decay and the rise and fall in emission intensity due to heating, on a log scale, and (b) represents normalized data for just the rise and fall in emission intensity on a linear scale. Also shown in the case of fracture (Fig. 9) are the corresponding PIE curves which were measured simultaneously. In Fig. 10b we show for comparison the EE response (on a linear scale) for both the electron bombarded surface and the fracture surface, measured at approximately the same heating rate. We see that they exhibit essentially the same kinetics.

The important points here are, first, both the predicted curves and the data show similar responses to increasing temperature, namely the rise and fall of emission intensity. The experimental data is of course not as clean as the predicted curves and has the background problem mentioned earlier. Nevertheless, close agreement in basic behavior can be seen. Second, both the PIE and EE induced by fracture (there is no positive ion after-emission following electron bombardment) behave similarly. We do observe in Fig. 9b a slight shift in the PIE

"glow curve" to longer times (higher temperatures) above the EE "glow curve". The proposed ESD mechanism for the PIE emission does show in a number of systems a temperature dependence in the ion yield, Y, although most cases studied consist of gases adsorbed on metal substrates. Our results would require that Y increase with temperature for BR.

A third point is the strong similarity between the response of the fractured filled-BR and the electron bombarded surface. This further supports our earlier statement that fracture and particle bombardment are producing the same type of excitations on the surface. A comparison of these two cases plotted as a function of temperature (instead of time), is shown in Fig. 11. It was not possible to heat the fracture surface to as high a temperature as the bombarded thin film, so the dashed curve for the fracture surface falls off at higher temperature. While the material was experiencing an increasing temperature, however, we see that it follows a similar rise and fall to the electron bombarded surface. The dotted curve in Fig. 11 represents the predicted response to thermal stimulation (shown on log intensity vs time in Fig. 8) plotted vs temperature. Although slightly narrower, the basic response predicted agrees fairly well with experiment using a single activation energy rather than a distribution. This agreement suggests that the electron traps are uniform in nature with a common activation energy. Analysis of a number of combinations of constants indicate that E_A lies in the range between 0.4-0.9 eV, which although somewhat uncertain, is considered meaningful. This range corresponds to the electron

affinities of a number of organic molecules as well as O_2 (Ø.45 eV) and H_2O (aprox. Ø.9 eV), two possible contaminants that could be contained in the polymer. Such entities could very well serve as electron traps.

Although the emission intensities are smaller for the case of the unfilled BR, we were able to measure the response of the EE and PIE to thermal stimulation of the unfilled material, shown in Fig. 12. Again, the top curve (Fig. 12a) is the initial decay followed by the "glow curve" on a log scale and Fig. 12b are the "glow curves" on a linear scale. The corresponding curves plotted vs temperature are shown in Fig. 13. The only difference when compared with the previous curves is a slight narrowing of the "glow curve" in both time and temperature, actually coming closer to the predicted curve than the experimental curves for the cases shown in Fig. 11. One possibility is that the intensity of the particle bombardment (and therefore the dose) is less, and that this may result in a small change in the parameters influencing the emission kinetics. Further studies of the dose dependence of the response of the electron bombarded surfaces needs to be carried out. What we desire to emphasize here, however, is that the unfilled material again shows nearly identical behavior to the filled material, suggesting that the mechanisms for producing EE_3 are the same for both materials; lower intensities result for the case of cohesive fracture because the strength of the charge separation is reduced.

IV. CONCLUSION.

To summarize, we have compared the EE_3 (after-emission) for the filled and unfilled BR and shown that they have nearly identical kinetics (which can not be represented by a simple first order, isothermal process) and suggest that they share common mechanisms. This mechanism involves the consequences of opening a crack with charged surfaces and evolved gases, thus inducing a discharge and subsequent particle bombardment of the fracture surfaces. This is supported by the presence of phE and RE during the fracture of the unfilled BR which, although weak, indicates the occurrence of a micro-discharge during crack propagation. We have shown that isothermal EE decay curves can be generated by simple electron bombardment and these decay curves are identical to those produced by fracture. We have presented a simple trap model based on TSL theory and showed that both isothermal and thermally stimulated behavior could be predicted numerically which was very similar to that observed experimentally. We also detected a phE_3 decay which paralleled the EE_3 decay, as predicted from this simple trap model. Thermal stimulation of both the EE and PIE produced by fracture led to nearly identical curves, again showing that PIE is intimitely linked to the EE, consistent with the proposed ESD mechanism for PIE. Finally, we showed that the fracture surfaces of the unfilled BR responded to thermal stimulation in the same basic manner as the filled BR, again consistent with the simple trap model. This further supports our statement that the EE_3 mechanisms are the same for the two types

of materials.

These results, built on predictions from our earlier studies,[1-4] thus confirm a number of features of the mechanistic model and suggest additional experiments. For example, the ion masses produced by ESD should be determined with a mass spectrometer and compared with the fracture induced species observed earlier.[15,18] Also, the simple trap model should allow us to predict <u>isothermal</u> EE_3 curves at various temperatures which could be measured quite accurately. Finally, populations of trapped and free electrons can be altered by the use of photon stimulation which in turn should affect the emission rates. Thus, by illumination of the fracture surface with the proper frequency photons, we may be able to probe the electronic states involved in the EE_3.

V. ACKNOWLEDGMENTS.

We wish to thank A. N. Gent, University of Akron Institute of Polymer Science, for supplying us with the polybutadiene samples. We also wish to thank R. A. McGough for carefully carrying out the numerical integration of the model rate equations and E. E. Donaldson for helpful discussions.

This work was supported by the Office of Naval Research Contract N0014-80-C-0213, the National Science Foundation Grant DMR 8210406, and a grant from the M. J. Murdock Charitable Trust.

REFERENCES

1. J. T. Dickinson, L. C. Jensen, and A. Jahan-Latibari, J. Vac. Sci. and Technol., to be published.

2. J. T. Dickinson, L. B. Brix, and L. C. Jensen, J. Phys. Chem., to be published.
published.

3. J. T. Dickinson, L. C. Jensen, and A. Jahan-Latibari, J. Mat. Sci., to be published.

4. J. T. Dickinson, J. Mat. Sci., to be published.

5. J. T. Dickinson, in Adhesives Chemistry -- Developments and Trends, L. H. Lee, ed., (Plenum Publishers, New York), to be published.

6. L. A. Larson, J. T. Dickinson, P. F. Braunlich, and D. B. Snyder, J. Vac. Sci. and Technol. 16, 590 (1979).

7. H. Glaefeke, in Thermally Stimulated Relaxation in Solids, ed. by P. Braunlich (Springer Verlag, Berlin, 1979), p. 229.

8. V. Bichevin and H. Kaambre, Phys. Status Solidi (A) 4, K235 (1971).

9. R. Chen and Y. Kirsh, Analysis of Thermally Stimulated Processes (Pergamon Press, Oxford, 1981) pp. 16-23.

10. R. H. Partridge, in The Radiation Chemistry of Macromolecules, Vol.I, ed. by M. Dole (Academic Press, New York, 1973), Chapter 10.

11. G. G. A. Bohm, J. Polm. Sci., 14, 437 (1976).

12. See articles contained in Desorption Induced by Electron Transitions: DIET I, ed. by N. H. Tolk, M. M. Traum, J. C. Tully, and T. E. Madey (Springer Verlag, Berlin, 1983).

13. J. T. Dickinson, L. C. Jensen, and M. K. Park, Appl. Phys. Lett. 41 443 (1982).

14. J. T. Dickinson, L. C. Jensen, and M. K. Park, Appl. Phys. Lett. 41, 443 (1982).

15. J. T. Dickinson, L. C. Jensen, and M. K. Park, Appl. Phys. Lett. 41, 827 (1982).

16. A. Halperin and A. A. Braner, Phys. Rev. 117, 408 (1960).

17. D. Shenker and R. Chen, J. Computational Physics, 10, 272 (1972).

18. J. T. Dickinson, L. C. Jensen, and M. K. Park, J. Mat. Sci. 17 3173 (1982).

FIGURE CAPTIONS

Fig. 1. A comparison of the EE_3 (after fracture) for filled and unfilled BR. The solid curve (filled BR) has been normalized at a single point to the much weaker EE_3 from the unfilled BR.

Fig. 2. Electron emission (EE) and near-field electromagnetic radiation (RE) measured simultaneously for cohesive fracture of unfilled BR. The asterisk denotes the instant of separation of the two fracture surfaces.

Fig. 3. Electron emission (EE) and photon emission (phE) measured during the cohesive failure of unfilled BR.

Fig. 4. (a) The emission of electrons from a thin film of BR following bombardment of the film with 500eV electrons (.....). The solid curve (———) is a representative EE_3 curve following fracture of filled BR, normalized at a single point.
(b) The electron stimulated desorption of positive ions from BR during bombardment of the BR with 500 eV electrons.

Fig. 5. Energy level diagram for electrons in an amorphous insulator containing electron traps and a low lying recombination center. This model is based on the description of thermally stimulated luminescence given by Halperin and Braner.[16]

Fig. 6. Predicted isothermal emission curves (EE_3) for various activation energies, E_A. The values of the constants and initial values are: $A=0.035$, $B=1.0 \times 10^9$, $C=10.0$, $N=1.2 \times 10^6/cm^3$, $m_o=n_o=1.1 \times 10^6/cm^3$.

Fig. 7. Isothermal decay of electrons (EE_3) and photons (phE_3) following the fracture of filled BR. The two curves were normalized at a single point.

Fig. 8. Predicted electron emission response of an activated surface to thermal stimulation. From t = 0 to the arrow the surface emits electrons isothermally (room temperature). At the arrow a temperature increase of 3.2 K/s begins, generating a curve similar to a TSL glow curve. The constants and initial values are: $A=0.035$, $B=1.0 \times 10^9$, $C=10.0$, $N=1.2 \times 10^6/cm^3$, $m_o=n_o=1.1 \times 10^6/cm^3$, $E_A=0.56$ eV.

Fig. 9. Response of the filled BR fracture surface to thermal stimulation -- both EE_3 and PIE_3 are shown. a) The complete curve shown on a log scale. b) The response of

the emission to a temperature rise on a linear scale (arbitrary units), the two curves normalized at the peak.

Fig. 10. a) The response of the EE_3 from the electron bombarded EE to thermal stimulation. At the arrow the sample was heated at 3.2 K/s. b) The same data on a linear scale (arbitrary units) and compared to the response of a fracture surface heated at approximately the same rate. The two curves have been normalized at the peak.

Fig. 11. The response of the activated surfaces as a function of temperature for a) the electron bombarded BR, and b) the fractured filled BR.

Fig. 12. The response to thermal stimulation of unfilled BR after fracture -- EE_3 and PIE_3. a) The initial isothermal decay and thermal response on a log scale, and b) the thermal response on a linear scale (arbitrary units).

Fig. 13. The EE and PIE response to thermal stimulation of unfilled BR after fracture, plotted as a function of temperature, normalized at the peak.

COMPARISON OF EE
FROM FILLED AND UNFILLED BR

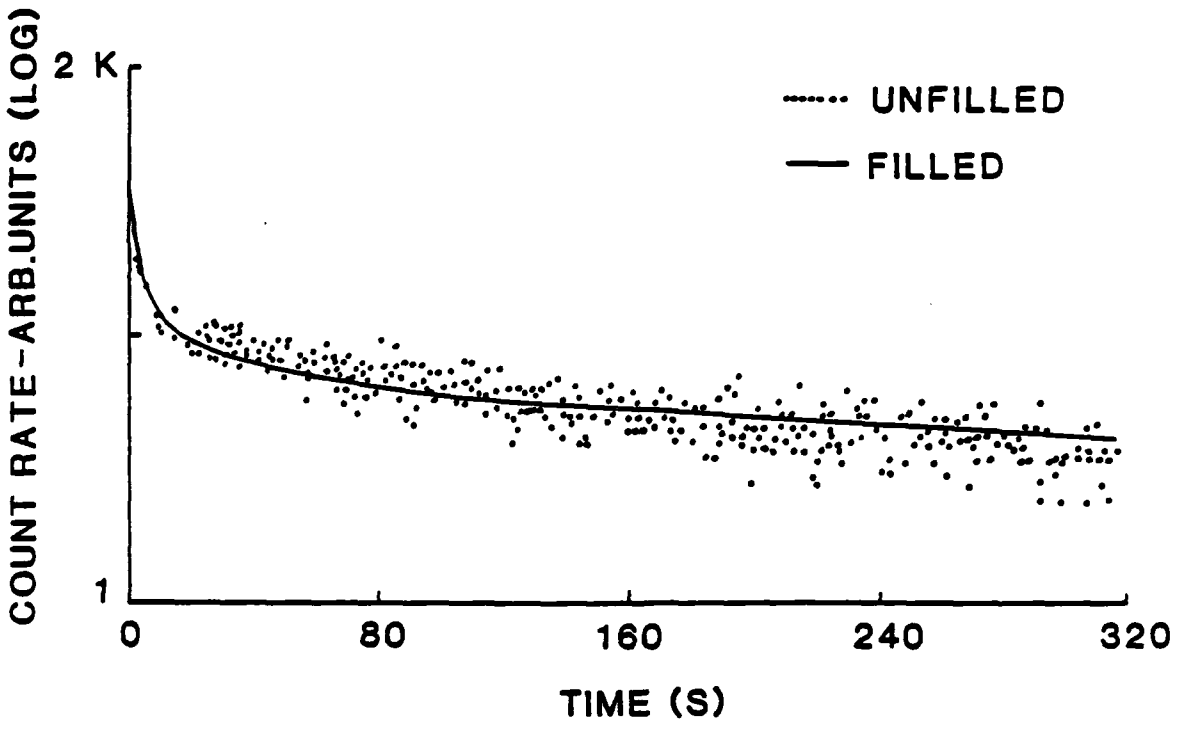

Fig. 1

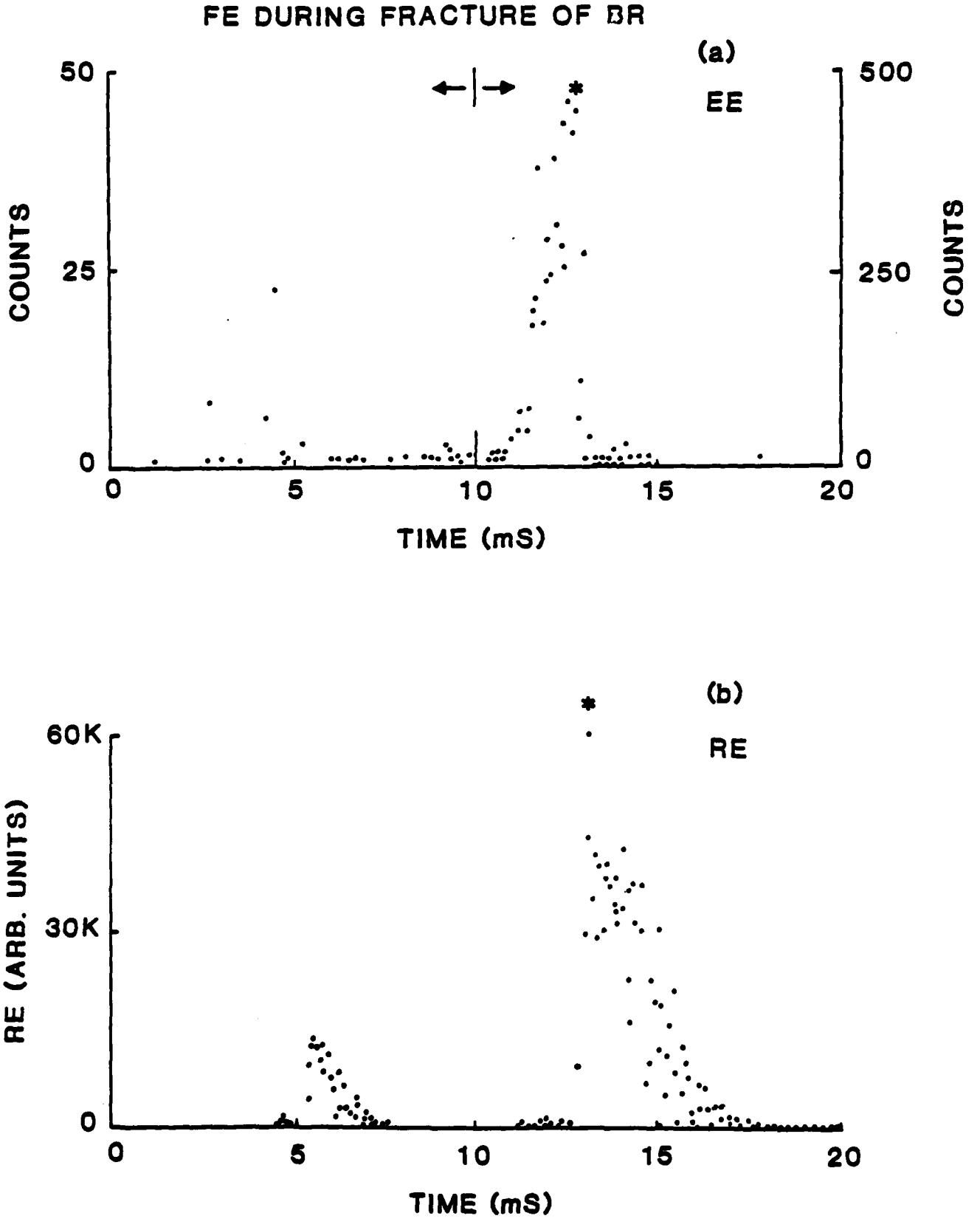
FE DURING FRACTURE OF BR
(a)
EE
50
25
0
COUNTS
500
250
0
COUNTS
0
5
10
15
20
TIME (mS)
(b)
RE
60K
30K
0
RE (ARB. UNITS)
0
5
10
15
20
TIME (mS)

Fig

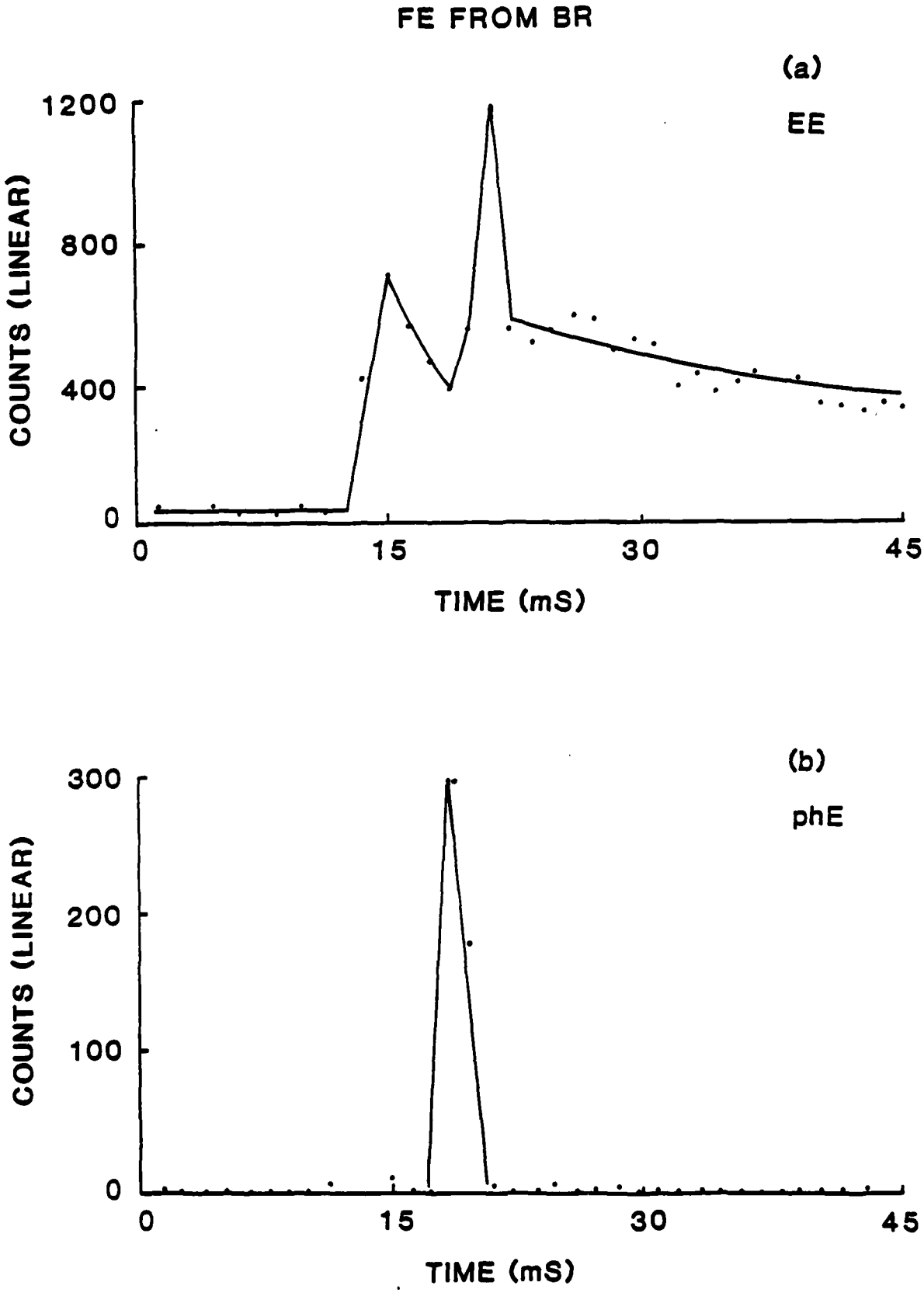
FE FROM BR
(a)
EE
1200
800
400
0
COUNTS (LINEAR)
0
15
30
45
TIME (mS)
(b)
phE
300
200
100
0
COUNTS (LINEAR)
0
15
30
45
TIME (mS)

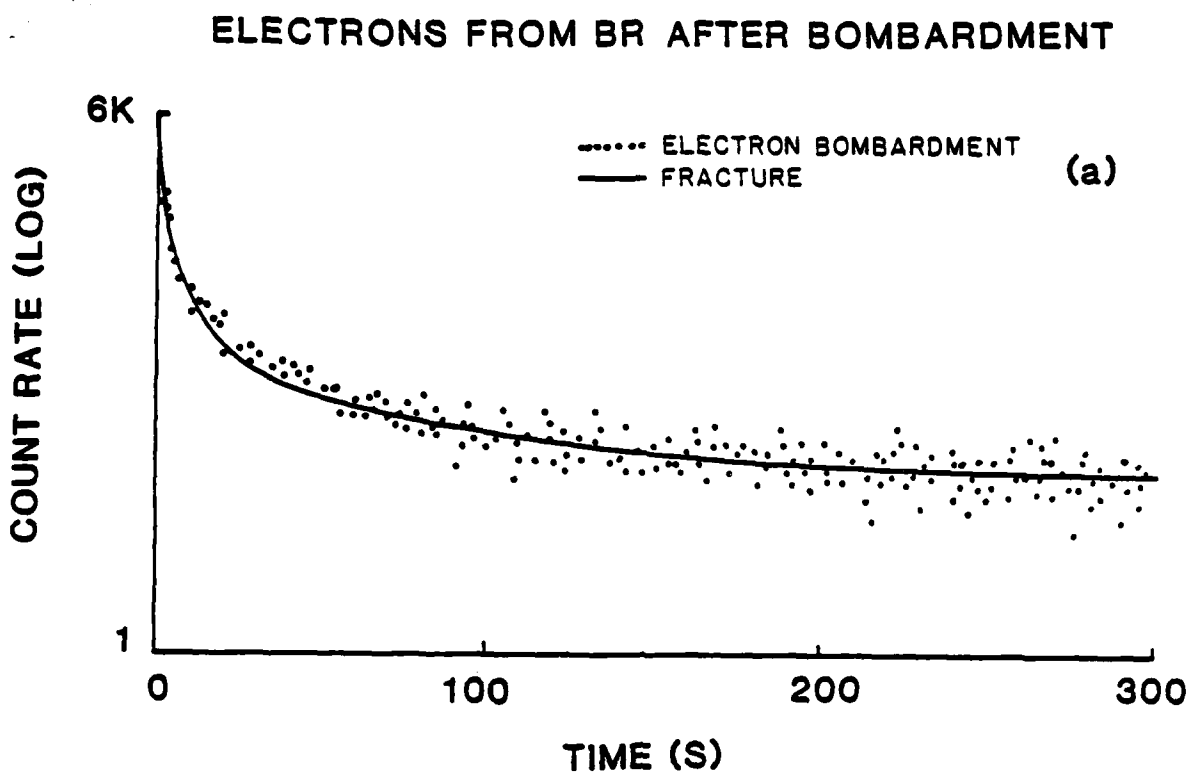
ELECTRONS FROM BR AFTER BOMBARDMENT
6K
1
COUNT RATE (LOG)
ELECTRON BOMBARDMENT
FRACTURE
(a)
0
100
200
300
TIME (S)

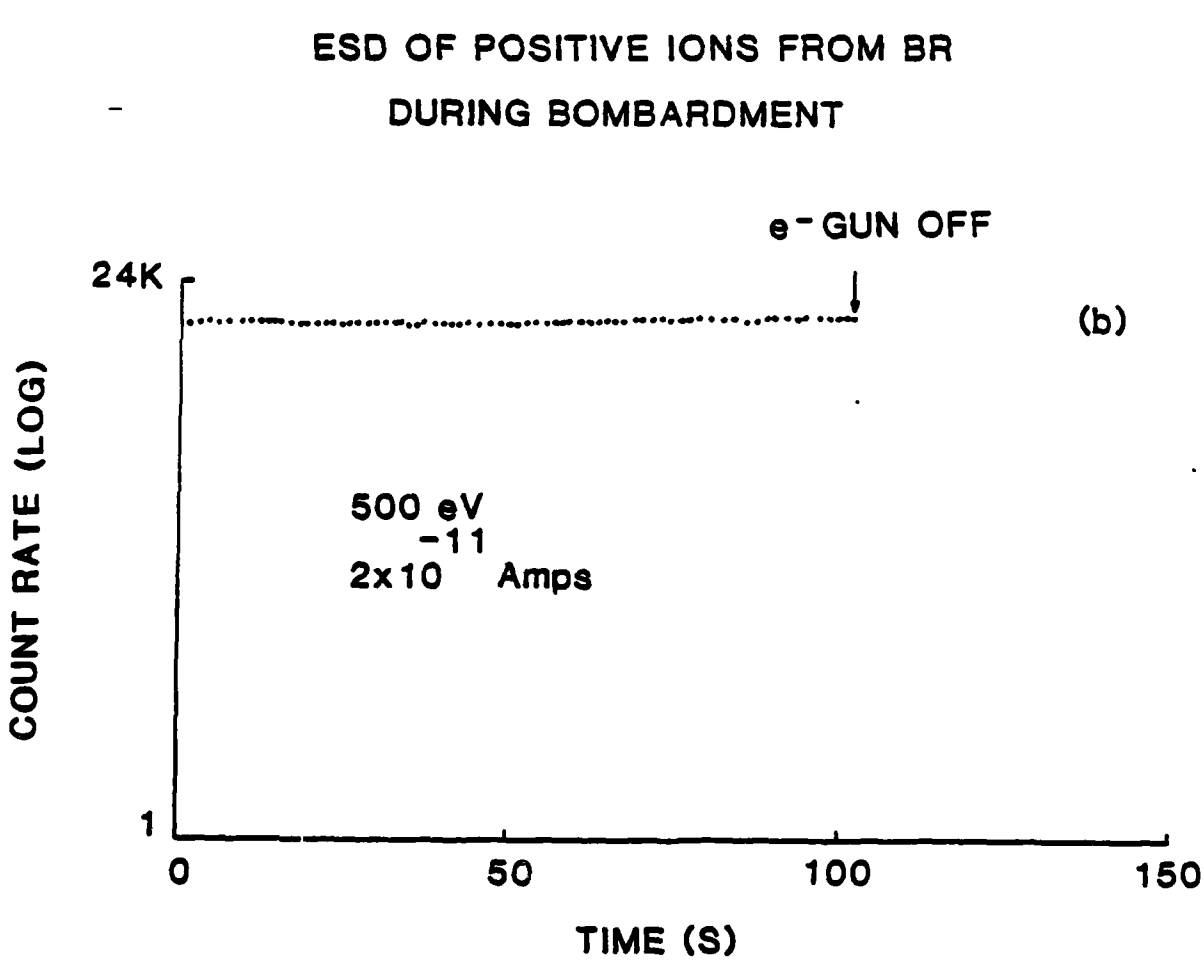
ESD OF POSITIVE IONS FROM BR
DURING BOMBARDMENT
e⁻ GUN OFF
24K
1
COUNT RATE (LOG)
(b)
500 eV
2x10⁻¹¹ Amps
0
50
100
150
TIME (S)

Fig. 4 (a+b) BR II

SIMPLE TRAP MODEL

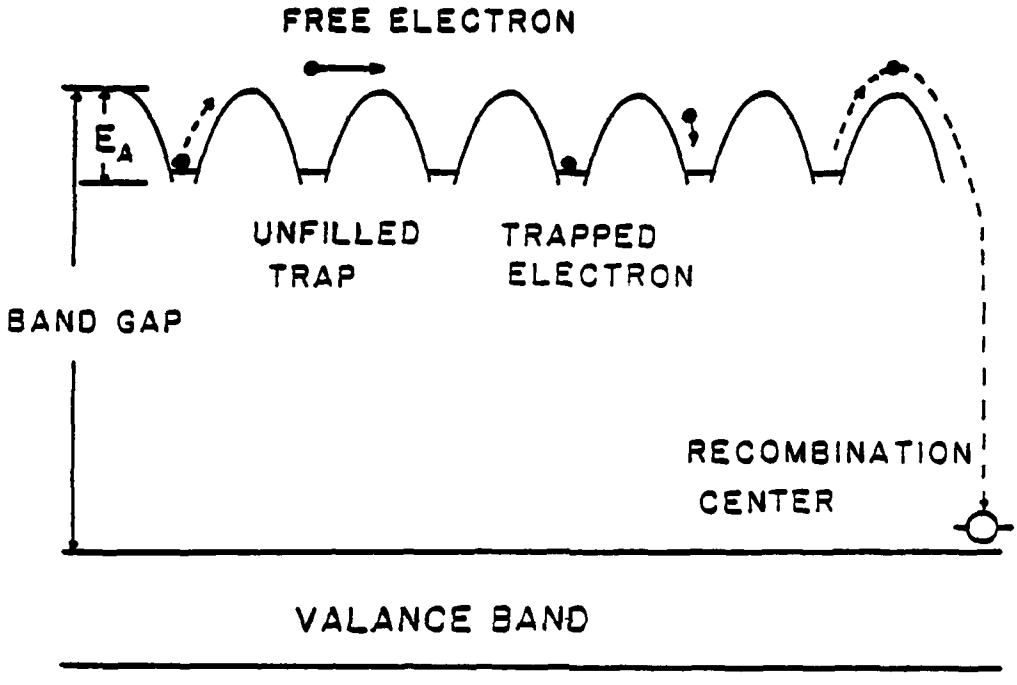

CALCULATED DECAY CURVES

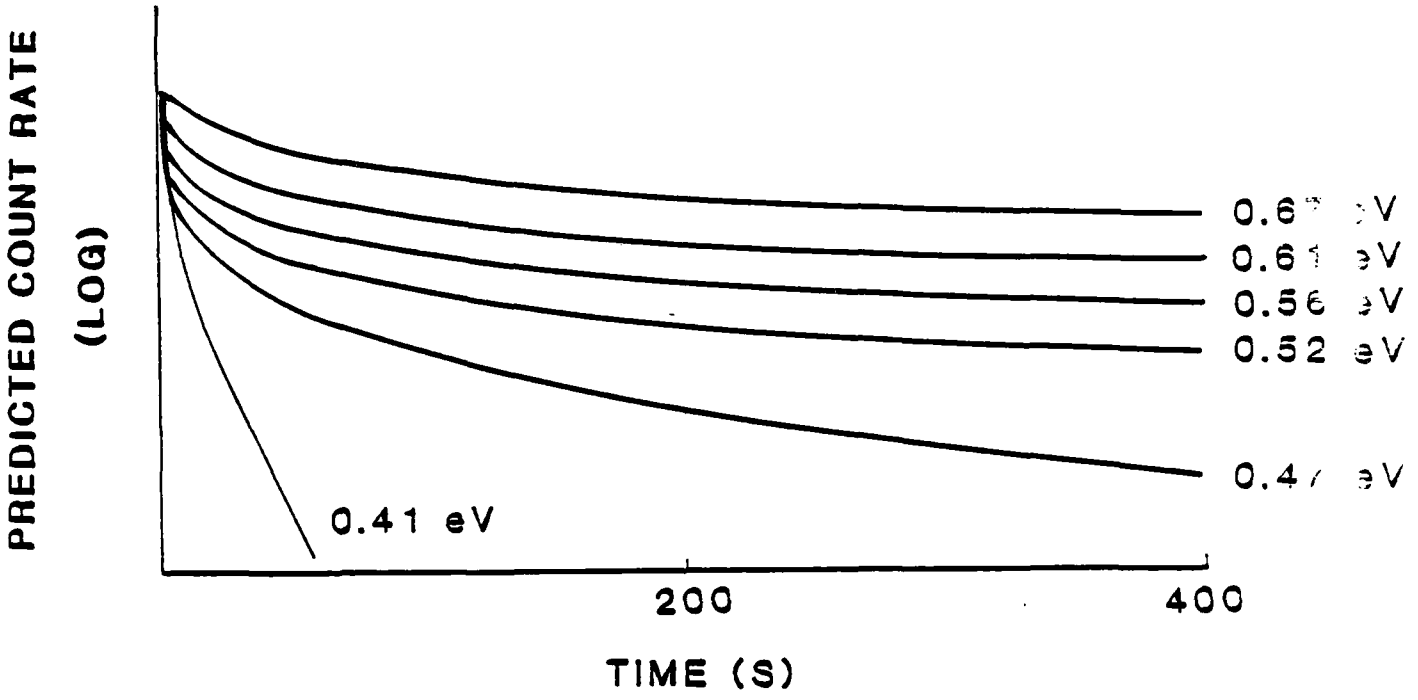

COMPARISON OF EE AND phE FROM FILLED BR

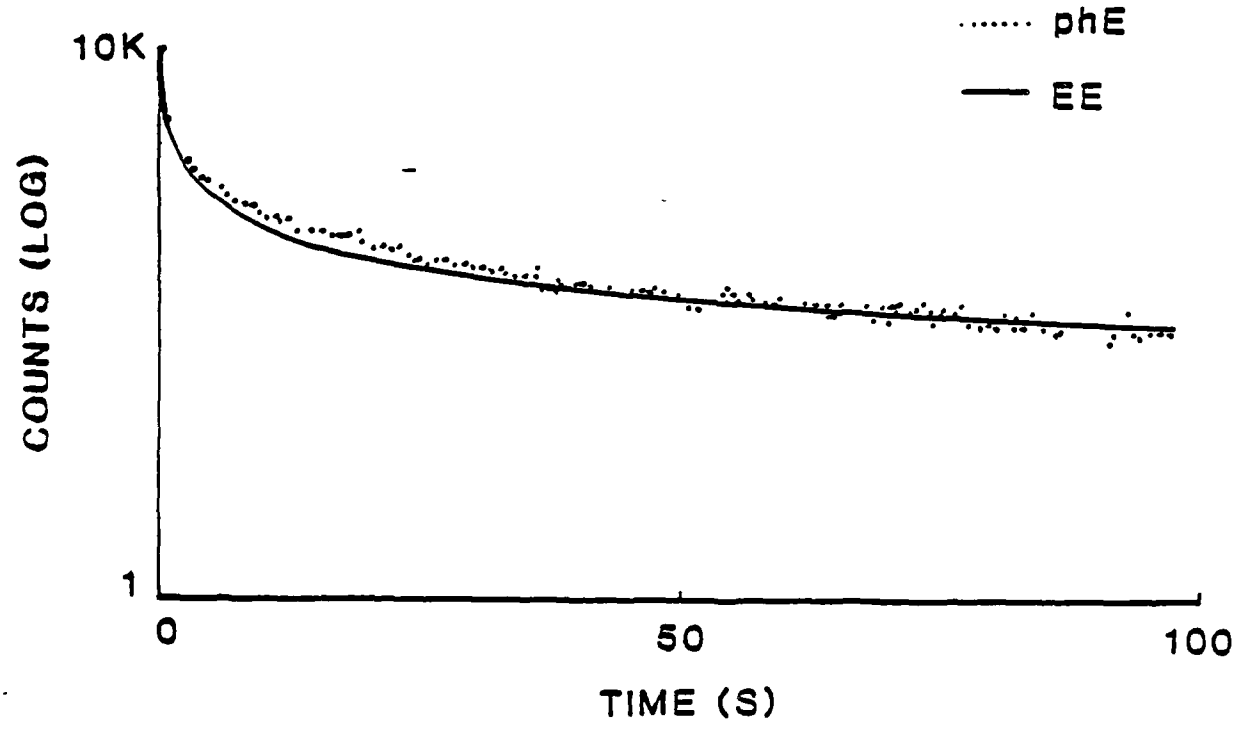

PREDICTED RESPOSE TO THERMAL STIMULATION

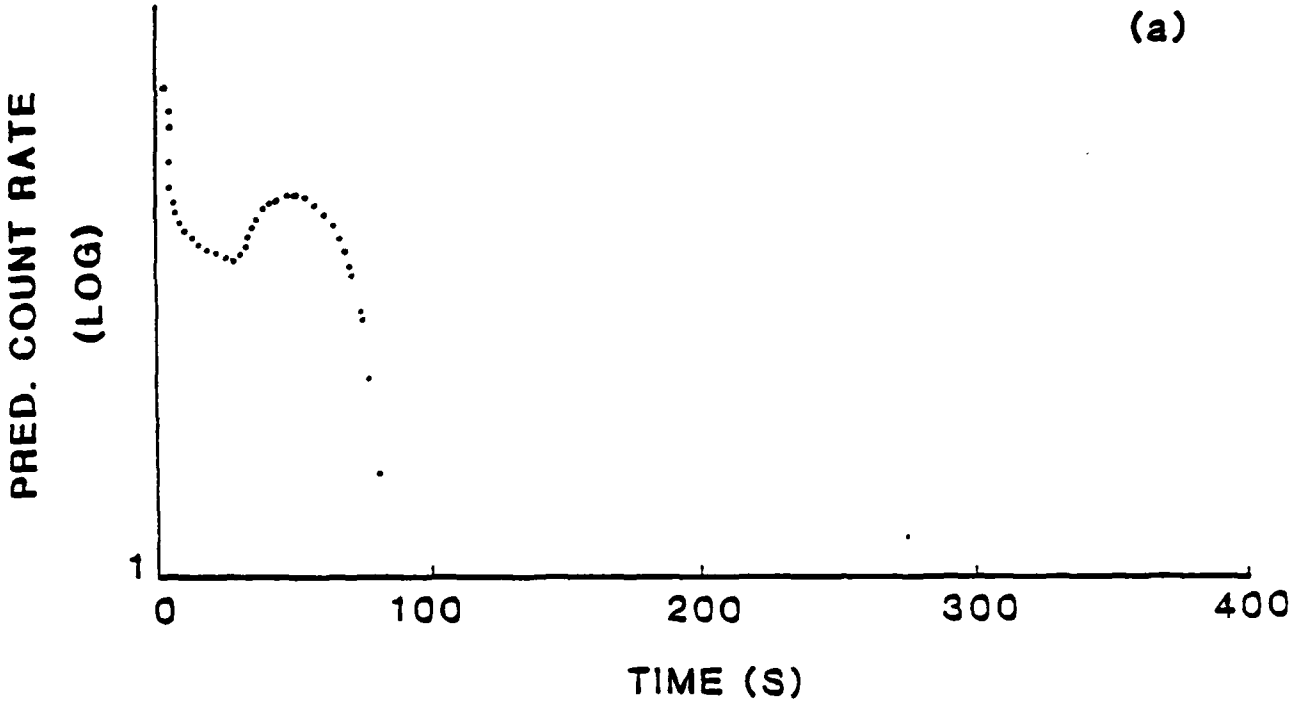

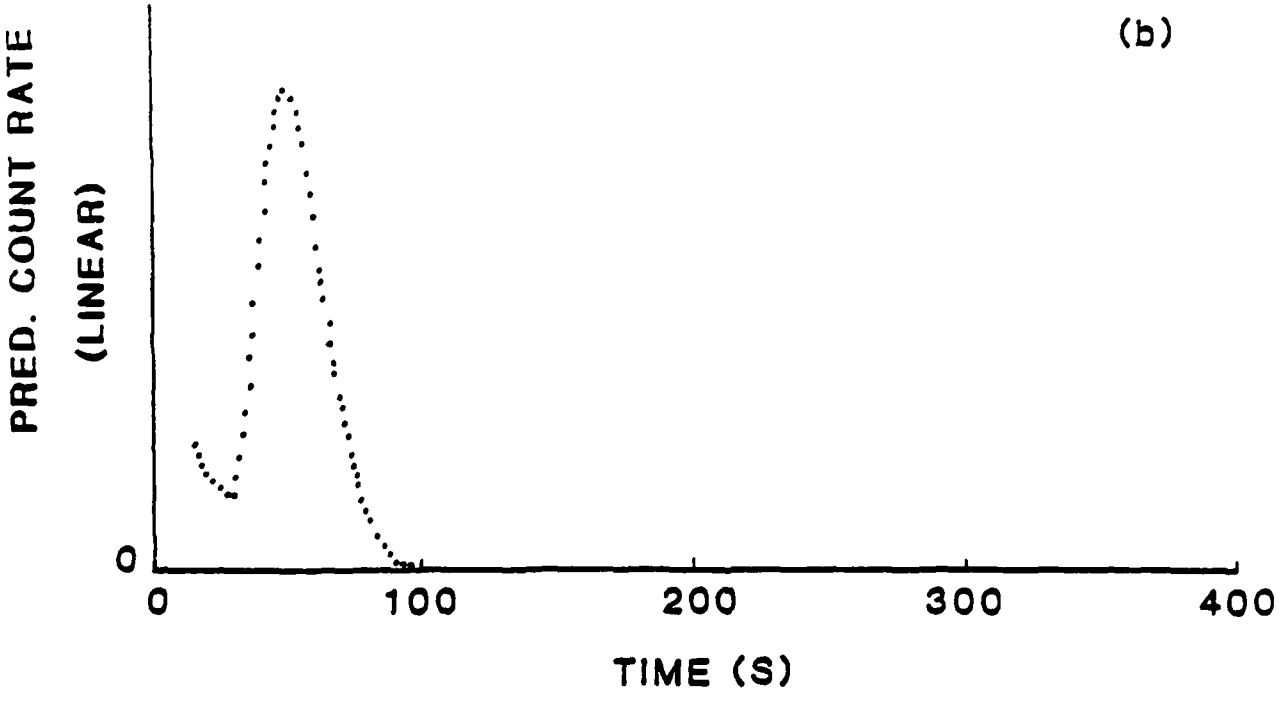

THERMAL STIMULATION OF FRACTURE SURFACE OF FILLED BR

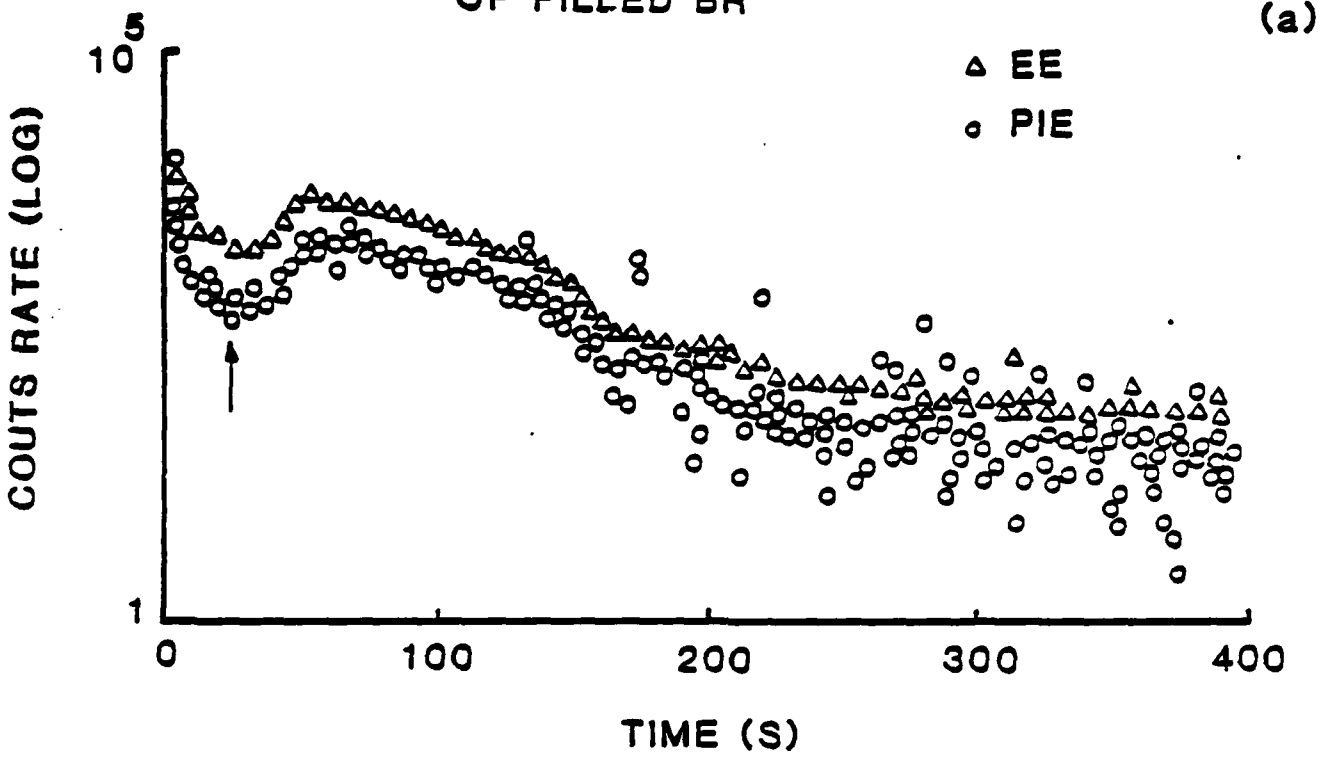

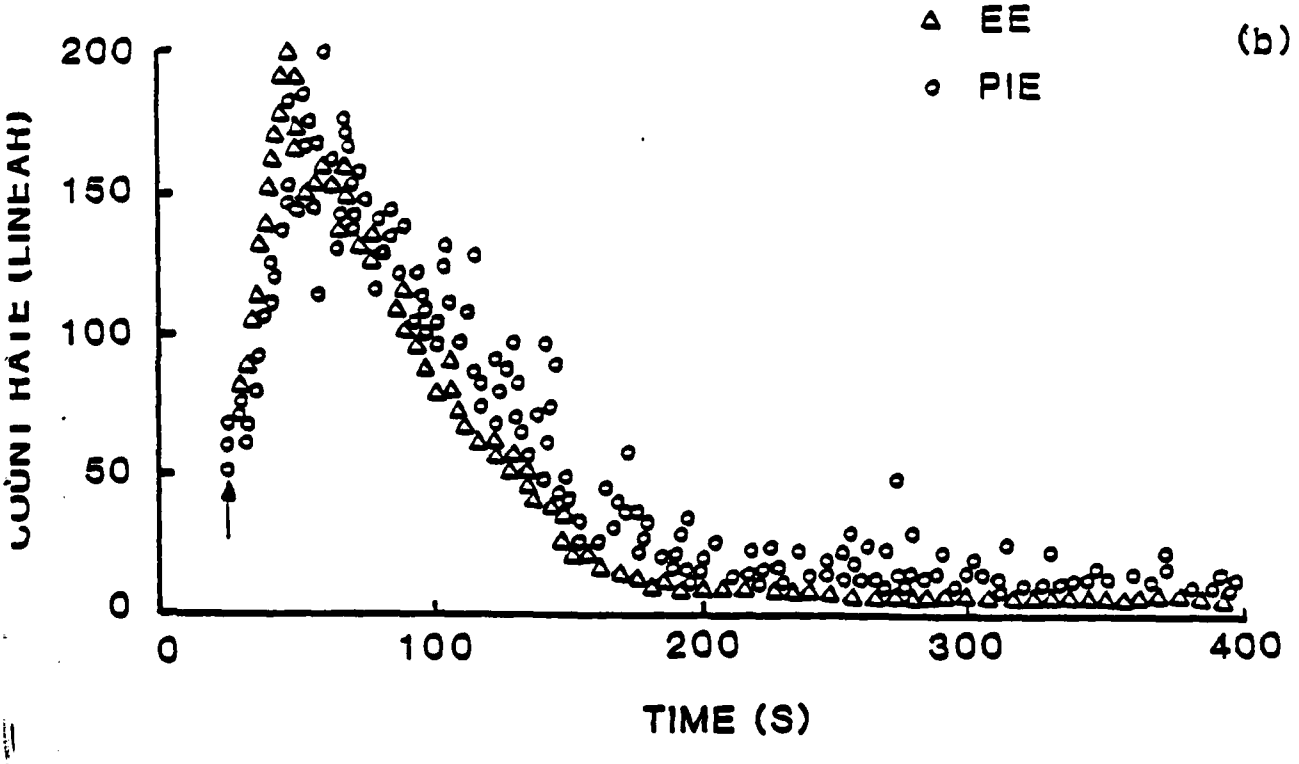

THERMAL STIMULATION OF ACTIVATED SURFACE

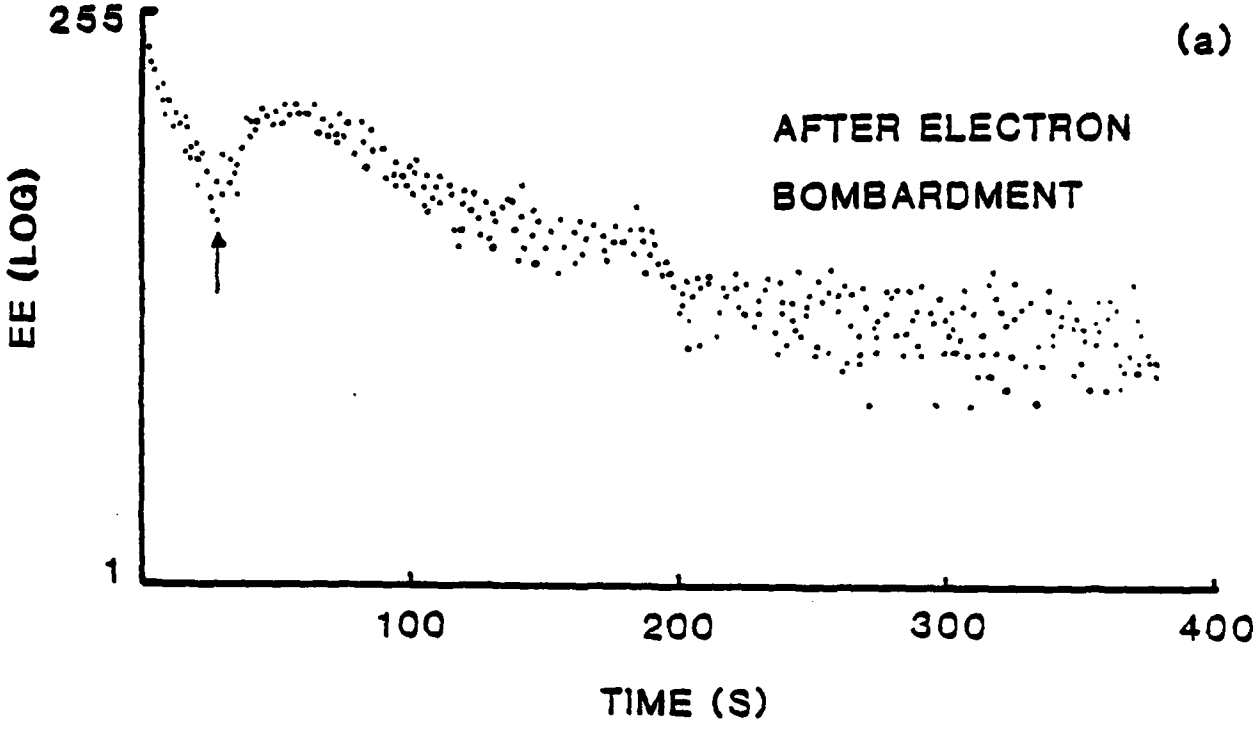

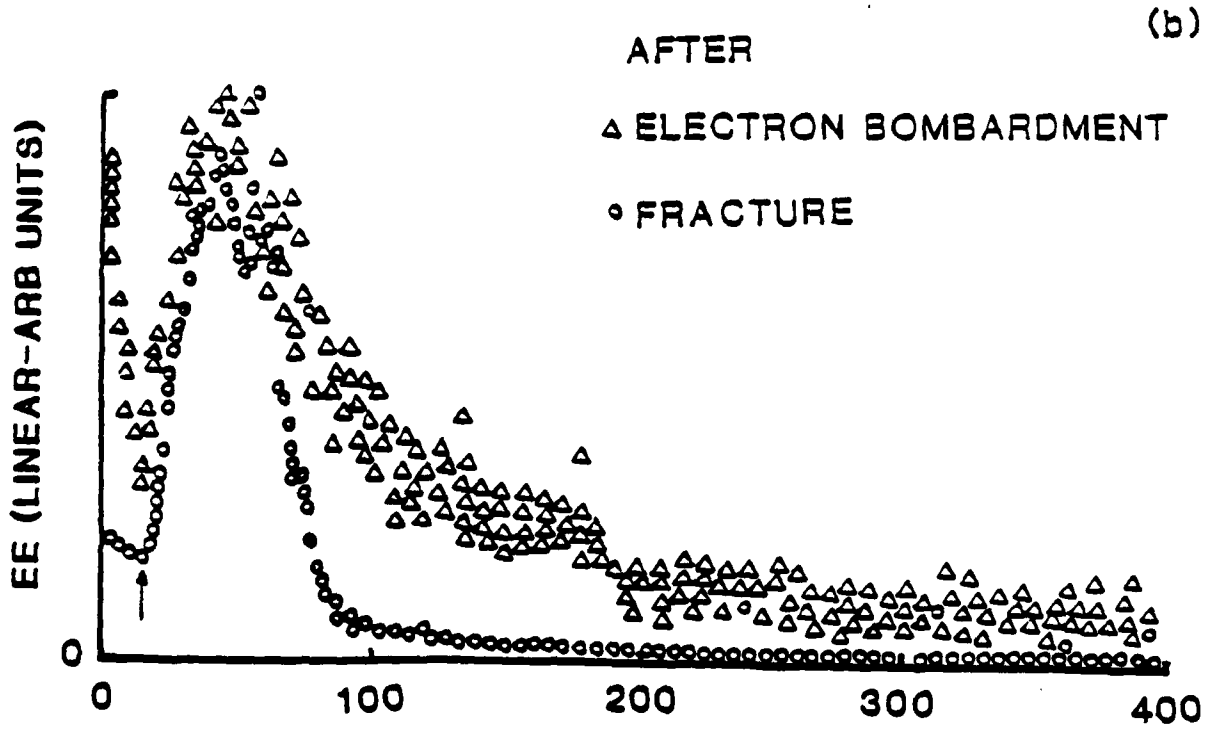

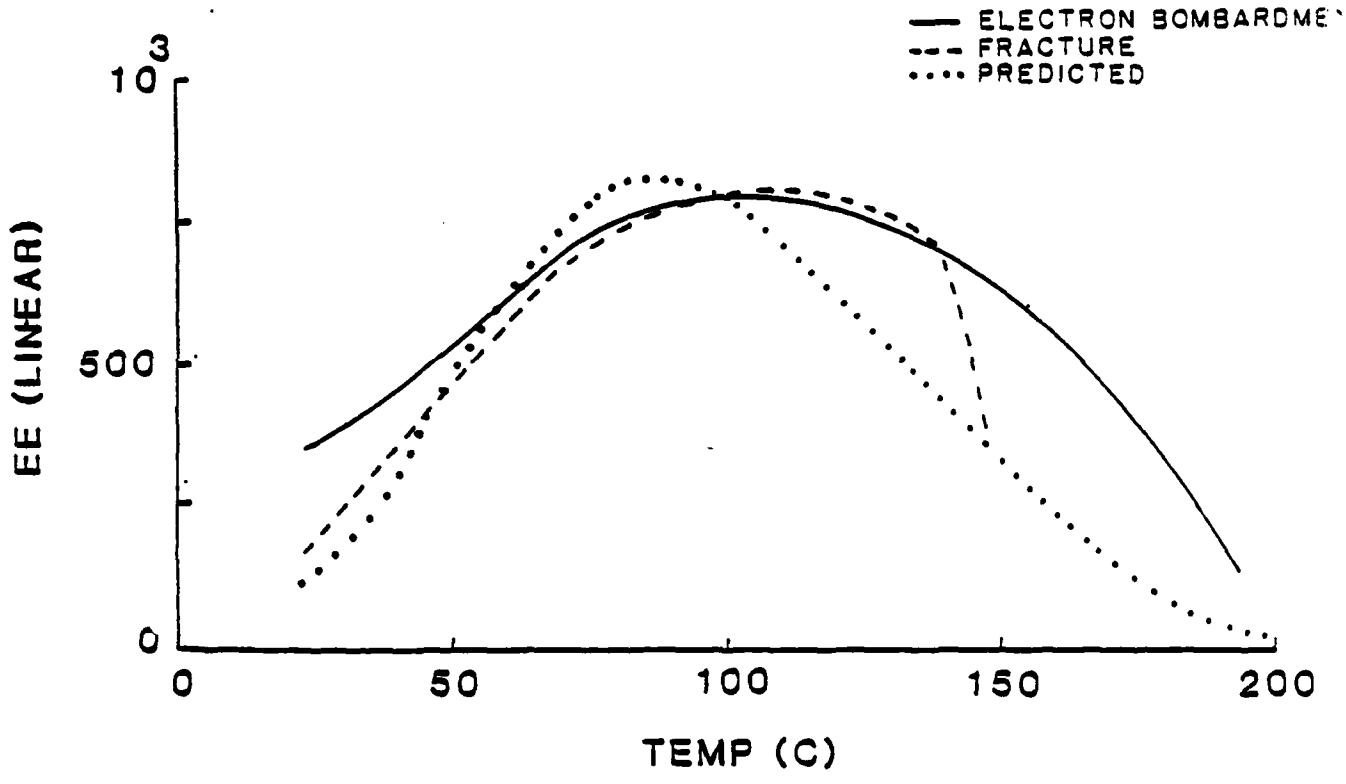
ELECTRON BOMBARDME
FRACTURE
PREDICTED
10^3
500
0
EE (LINEAR)
0
50
100
150
200
TEMP (C)

BR II

THERMAL STIMULATION OF FRACTURE SURFACE

UNFILLED BR

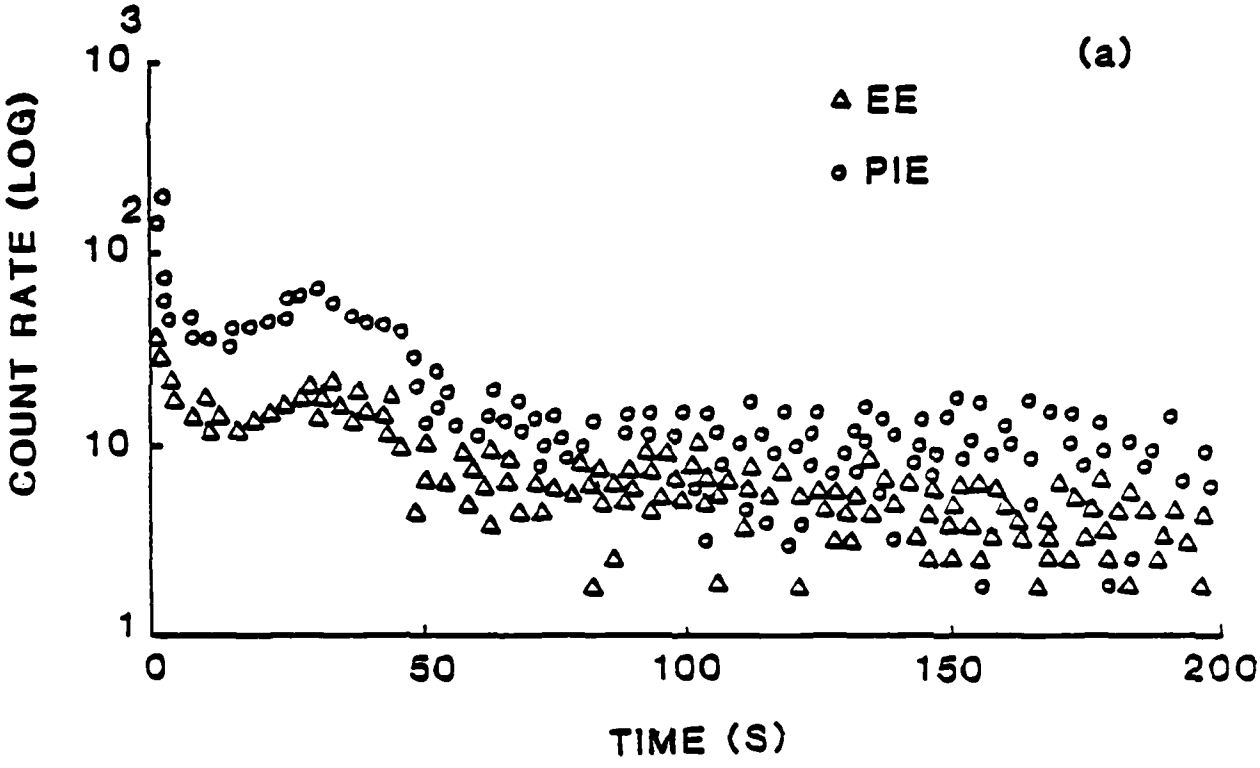

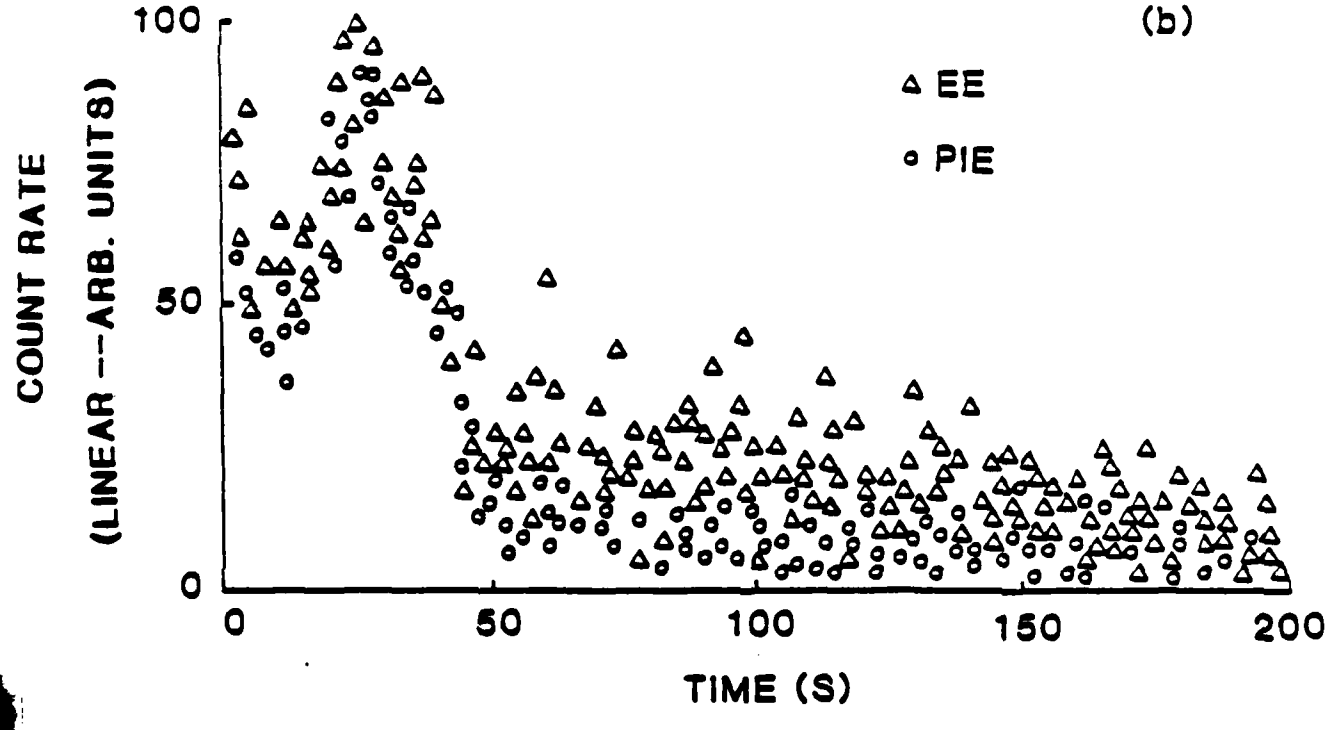

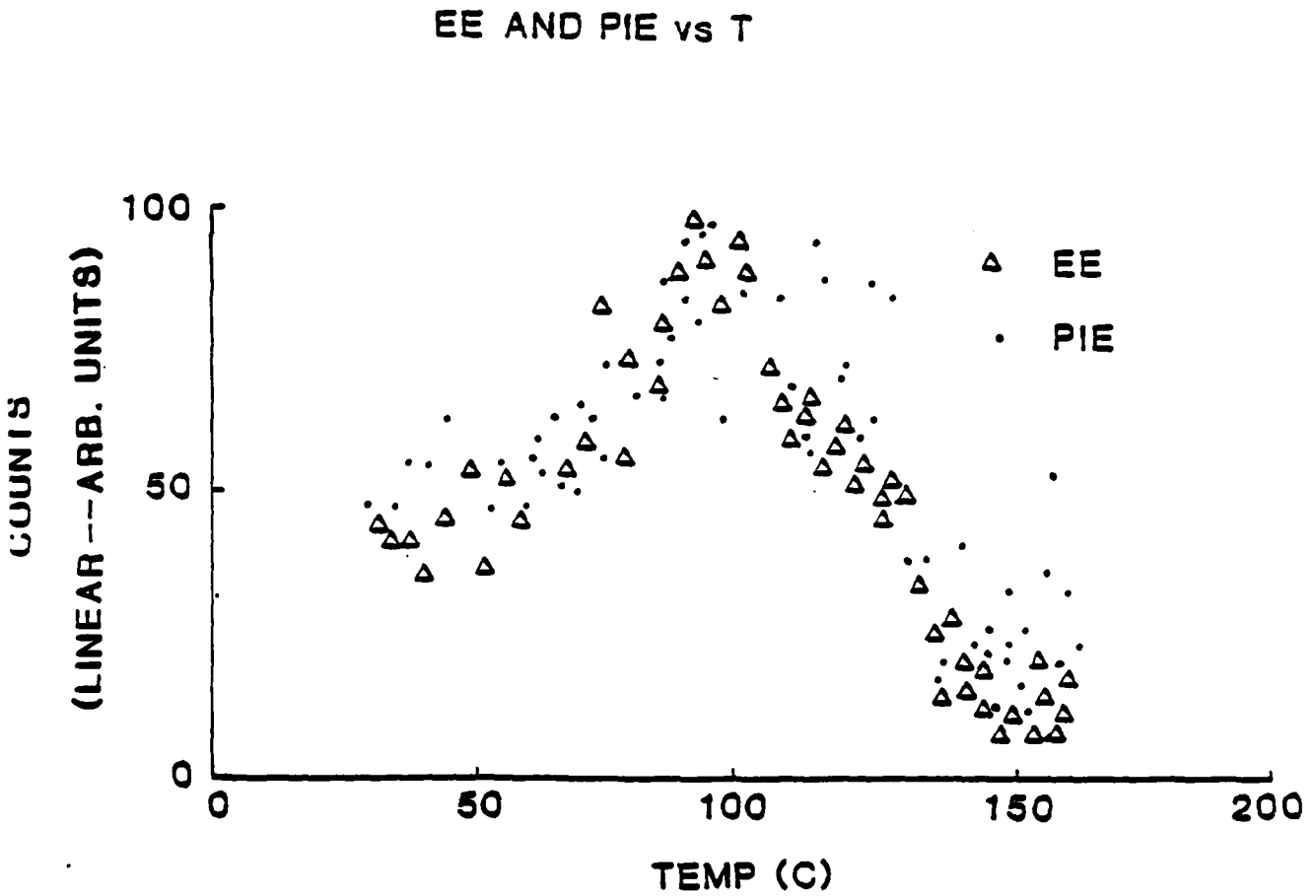
EE AND PIE vs T
COUNTS
(LINEAR -- ARB. UNITS)
100
50
0
0
50
100
150
200
TEMP (C)
EE
PIE

SR II

IV. FRACTO-EMISSION FROM SINGLE CRYSTAL PENTAERYTHRITOL TETRANITRATE (PETN)

M. H. Miles, J. T. Dickinson, and L. C. Jensen
Department of Physics
Washington State University
Pullman, WA 99164-2814

ABSTRACT

The emission of electrons, photons, and positive ions was monitored during three-point bending, compression, and fast compression (impact loading) of single crystal pentaerythritol tetranitrate (PETN). The emission appears to be fracture mode dependent with negligible emission from cleavage type fracture and very intense electron emission accompanying impact. Possible causes of this enhanced emission are discussed in terms of shear effects and frictional grinding of the crystal fragments. Evidence of a micro-discharge (electrical breakdown between fracture surfaces) during impact loading of the crystals is presented.

INTRODUCTION

The transformation of mechanical energy into other energy forms occurs during fracture of all solids. Fracto-emission (FE), e.g., the emission of electrons (EE), positive ions (PIE), visible photons (phE), and neutral particles (NE) during and following the fracture event[1-6] are manifestations of physical phenomena accompanying fracture. In previous studies, we have examined EE and PIE from several explosive organic molecular crystals. Results on RDX[3] showed a wide variation in the emission intensity for events that appeared to involve different modes of fracture. It is therefore anticipated that the mode of fracture is an important variable in FE phenomena. In this paper we present results of FE measurements on single crystal pentaerythritol tetranitrate (PETN) where we have purposefully varied the type of loading. In particular, we report here our first emission measurements accompanying impact, which we show leads to enhanced FE.

Included in our measurements are attempts to detect evidence of a micro-discharge previously observed in materials where a high degree of charge separation occurs. This involves the detection of bursts of visible photons and low frequency electromagnetic radiation accompanying fracture. In previous studies where fracture leads to intense charge separation on the fracture surfaces, we found the EE and PIE intensities to be correspondingly large. We have attributed this high intensity to the consequences of this discharge interacting with the

fracture surfaces.[3-6] Previous measurements of EE and PIE on PETN under slow compressive loading showed it to be a relatively weak emitter so that we expected any fracture induced discharge to be very weak. Nevertheless, in the case of impact loading we were able to detect evidence of such a discharge.

EXPERIMENTAL

Single crystals of pentaerythritol tetranitrate (PETN) were fractured in a vacuum of 10^{-5} Pa. Crystals fractured in flexure were mounted in a miniature three point bending fixture. Fracture was performed manually with a knife edge pushing on the center of the crystal. Typically this knife edge advanced at 0.1 mm/s during a test.

Single crystals were also fractured in compression between two parallel steel surfaces, similar to a vise. While straining the sample, separation of the two surfaces decreased at a rate of 0.5 mm/s.

Fracture by impact was achieved by coupling the compression device to a massive block that could be given a sharp blow with a heavy hammer. The impulse of this blow was transmitted to the "vise" holding the crystal via a 2 cm diameter steel rod penetrating into the vacuum via a bellows arrangement. Immediately following impact of the crystal following the sharp blow from the hammer, the two parallel surfaces quickly opened again due to the elasticity of the deformed bellows. The resulting impact, while considerably more energetic and violent than the other modes of loading the crystals, was below that required for explosive initiation of

the crystal. It should be emphasized that obtaining quantitative data on FE intensities for both slow compression and impact is quite difficult due to the obstruction of the vise surfaces which probably block a large portion of the emission. Furthermore, when we use two detectors, they generally viewed the sample from opposite sides of the vise and were therefore viewing different fracture surfaces. Ideally, for FE experiments one would like the crack to be opening up towards the detectors to maximize collection efficiencies. Obviously, both the slow compression and impact modes of loading are in this regard non-ideal. Nevertheless, we are still able to detect a number of FE components.

During straining of the crystals one or two types of emission were monitored (e.g., electrons, positive ions, photons, and/or low frequency electromagnetic radiation). The detectors used for charged particle detection were channeltron electron multipliers (CEM) which produce fast (10 ns) pulses with high detection efficiency for both electrons and positive ions. Background noise counts typically ranged from 1 to 10 counts/s.

The detectors were positioned within a centimeter of the sample with proper bias voltage on the front cone to attract the charged particles of interest.[2] It should be noted that for polymers we have shown that the principle particles detected for plus and minus bias on the CEM front cone were electrons and positive ions, respectively.

A Bendix BX754A photon counter tube with an S-20

photosensitive surface of 1 mm in diameter was used to detect visible photons; typical background count rates were 10-100 counts/s. We refer to this detector as our small photon detector. A second photon detector (Thorn-EMI 9924QB) with a factor of a hundred larger solid angle was introduced towards the end of this study and significantly improved the reliabilty of the photon measurements. We shall call this detector our large photon detector.

Because of expected weak signals, great care was taken to maximize sensitivity to the emission of low frequency electromagnetic waves (RE--for radiowave emission). A 20,000 turn solenoid of No. 30 magnet wire was wound on a 1 cm glass cylinder form and placed 2 mm from the sample. Such an antenna couples to a changing B field. It should be emphasized that this arrangement is detecting the near-field electromagnetic emission because of the close proximity of the solenoid to the source. The intensity of these oscillating fields is so weak that we would not be able to detect them at distances of several wavelengths. Such measurements would have to be made to assure absolutely that a true radiation field existed. Since our primary interest here is finding evidence of a micro-breakdown during fracture, we are chiefly concerned with simply detecting electromagnetic radiation accompanying fracture. A simultaneous burst of visible photons in coincidence with the observed RE burst reinforces the interpretation of these signals as being caused by a microdischarge.

The antenna coil was connected to the input of a wide-

band differential amplifier with high common mode rejection to minimize pick-up noise and amplified with a tuned amplifier set to the ringing frequency of the coil-amplifier circuit (8 KHz). The signal was then digitized at a rate of 250 kHz. The resulting signal was squared (to remove the negative part of the ringing signal) and plotted; the observance and time of onset of RE (relative to impact) were considered the most important information.

RESULTS

Fracture of single crystals of PETN in three point bending produced clean, cleavage type fracture surfaces. For PETN we recorded RE and phE for six samples and EE for two samples. No detectable EE was observed for this type of fracture. For one PETN sample, a small photon emission peak of 35 photons occurred in one channel (over the noise level of one photon per channel). No accompanying RE was observed. Excluding this rather singular event, PETN appeared not to emit in any significant way during cleavage-type fracture.

Compressional crushing of crystals was expected to alter the mode of fracture and also increases the freshly created fracture surface area. As reported earlier[2], loading PETN crystals in slow compression does lead to detectable EE.[2] Table 1 presents recent results of compressional fracturing of four single crystals of PETN fractured by compression while monitoring both EE and phE (using the small photon detector). Data were acquired at 0.1 s/channel. Fig. 1 shows the time

dependence of the EE and phE (small photon detector) measured simultaneously for sample 3 during compression of the sample. At approximately 25 s (not shown in the figure) the gap between the steel surfaces was reopened. A rise in EE was observed, similar to the EE behavior reported earlier,[2,3] but no detectable rise in phE was seen. The rise in EE is consistent with previous interpretations[2,3] that exposure of the crushed material allows the electrons to reach the detector. Furthermore, the most intense phE occurs during fracture and is believed due to a microdischarge occurring during failure of the crystal. In some other materials, very careful measurements of the phE after fracture has yielded a parallel phE signal falling with the EE, suggesting a parallel relaxation mechanism during this after-emission. We suspect that it here it is simply too weak to be observed, particularly with the small photon detector.

Seven PETN single crystals were fractured by fast compression (impact). Data were acquired at 0.1 s/channel. In dramatic contrast to the absent or relatively weak emission from three point bending and slow compression of PETN, we observed abundant emission from the impact of PETN. Table 2 summarizes the data for this type of loading. Fig. 2 shows the EE and phE (small photon detector) of sample 5, where the highest point in every ten channels is displayed. The EE peak is seen to be 950 corresponding to a minimum count rate of 9500 counts/s. The corresponding phE peak was 36 counts, for a minimum peak count rate of 360 counts/s. The rise in both the photon and electron

peaks occurred simultaneously in a time equal to or less than 0.1 s, both in the same channel, consistent with both peaks occurring during fracture.

Fig. 3 shows the emission of sample 7, which exhibited larger EE and phE peaks, each approximately 2400 counts (in 0.1 s) high. The EE curve (Fig. 3a) shows a clearly defined decay lasting many seconds after impact. The phE (Fig. 3b) curve shows almost all counts above background occurring in one channel, well aligned with the rise in EE.

Fig. 4 shows the EE (the only FE component that was measured) which occurred upon the second impact of crystal 8. Here the peak emission is the largest we observed, 24,000 counts (in 0.1 s), with a long and sustained decay following the initial rapid decay. As is the case for a wide range of other materials, the intensity and duration of the decay curves for impact loaded PETN are generally greater when larger peak emissions occur.

Fig. 5 shows the EE and phE from impact loading of sample 9. Peak EE is 9100 counts (0.1 s) and peak phE is 60 counts (0.1 s). Again the EE shows the long decay curve whereas most of the phE occurs in a single channel, presumably only during fracture.

In Fig. 6 we show the EE and PIE from sample 10, measured simultaneously. Both show a decay curve lasting many seconds. If we normalize the two curves at any point other than the initial peak, the two curves are approximately the same. This behavior has been observed in a number of other systems and

is due to a PIE mechanism which directly involves the emission of electrons; therefore the PIE intensity is proportional to the EE intensity.

For impact loading using the large photon detector (Thorn-EMI 9924QB) we were able to detect phE both during and following impact. Photon data were acquired at 10^{-3} s/channel for samples 12, 13, and 14 summarized in Table III. The phE from samples 13 and 14 are shown in more detail in Fig. 7. Although the phE after impact of the crystal is only about 100 ms in duration it is suggestive of a relaxation process similar to that observed in polymers.[5,6]

Also, for impact loading, we were able to observe small but clearly discernible emission of electromagnetic radiation (RE) during failure of the crystal. Figures 8 and 9 show the RE and simultaneous phE (using the small photon detector) for two different samples on a millisecond time scale. Figure 8 is the second impact of 13 and Fig. 9 is the first impact of 14. The phE is plotted in histogram form (which is how the data is acquired) to show that the onset in RE and the first detectable phE occur in the first channel of detectable phE. The finite time during crushing of the crystal and the re-opening of the metal surfaces may explain the somewhat complicated shape of the phE curve. Thus, in the case of impact of PETN between two metal surfaces, it appears that a microdischarge is occurring.

Many of the impacted PETN samples were struck several times. It was not uncommon for the second impact to produce significantly more emission than the initial impact. To

illustrate we have included in Table II the results of the second impact of samples 8 and 11.

The experimental results presented here are suggestive of two clearly separated time scales. A sub-millisecond time scale related to EE, phE, and RE due to a microdischarge during fracture of the PETN, and EE and PIE that continues for many seconds following energetic fracture due to a relaxation of an excited surface.

As mentioned earlier, the stress levels experienced by the samples during impact were not controlled and varied considerably. Also, the two detectors used in a typical experiment usually view opposite sides of the impacted crystals. Thus, although the onset of the various emissions appear to be nicely coupled, the magnitudes of peak and total counts showed large variability both between different impacted crystals and between different emissions on the same impacted crystal. However, it should be noted that the first two crystals impacted (samples 5 and 6) were smaller in size than later samples and their emissions were notably smaller.

To gain further information on the role of the mode of fracture we examined the emission accompanying surface scratching or abrasion between a PETN crystal and a sharp, pointed stainless steel blade pulled across the crystal with a small load pushing the point into the crystal. This produced a scratch on the surface of the crystal with considerable metal/crystal and crystal/crystal rubbing. Data taken for sample 15 were collected at 0.1 s/channel for scratches 15A,

15B, 15C and at 0.01 s/channel for 15D-15F. Total and peak EE counts are given in Table IV. Scratches 15A and 15C were produced by slow movement of the sharp point over the surface. However, scratch 15B was unusual in that the sharp point had initially fallen over an edge of the crystal. In pushing it back onto the crystal, it jumped rapidly across the edge. Thus, the rate of deformation was considerably higher and it also produced sizeable chipping of the edge as the point came up onto the crystal surface. Most of the visual damage and presumably most of the emission was due to this rapid motion. This result suggested that the strong emission was dependent on the rate of the damage.

To test this hypothesis, the last three "fast" scratches were produced by giving a sharp blow with a heavy hammer to a massive block attached to the steel rod which in turn moved the steel point on the crystal surface. This produced sudden rapid motion of the steel point. As predicted, this rapid abrasion produced intense emission. Figure 10 shows the EE for scratches 15D and 15E where the emission from the two scratches showing the intense peaks during abrasion and the accompanying long decay following motion of the metal point.

DISCUSSION

We have demonstrated that in three point knife edge cleavage fracture of single crystal PETN, EE, phE, and RE are not detectable. This is in contrast to results on RDX[3] where an EE peak accompanying cleavage fracture was always observed and was followed by an observable decay. Slow compressional

crushing of PETN does, however, produce EE in agreement with our previous work.[2] Fast compressional crushing (impact) of PETN leads to greatly enhanced EE compared to the slow compressional crushing. In addition, we also observed phE and electromagnetic radiation (RE) accompanying impact fracture of PETN. Similarly, we observed EE accompanying abrasion or scratching of the PETN surface with a metal point and this emission also exhibited a strong rate dependence.

In the case of cleavage fracture, we suggest that principally mode 1 fracture is occurring wherein only certain crystal faces are separated without surface contact sliding or rotation (i.e. absence of surface friction of any type). The latter occurs, however, in more energetic types of fracture and in the abrasion experiment. Recent work of Hauser et al.[7] suggests that the appearance of molecular fracture products is indeed energy dependent and it is likely that the relative amounts of mode 2 and mode 3 fracture are more dissipative. The work reported here, and earlier work on RDX[3] and PETN and HMX,[2] indicate that intense long lasting emission occurs for multiple fracture involving surface frictional grinding, i.e. mode 2 and mode 3 fracture. The three classical modes of fracture usually neglect considerations of plastic flow and possible dislocation mechanisms which may play important roles in both FE and in hot spot formation.[8,9]

For the fracto-emission components observed here, we have previously proposed a mechanistic model,[3-6] the basic features of which consist of the following:

1. The fracture event yields charge separation on surfaces producing an electric field, E, usually across the crack gap, but also along the surface due to the patchy nature of this charge separation.
2. Desorption of volatiles and/or fracture products raises the pressure, P, in the crack tip. (We note that Field et. al.[8] have shown that fracture of PETN leads to gaseous emission.)
3. A gas discharge (whose intensity is dictated by P, E, and a distance d characterizing the crack width) occurs, producing the RE and phE observed <u>during</u> fracture. Electron and ion bombardment of the crack walls occurs during this discharge.
4. Bombardment of the fracture surfaces creates primary excitations, usually explained in inorganic crystals in terms of electron-hole production, raising electrons into traps near the conduction band, which then undergo thermally stimulated migration until recombination with a hole occurs. This recombination can yield an emitted electron (thermally stimulated electron emission[10]), say by an Auger process[11], or a photon (thermal luminescence).[12] Since these are thermally stimulated processes they occur with kinetics dictated by activation energies and populations of electrons, traps, and recombination sites and generally decay with time[6].
5. A portion of the electron emission strikes adjacent patches of positive charge yielding PIE via an ESD

mechanism.[13] Some of these positive ions are neutralized as they leave the surface, yielding an excited neutral component of FE that we have observed.[14]

A number of important properties of FE are explained by this model and are discussed in references 3-6. Of importance here is the role of the mode of fracture in producing the necessary conditions for phenomena such as a discharge to occur. PETN is non-piezoelectric and therefore may explain why cleavage type fracture does not produce detectable FE (i.e., no charge separation). However, the other modes of fracture involving frictional grinding of crystal surfaces may lead to charge separation of sufficient magnitude to produce the effects observed. It should be mentioned that when noncrystalline, unfilled elastomers are torn, they yield FE including RE.[3-6] This further supports the existence of a mechanism whereby a homogeneous non-piezoelectric material may produce charge separation when fractured.

We have not ruled out the possibility that the metal/crystal interaction that occurs in the compression and impact loaded cases is involved. Here we would imagine contact charging occurring before and during fracture followed by separation of metal/PETN surfaces which in turn leads to charge separation and a discharge. The fact that the EE <u>increased</u> with the rate of abrasion of PETN with a metal point does not fully agree with this mechanism. The time of contact between disimilar materials greatly influences the degree of charge separation so that larger effects would be expected at lower

velocities and/or where the metal point remained stationary on the crystal for longer times. Furthermore, the compressional nature of the loading really does not encourage separation of the crystal surfaces from the metal surface. Although additional studies of both abrasion and compression are needed, at this time we do not believe the FE observed is due to the metal/crystal interface.

The two compressional types of loading obviously lead to considerably larger surface areas. Examination of the fragments with optical microscopy show that the compressed materials form a pulverized "cake" with some extrusion out of the vise. Rough estimates of upper limits on the ratios of surface areas exposed to the vacuum relative to the cleavage fracture surface areas are: slow compression--100, fast compression (impact)--500. Such estimates indicate that surface area alone could not explain the extreme range of FE intensities observed during fracture.

We thus conclude that the intense EE and detectable phE and RE obtained by mechanical action involving fast compression (impact) of PETN single crystals is a manifestation of the modes of failure involving slipping and rubbing between crystal surfaces and is highly strain rate dependent. The role of this type of fracture in producing charge separation in a non-piezoelectric material and the subsequent microdischarge is believed to be important in the observed FE from these materials.

So far our most vigorous impacts were below the

intensity required to produce a self-sustaining reaction in PETN. It is unknown at this time how the EE and other emission components vary as the impact velocity is increased towards initiation. It seems reasonable that before a self-sustaining and growing hot spot is nucleated that many sub-critical hot spots will be produced. It is quite possible that some of the fracto-emission features might correlate with the growth or decay of these centers of reactivity.

Finally, we should point out that the explosives literature contains evidence that freshly produced fractured surfaces are much more reactive than crystal surfaces that have been allowed to passivate. Hanna and Polson[15] found that if an electrical spark was discharged to lead azide within a few seconds of crushing the material, then the initiation threshold was greatly reduced from a spark energy of 10^{-7} Joules to a value of the order 10^{-10} Joules. Charging effects have long been of interest to workers in explosives. One interesting example is the work of Fox[16] who measured the fluctuations of charge on the surface of lead azide crystals during growth. Such charge fluctuations are known to sometimes produce explosions.

ACKNOWLEDGMENTS

The authors would like to thank Dr. Howard Cady and Dr. Jerry Dick, Los Alamos National Laboratory, for providing us with the single crystals of PETN. We gratefully acknowledge the support of this work from the Office of Naval Research Power

Program under Contract N00014-80-C-0213.

REFERENCES

1. J. T. Dickinson, E. E. Donaldson, M. K. Park, J. Mat. Sci. 16, 2897 (1981).

2. M. H. Miles and J. T. Dickinson, Appl. Phys. Lett. 41, 924 (1982).

3. J. T. Dickinson, M. H. Miles, W. L. Elban, and R. G. Rosemeier, J. Appl. Phys. 55, 3994 (1984).

4. J. T. Dickinson, L. B. Brix, and L. C. Jensen, J. Phys. Chem. 88, 1698 (1984).

5. J. T. Dickinson, L. C. Jensen, and A. Jahan-Latibari, J. Vac. Sci. Technol. A 2, 1112 (1984).

6. J. T. Dickinson and L. C. Jensen, submitted to J. Poly. Sci.: Poly. Physics Ed.

7. H. M. Hauser, J. E. Field, and V. K. Mohan, Chem. Phys. Lett. 99, 66 (1983).

8. J. E. Field, G. M. Swallowe, and S. N. Heavens, Proc. Royal Soc. Lond. A 382, 231 (1982).

9. W. L. Elban, C. S. Coffey, R. W. Armstrong, K. C. Yoo, and R. G. Rosemeier, "Microstructural Origins of Hot Spots in RDX Explosive and Several Reference Anext Materials," Naval Surface Weapons Center Report, No. MP83-116.

10. H. Glaefeke, in Thermally Stimulated Relaxation in Solids, ed. by P. Braunlich (Springer Verlag, Berlin, 1979), p.229.

11. V. Bichevin and H. Kaambre, Phys. Status Solidi (A) 4, K235 (1971).

12. R. Chen and Y. Kirsh, Analysis of Thermally Stimulated Processes (Pergamon Press, Oxford, 1981), pp. 48-52.

13. M. L. Knotek and P. J. Feibelman, Phys. Rev. Lett. 40, 964 (1978).

14. J. T. Dickinson, L. C. Jensen, and M. K. Park, Appl. Phys. Lett. 41, 443 (1982).

15. H. A. Hanna and J. R. Polson, Iowa Army Ammunition Plant Technical Report No. 98A.

16. P. G. Fox, J. M. Jenkins, G. W. C. Taylor, Explosivstoffe 8, 181 (1969).

LIST OF TABLES

Table I

Sample	Emission	Total Counts	Peak Count
1	EE	340	20
	PhE	5200	50
2	EE	59000	65
	PhE	4000	80
3	EE	37500	50
	EE	500	25
	PhE	3000	150
4	EE	2600	40
	PhE	1500	30

Table II

Sample	Emission	Total Counts	Peak Counts
5	EE	4300	950
	PhE	38	36
6	EE	1300	50
	PhE	130	130
7	EE	16700	2400
	PhE	2400	2400
8	EE	2500	90
	PhE	90	70
second impact	EE	1250000	24000
	PhE	20	10
9	EE	370000	9100
	PhE	90	70
10	EE	17500	4700
	PIE	3500	2700
11	EE	213000	5500
	PIE	16000	700
second impact	EE	2100000	3100
	PIE	2400	100
Averages	EE	440000	5500
	PhE	460	450
	PIE	7300	1200

Table III

Sample	Emission	Total Counts	Peak Counts
12	PhE	49000	7400
	RE		
13	PhE	26000	5300
	RE		
second impact	PhE	3000	900
	RE	Detected	
14	PhE	14000	6200
	RE	Detected	
second impact	PhE	7800	4700
	RE	Detected	

Table IV

Sample Experiment	Emission	Total Counts	Peak Counts
15A Slow Abrasion	PhE	Below Noise	0
	EE	6200	50
15B Damaging Edge	PhE	27400	13000
	EE	1060000	59000
15C Slow Abrasion	EE	45000	1500
15D Fast Abrasion	EE	100000	2200
15E Fast Abrasion	EE	405000	5700
15F Fast Abrasion	EE	109000	22000

FIGURE CAPTIONS

Figure 1. (a) Electron emission and (b) photon emission during and following slow compression of PETN. (Ø.1 s/ channel).

Figure 2. (a) Electron emission and (b) photon emission due to impact of sample 5. (Ø.1 s/channel; highest point in ten channel intervals displayed).

Figure 3. (a) Electron emission and (b) photon emission due to impact of sample 7. (Ø.1 s/channel).

Figure 4. Electron emission accompanying impact of sample 8. (Ø.1 s/channel.)

Figure 5. (a) Electron emission and (b) photon emission for impact of sample 9. (Ø.1s/channel).

Figure 6. (a) Electron emission and (b) photon emission for impact of sample 1Ø. (Ø.1s/channel).

Figure 7. (a) Photon emission for impact of sample 13 and (b) photon emission for impact of sample 14. (1 ms/channel).

Figure 8. (a) Response of solenoid (radiowave emission) and (b) photon emission for impact of sample 13.

Figure 9. (a) Radio wave emission and (b) photon emission for impact of sample 14.

Figure 1Ø. Electron emission due to two rapid surface abrasions or scratches of a PETN crystal surface with a stainless steel point. (1 s/channel).

PETN

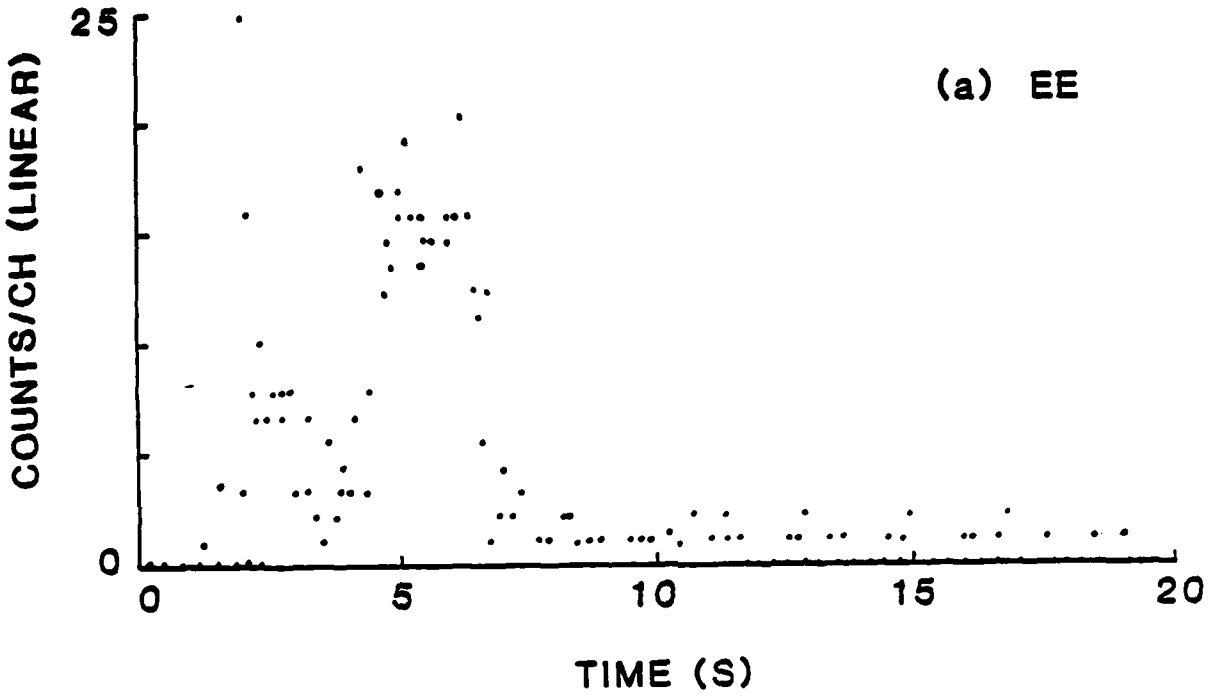
25
0
COUNTS/CH (LINEAR)
(a) EE
0
5
10
15
20
TIME (S)

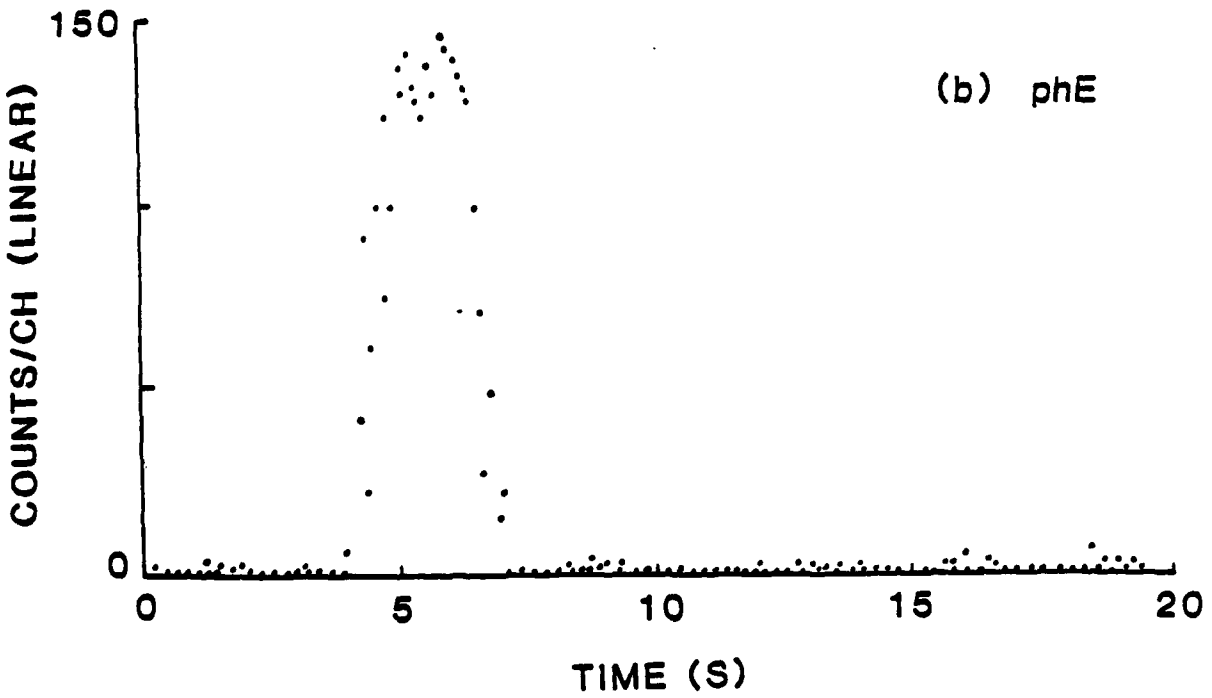
150
0
COUNTS/CH (LINEAR)
(b) phE
0
5
10
15
20
TIME (S)

Fig -

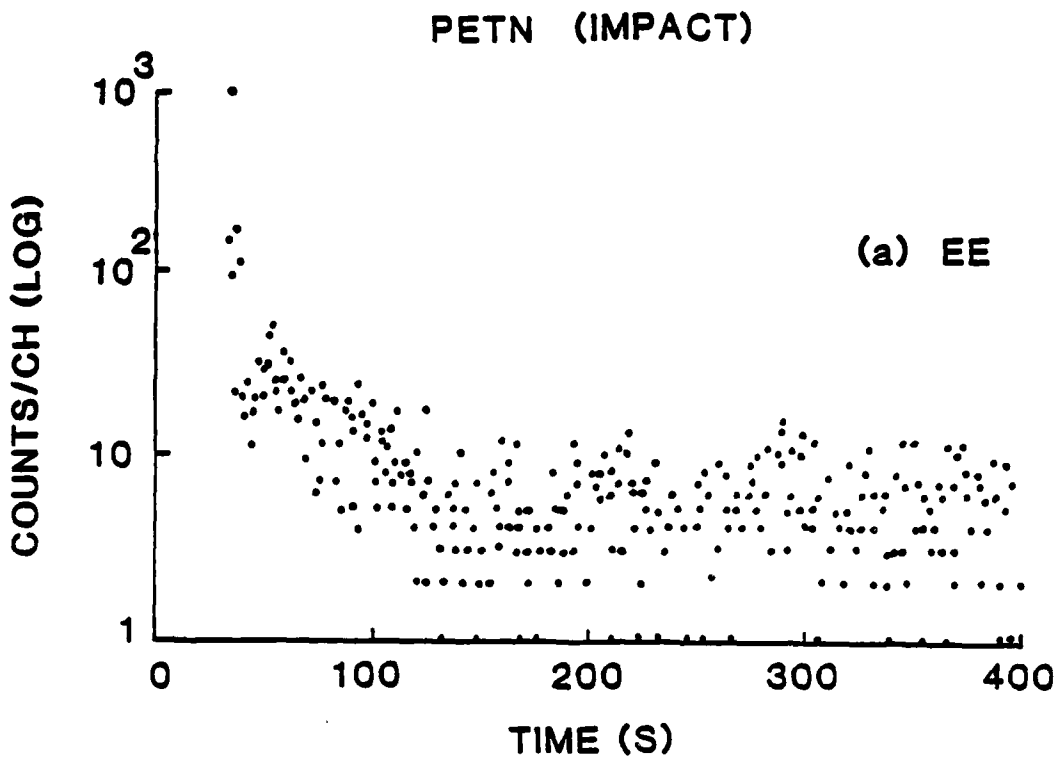
PETN (IMPACT)
COUNTS/CH (LOG)
10^3
10^2
10
1
(a) EE
0
100
200
300
400
TIME (S)

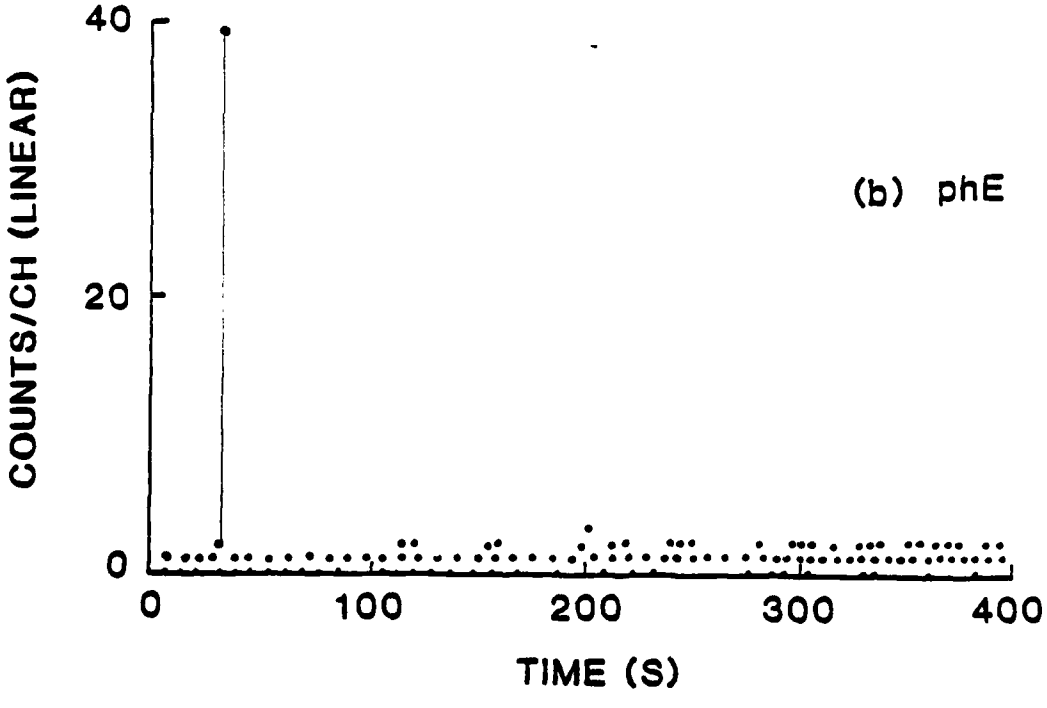
COUNTS/CH (LINEAR)
40
20
0
(b) phE
0
100
200
300
400
TIME (S)

PETN (IMPACT)

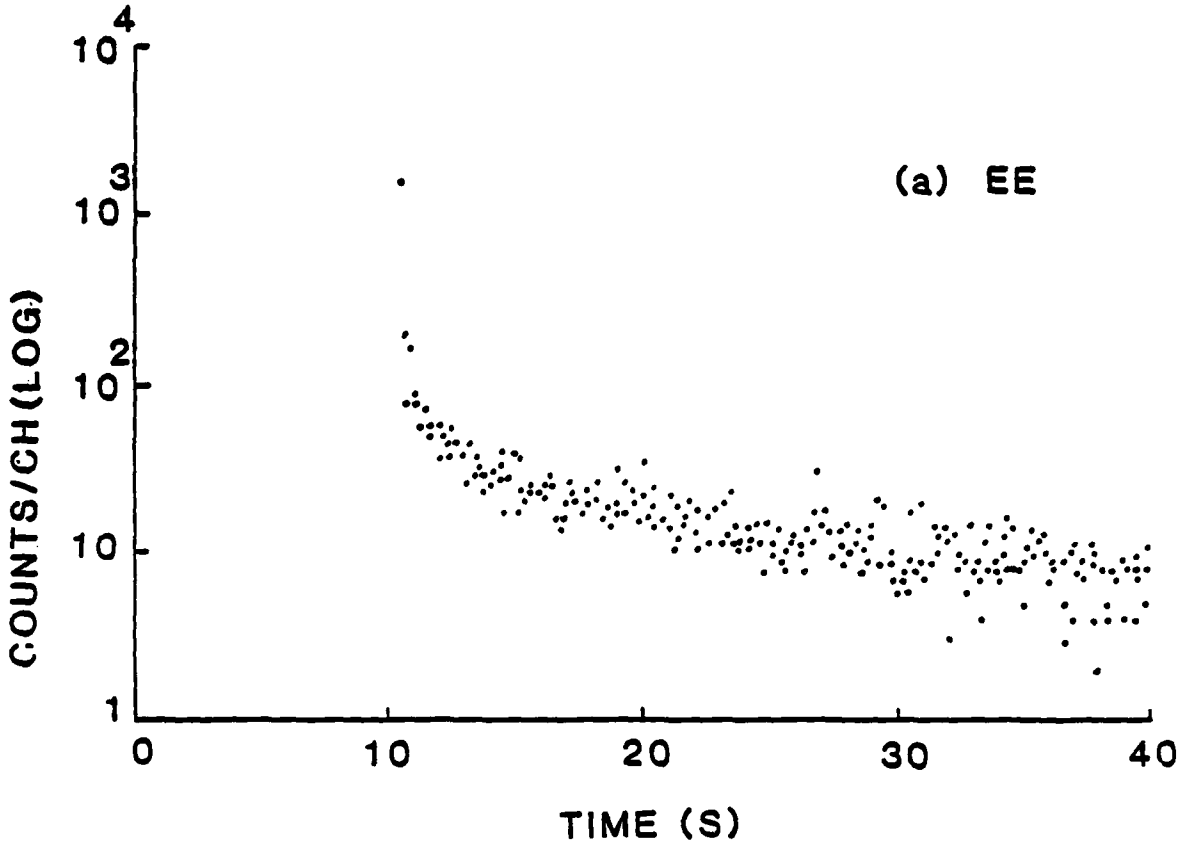

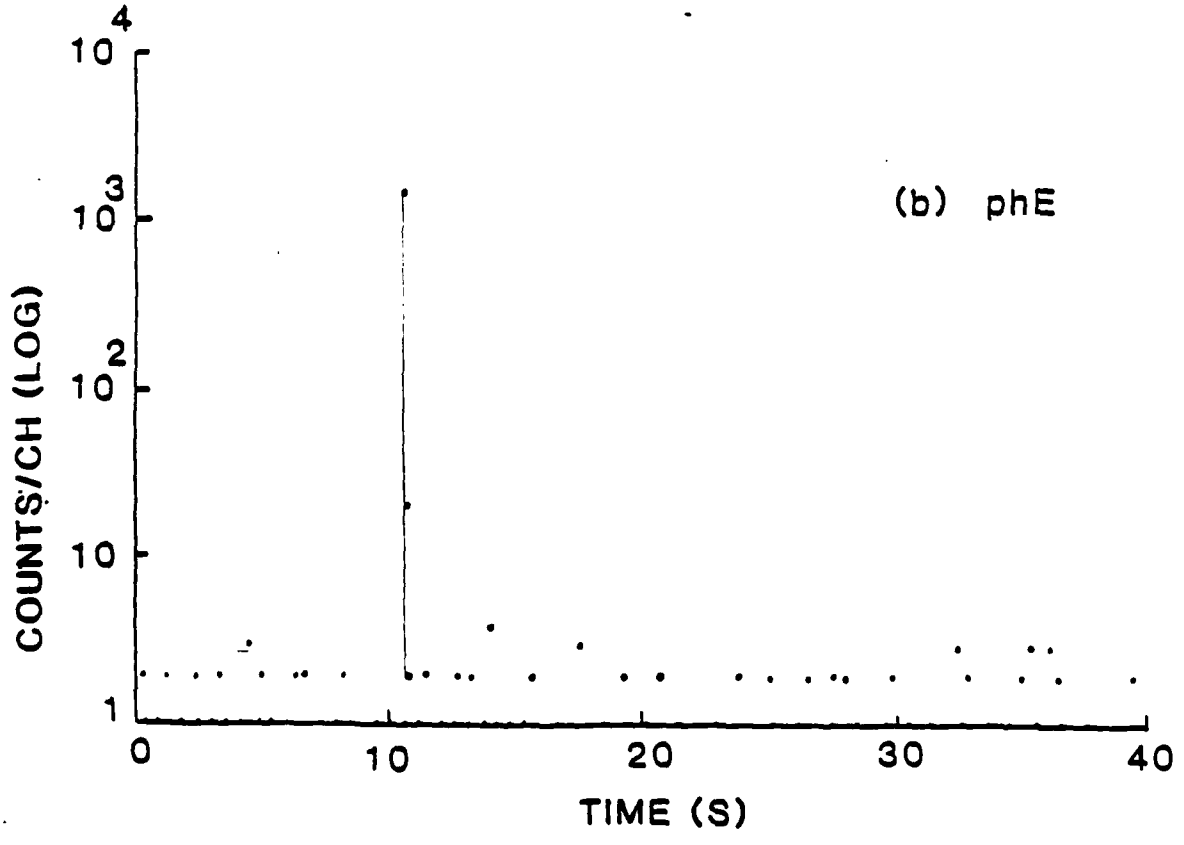

Fig 3

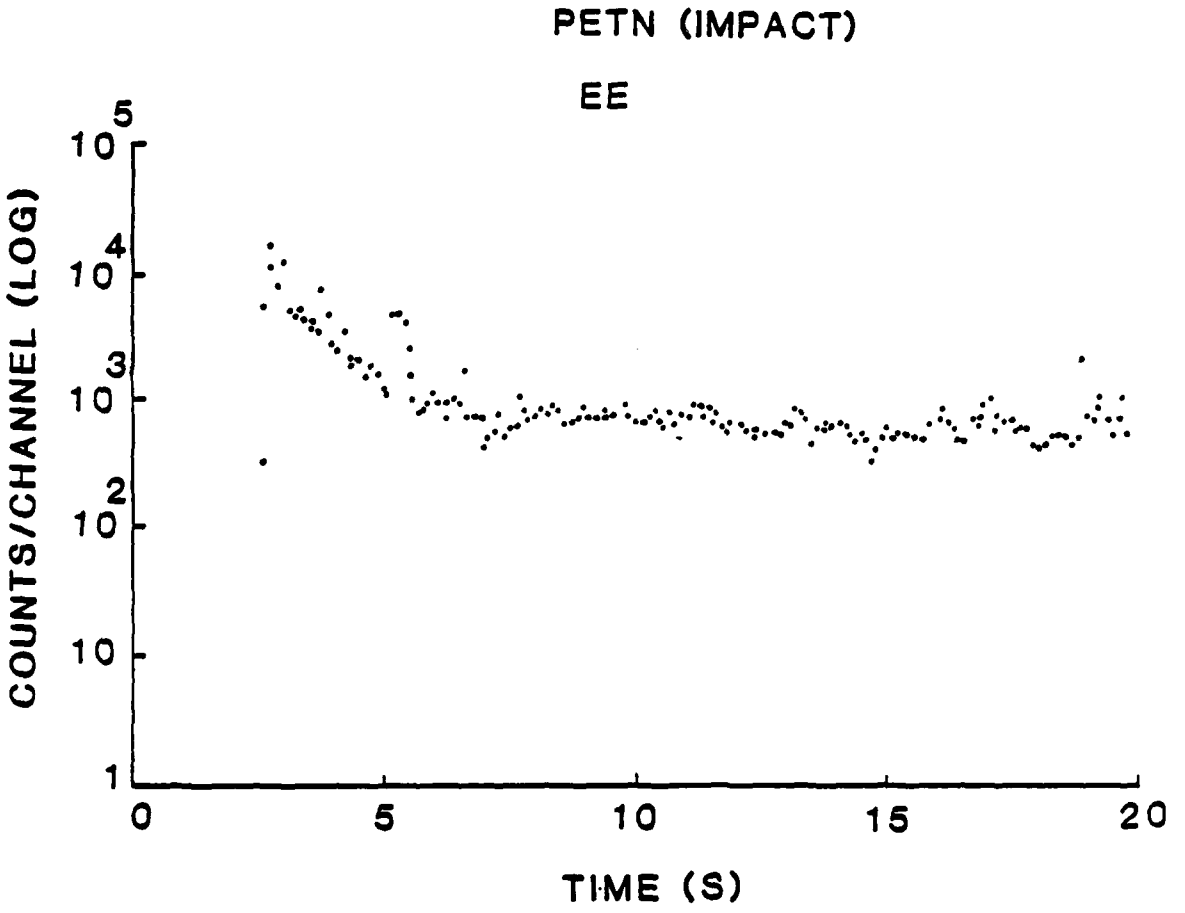
PETN (IMPACT)
EE
COUNTS/CHANNEL (LOG)
10^5
10^4
10^3
10^2
10
1
0
5
10
15
20
TIME (S)

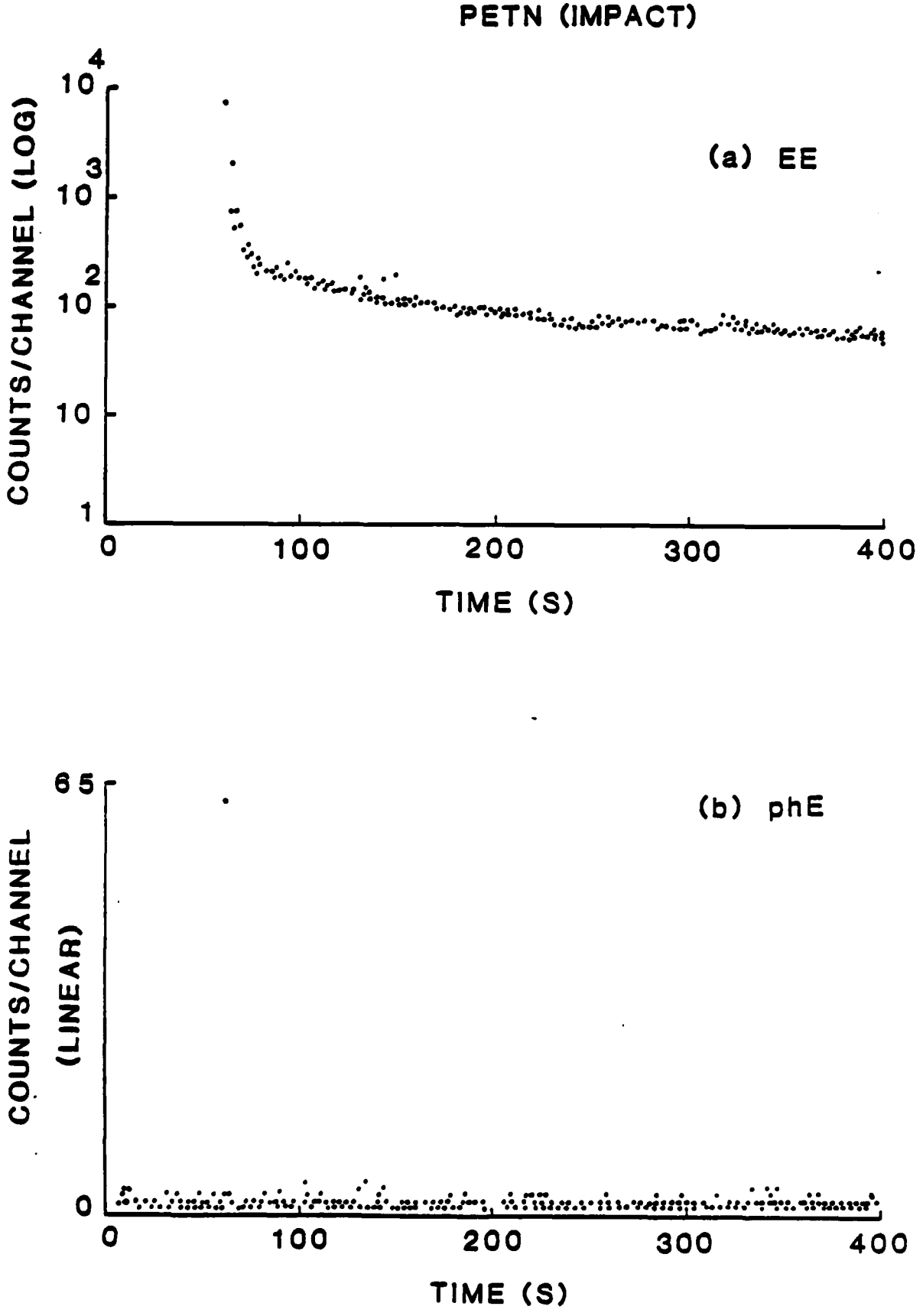
PETN (IMPACT)
(a) EE
COUNTS/CHANNEL (LOG)
10^4
10^3
10^2
10
1
0
100
200
300
400
TIME (S)
(b) phE
COUNTS/CHANNEL (LINEAR)
65
0
0
100
200
300
400
TIME (S)

Fig 5

PETN (IMPACT)

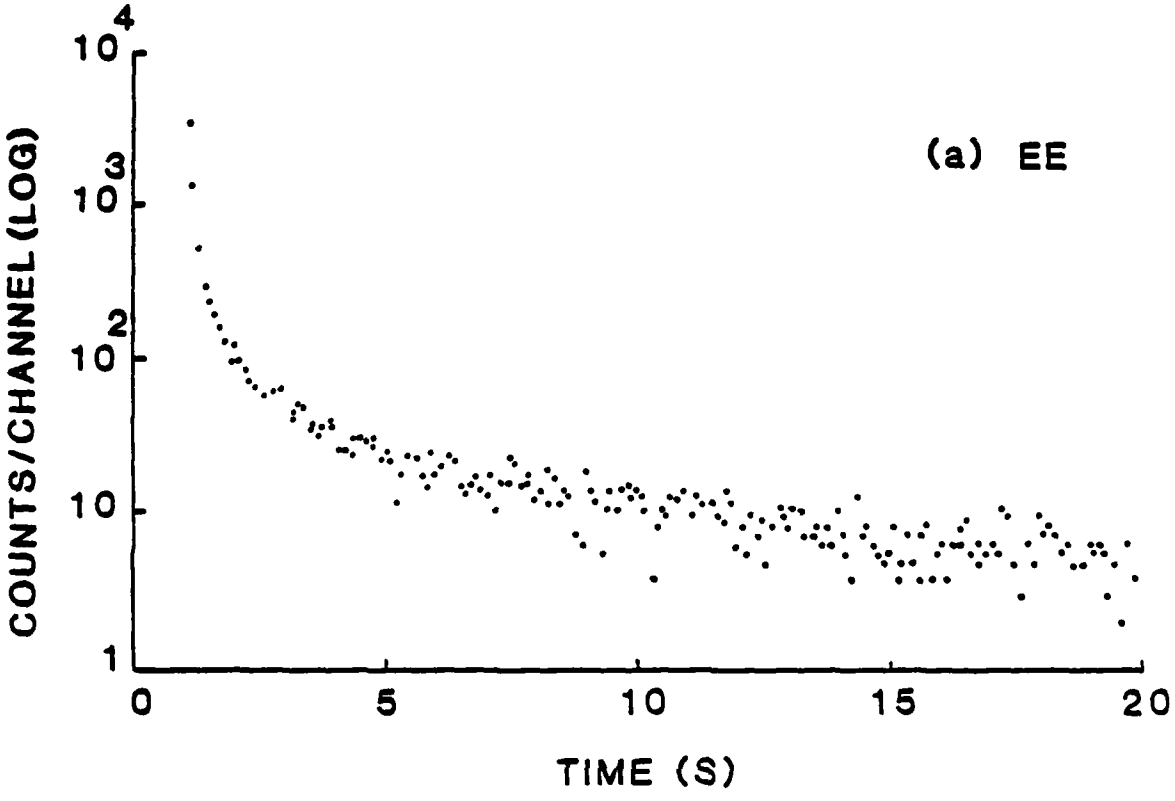

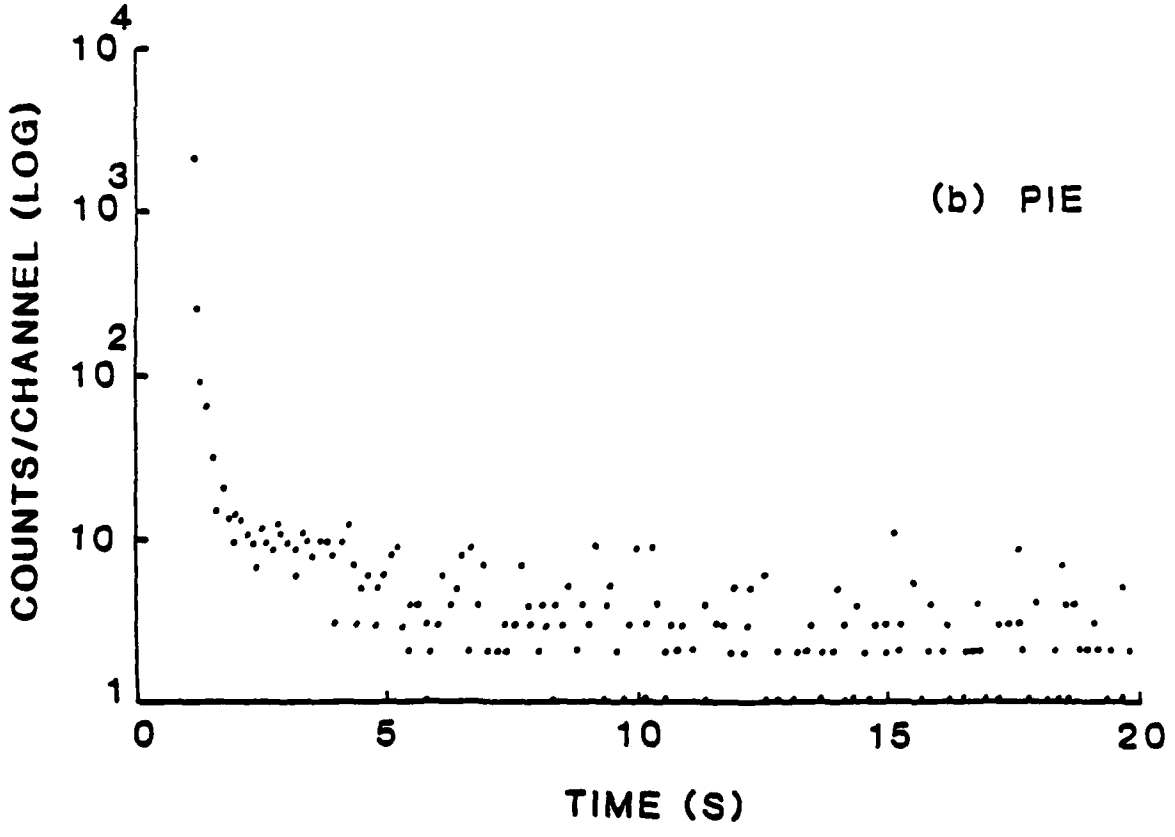

Fig 6

PETN (IMPACT)

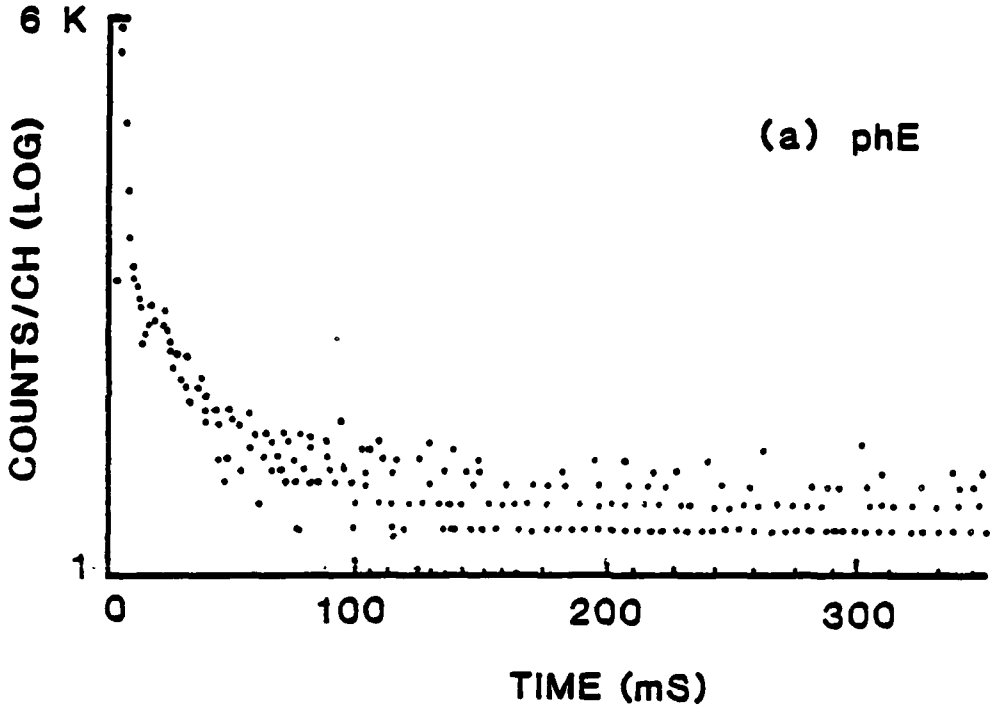

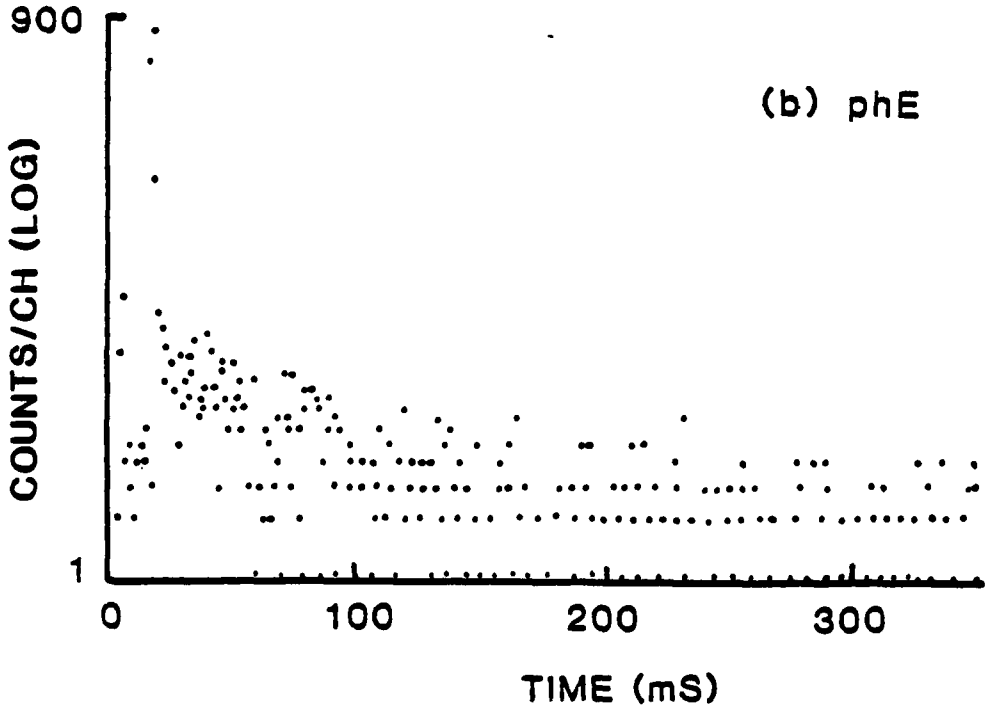

Fig 7

PETN (IMPACT)

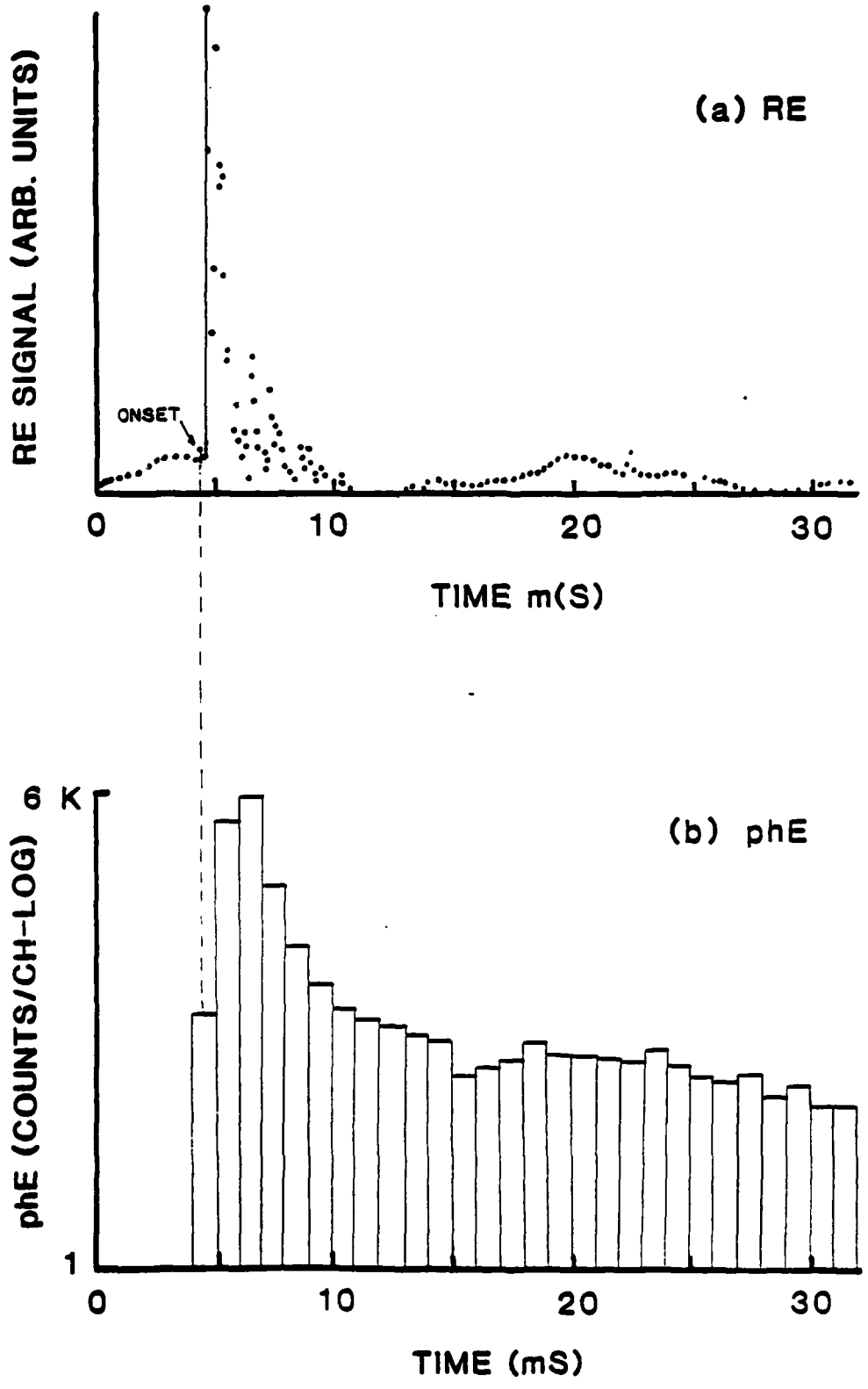
RE SIGNAL (ARB. UNITS)
(a) RE
ONSET
0
10
20
30
TIME m(S)
phE (COUNTS/CH-LOG)
6 K
1
(b) phE
0
10
20
30
TIME (mS)

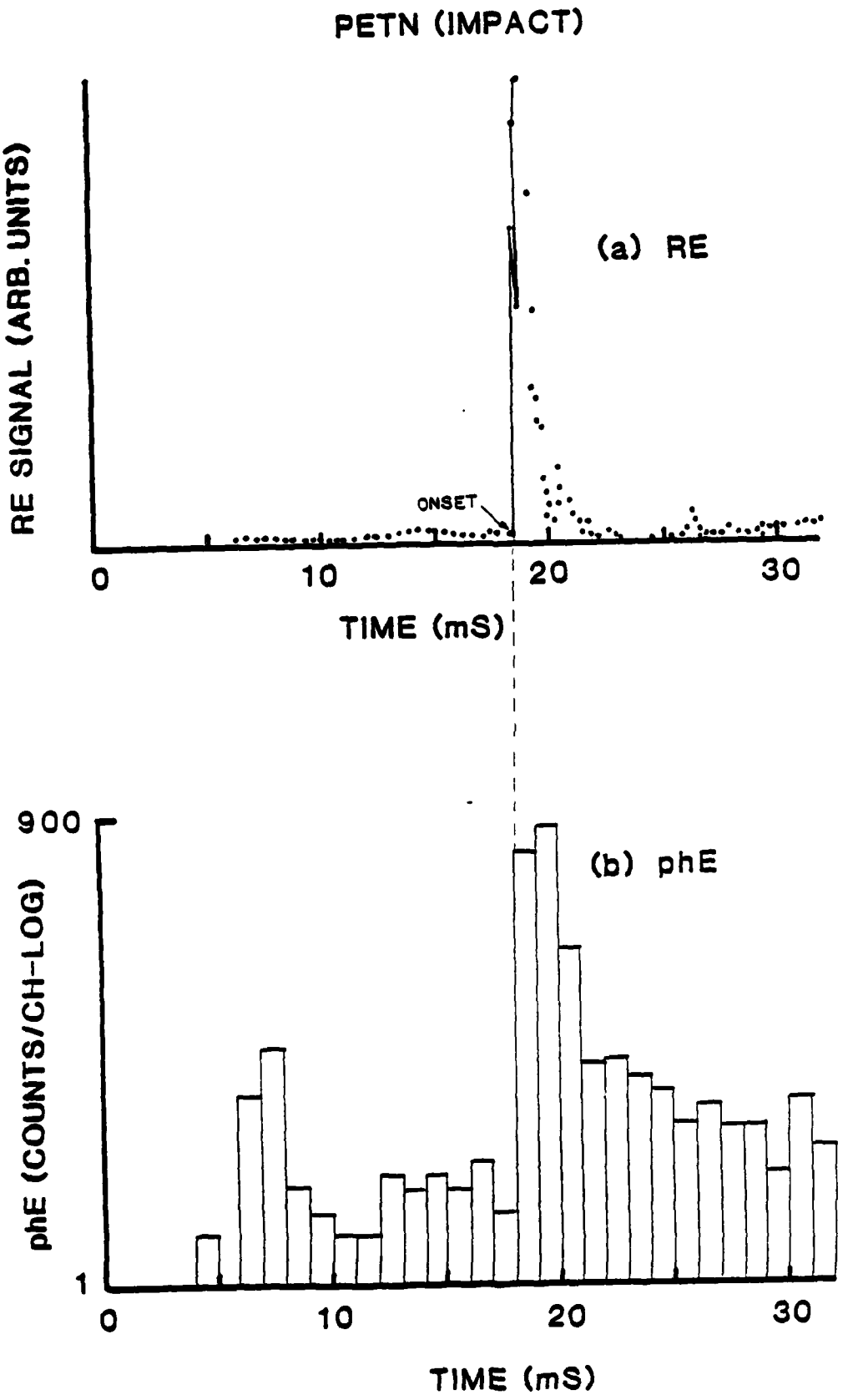
PETN (IMPACT)
RE SIGNAL (ARB. UNITS)
(a) RE
ONSET
0
10
20
30
TIME (mS)
900
1
phE (COUNTS/CH-LOG)
(b) phE
0
10
20
30
TIME (mS)

Fig 9

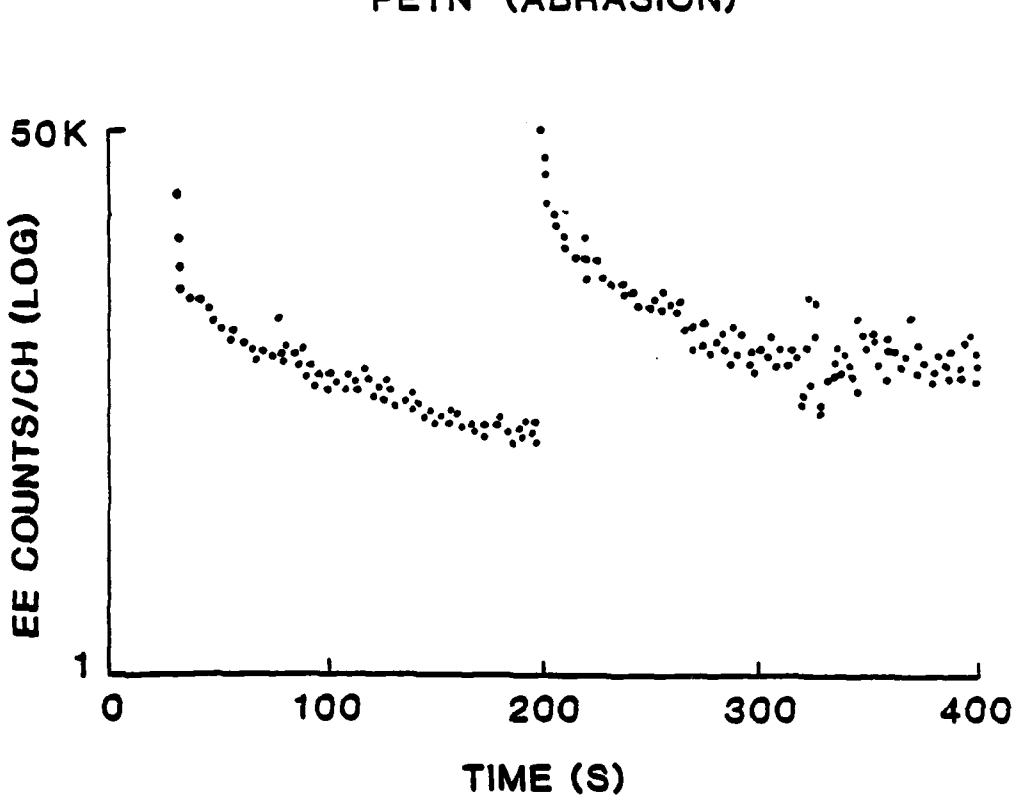

Fig 10

V. ELECTRICAL BREAKDOWN INDUCED BY FRACTO-EMISSION

M. L. Klakken, J. T. Dickinson, and L. C. Jensen
Department of Physics
Washington State University
Pullman, WA. 99164-2814

ABSTRACT

Fracto-emission is the emission of particles (e.g. electrons, ions, neutral species and photons) during and following fracture. In this study, we investigate the possibility that fracture can induce electrical breakdown in air at atmospheric pressure. Fracture of a number of materials were found to induce electrical breakdown including quartz, sapphire, alumina, boron nitride, PZT, glass-filled polybutadiene and alumina-filled epoxy. These measurements indicate that fracturing induces electrical breakdown due to the emission of charged particles from the fracture which once released from the fracture area, become available for normal breakdown phenomena.

I. INTRODUCTION

Emission of particles (electrons, positive and negative ions, neutral species and photons) is known to occur when certain materials are fractured in vacuum[1-4]. This emission is collectively known as fracto-emission (FE). FE has been observed from a number of insulating materials such as alumina-filled epoxy, polybutadiene, polyisoprene, quartz, and mica, as well as from failure of pressure-sensitive adhesives.

Recently[3,4] we have presented a model for the charged particle emission accompanying fracture which explains a wide range of FE characteristics and dependences on materials, temperature, etc. A brief summary of this model is presented here. As a crack propagates in vacuum, liberated fragments and/or desorbed volatiles will raise the pressure between the newly formed surfaces. Charge concentrations on the newly formed surfaces may also occur in a wide range of materials due to a variety of charge separation mechanisms. This can produce an intense electric field between the surfaces, which can cause a gaseous discharge in the crack tip. Evidence of this discharge for samples fractured in vacuum include the observation of bursts of photons and radio wave emission during fracture[3]. This micro-discharge produces charged particles (electrons, positive and negative ions) which tend to follow the electric field lines, thus bombarding the newly formed surfaces. This particle bombardment creates a non-

equilibrium electron energy distribution in these surfaces, e.g. electrons in high lying traps which can then undergo thermally stimulated migration and subsequent recombination with holes. Such a recombination can yield an emitted electron (thermally stimulated electron emission - TSEE[5]) or a photon (thermally stimulated luminescence - TSL[6]) from the fracture surface. A portion of the electron emission can strike an adjacent charge patch which would yield positive ion emission and excited neutral emission via an electron stimulated desorption mechanism[7]. Thus, during and following fracture, a number of FE components are being emitted into the region near the crack.

Imagine that such fracture induced products (electrons, ions and excited neutral species) are released from a crack in the vicinity of a high voltage gap in air, which represents one of the electrode configurations studied here. The region is filled with gas molecules and a localized electric field exists. The possibility of these particles leading to the "avalanche effect"[8-11] is quite likely if both the number of charged particles released and the electric field strength are sufficiently high and the field geometry relative to the crack is suitable. In our case, when the result of the fracture was an arc or spark across the electrodes, we referred to the consequence as a gaseous electrical breakdown.

Another type of electrode arrangement of interest here involves electrodes attached to the sample such that when the

sample is broken, the fracture surface might itself be a conduction path and could participate in the breakdown. Thus, events occurring in the nearby air plus events on the fracture surface (e.g. a sudden increase in free or weakly bound electrons) might in combination lead to breakdown, which we shall call surface electrical breakdown. In this paper, we will examine the resulting breakdown for these two electrode arrangements due to fracture.

II. EXPERIMENTAL

The measurements described here were performed on materials fractured in air. For the gaseous electrical breakdown measurements, the sample was fractured in tension or in a three-point bending mode (see Fig. 1). In addition, the consequences of adhesive failure involving the peeling of 3M Magic Transparent tape from a polymethylmethacrylate (PMMA) surface was also studied. For the gaseous breakdown studies, the electrodes consisted of a wire sharpened to a point (radius of curvature approx. 0.15 mm) positioned over a thin circular aluminum disk, 2.5 cm in diameter. The electrodes were positioned so that the pointed electrode was about 5 mm from the region where the sample would fail. For tensile samples this location was directly opposite a notch placed in the sample. For the three-point bending specimens, the pointed electrode was positioned 3 mm from the front surface

placed in tension. In the case of peeling tape from PMMA, the pointed electrode was positioned 2 mm from the edge of the tape-PMMA interface. For all the samples, the gap was adjusted so that the top and bottom electrodes were above and below the sample, respectively.

The gap of the electrodes for the gaseous experiment was typically 1 mm. After the electrodes were in position, the high voltage was slowly raised until a self-sustaining electrical breakdown occurred and then the high voltage was lowered by approximately 10 volts. At this point, any injection of a significant amount of charge would cause breakdown. Occasionally, spontaneous breakdown would occur (presumably due to background radiation) without the sample being broken. Thus, if spontaneous breakdown did occur before breaking the sample, we were assured that the applied voltage was indeed adequate so that injection of charge from a nearby fracture would lead to breakdown which would be correlated in time with the fracture event.

The variables measured were the current through the gap and the stress applied to the sample, both as a function of time. The electrical circuit for the current measurement is shown in Fig. 2. The purpose of the 2.2 M resistor was to limit the current during breakdown to approximately 1 mA. The 43 k resistor provides a voltage directly proportional to the current through the gap. This voltage was digitized using a LeCroy 8212 Data Logger and stored on a disk. The applied

stress was measured using a load cell, Sensotec Model 11. The cell's output was amplified and also digitized.

Acoustic emission (AE) from the fracture/breakdown event was used for the stop pulse needed for the digitizer. AE was detected using an acoustic transducer, A.E.T. Model AC175L, which was attached to the fracture device holding the sample, approximately 4 cm from the sample. The output from the AE transducer was amplified and discriminated to provide a stop pulse at fracture.

The surface breakdown experiment measured the same two variables, applied stress and current, in the same manner as the gaseous breakdown experiment. However, the electrodes in this case differed in that they were applied directly onto the sample so that one fracture surface was between them (see Fig. 1). Silver paint (GC Electronics) was used for the electrode material and the sample was carefully notched so it would fracture in the desired location. The voltage was applied to the electrodes prior to fracture in the same manner as in the gaseous experiment.

The samples used in these studies included single crystal quartz, single crystal sapphire, polycrystalline alumina, polycrystalline boron nitride, polycrystalline PZT (lead zirconate titanate), the elastomer polybutadiene (BR) filled with glass beads, alumina-filled epoxy and 3M Magic Transparent tape attached to PMMA. The quartz samples were cut in the shape of a disk with a diameter of 6.5 mm and

thickness of 1.2 mm. The face of the disk was the (-2,1,1,0) plane and when fractured, the fracture surfaces tended to be perpendicular to the face. The sapphire samples, which had a rectangular shape, was of unknown orientation and had an average cross-sectional area of 35 mm^2. The polycrystalline PZT samples, which were also rectangular in shape, were polarized in the direction perpendicular to the applied stress (three-point bend) direction such that the fracture was perpendicular to the direction of the aligned electric dipoles. In studies currently in progress, this yields considerably more charged particle emission than unpolarized PZT. The average cross-sectional area of the PZT samples were 50 mm^2. The BR contained approximately 34% by volume small glass beads, about 50 m in diameter. These samples had a cross-sectional area of approximately 15 mm^2; they were notched in the center and broken in tension. Again, the filled BR was found to be an intense FE emitter, due to the charge separation at the glass-polymer interface[3]. The alumina-filled epoxy consisted of one part by weight EPON 828 (Z-hardener) epoxy to three parts of irregularly-shaped alumina particles with an average diameter of 10 m. The average cross-sectional area of the alumina-filled samples were 25 mm^2; they were also notched in the center and broken in tension. Filled epoxy fracture exhibits considerable interfacial failure and intense FE[3,4]. The tape was simply pressed on a PMMA surface and peeled from the surface in a U-

peel mode. The charge separation and intense FE from such a system has been well documented[1].

III. RESULTS

All the materials mentioned above were found to induce breakdown upon fracture. In the diagrams described below, the arrow on the time axis of the current data indicates the time that breakdown occurred and the arrow in the stress data represents the point where complete failure occurred, i.e. when the stress showed a sudden release. Figures 3-7 show results obtained from the fracture of five inorganic materials: quartz, sapphire, alumina, boron nitride and PZT, all fractured in a three-point bending mode. Breakdown occurred at the following approximate times relative to failure for these particular samples:

quartz	-Ø.2 ms
sapphire	12Ø ms
alumina	75 ms
boron nitride	26 ms
PZT	-Ø.16 ms

where the minus sign indicates that the burst of current between the electrodes occurred prior to catastrophic failure. Although the times varied somewhat for a given material, the values shown are typical.

Figure 8 represents a typical gaseous breakdown result

for a filled-epoxy sample. The sample was broken in tension with the pointed electrode approximately 5 mm from the crack. Breakdown occurred only after the sample was broken and the time lag between failure and breakdown was approximately 7.5 ms. Also note that two bursts of current were observed approximately 3.5 ms apart, suggesting a modulation of the amount of charge being transported to the high voltage gap.

Not every fracture event caused breakdown. In general, those materials that produced intense electron and positive ion emission in vacuum were more reliable producers of breakdown in air. In the case of the filled-epoxy samples, we found a relationship between the spatial positioning of the fracture path relative to the high voltage electrodes and the probability of breakdown. Three types of fracture paths are shown in Fig. 9. If the sample broke along paths B or C, we observed no breakdown. But if the sample broke along path A, breakdown occurred each time and the time lag between fracture and breakdown depended on the departure from a straight crack (path B), which is the distance between points A and B. We shall denote this distance as AB. Fig. 10 shows the time intervals of the current due to breakdown relative to the stress release (for the sample with AB=0.8 mm and AB=0.3 mm) for two different path differences. For AB=0.3 mm, there is a 13 ms time delay and for AB=0.8 mm, there is an 8 ms time delay. Not shown was a sample where AB=2 mm that yielded a time delay of approximately 110 ms.

Results for the peeling of Magic Tape from PMMA and the fracture of BR filled with glass beads are shown in Figures 11 and 12. The peeling of tape showed a time lag of approximately 5.5 ms between the onset of peeling and breakdown. BR was seen to induce breakdown approximately 330 ms after the onset of sample failure. Since BR is an elastomer, the much slower crack velocity resulted in a considerably longer time interval between the onset of failure and completion (i.e. separation of the surfaces), approximately 100 ms.

Results for the breakdown which occurred with the electrodes attached to the surfaces of the sample are shown in Figure 13, where the material was alumina filled-epoxy fractured in tension. Breakdown occurred 1.5 ms after break for this sample but other time intervals were also observed ranging from the instant of the break to 2 ms. A small increase in current, seen here at approximately 0.3 ms after catastrophic failure or 1.2 ms before the breakdown, was often observed. In all cases this precursor current appeared approximately 0.3 ms after failure. The maximum current in this time interval was approximately 10 A.

IV. DISCUSSION

In the two electrode configurations illustrated here, breakdown was found to be induced by fracture. The gaseous

breakdown for the filled-epoxy samples seemed to depend largely upon the location of the pointed electrode relative to the crack path. This result indicates that the charged particles available for inducing breakdown leave these particular samples in an asymmetric fashion, suggesting a distribution that has a maximum at approximately 130 degrees, shown in Fig. 9 as the angle . Such an asymmetry in the distribution pattern might be due to the fact that these samples were not stressed in pure tension due to constraints of the clamps holding the sample. Thus, the fracture did involve some slight twisting motion which may have led to an assymetric emission pattern.

For a number of trials, quartz and PZT showed breakdown slightly before the instant of failure. These particular samples showed considerable FE intensity when fractured in vacuum with occasional charged particle emission (of lower intensity) prior to catastrophic failure. We attribute this emission to micro-cracking (crack formation). This in turn yields sufficient charged particle emission prior to failure to cause breakdown.

Sapphire and alumina samples produced breakdown approximately 40% of the time, small compared to the other materials tested. These Al_2O_3 samples were quite small in cross section and since FE intensities decrease with decreasing surface area[3], we suspect we were not producing sufficient charge intensity to induce breakdown for every

fracture.

The experiments using the electrodes attached directly to the alumina-filled epoxy yielded a small burst of current at approximately 0.3 ms after fracture followed by breakdown approximately 1 ms later. We considered a number of possible explanations, including: (1) changes in capacitance due to the formation of the air gap, (2) changes in polarization in the dielectric due to changing fields during and after fracture, (3) changes in the electric displacement vector due to the creation of fringing fields at the crack edges, (4) possible changes in the applied voltage due to the response of the high voltage supply, and finally (5) an actual surface current due to free charge carriers produced by fracture. All but the last possibility were shown to be in the wrong direction and/or would occur at times much faster than observed. For a current to occur as observed, it would require discrete charge distributions at some distance from the electrodes moving under the influence of the applied field. Obviously, if this response is a surface current it is not leading to a surface avalanche current. Instead we observe breakdown at 1.5 ms after fracture. We suggest that the breakdown observed is in fact just another instance of gaseous breakdown. The 1 ms delay in breakdown may be due to turbulence in the gap sweeping out charge from the region between the electrodes. As these air currents damp down additional emission from the surface might then be able to induce breakdown.

V. CONCLUSIONS

We have shown that for two electrode configurations supporting high voltage, fracture can indeed induce gaseous electrical breakdown. The likely mechanism involves the release of charged particles created by fracture (components of fracto-emission) which subsequently contributes to an avalanche in the voltage gap. The time relations between dynamic crack propagation (catastrophic failure) and breakdown indicate that charge mobility in the gases in and near the crack is critically involved. In the case of quartz and PZT, crack formation (micro-cracking) prior to failure apparently emitted enough FE to induce breakdown before failure. No evidence of a complete electrical breakdown across the fracture surface of the filled epoxy was observed but rather a gaseous breakdown occurred approximately 1 ms after fracture.

VI. ACKNOWLEDGEMENTS

This work was supported by the National Science Foundation (Ceramics) Grant No. DMR-8210406, Sandia National Laboratory, the Office of Naval Research under Contract N00014-80-C-0213, and the M. J. Murdock Charitable Trust. We would also like to thank Dr. A. N. Gent, University of Akron Institute of Polymer Science for supplying the polybutadiene samples and Dr. W. D. Williams of Sandia National Laboratory

for supplying the PZT and epoxy-filled alumina samples.

REFERENCES

1) J. T. Dickinson, M. K. Park, E. E. Donaldson and L. C. Jensen, J. Vac. Sci. Technol. 20, 436 (1982).

2) J. T. Dickinson, E. E. Donaldson and M. K. Park, J. Mat. Sci. 16, 2897 (1981).

3) J. T. Dickinson, L. C. Jensen and A. Jahan-Latibari, J. Vac. Sci. and Technol., to be published.

4) J. T. Dickinson, in Adhesive Chemistry--Developments and Trends, ed. by L. H. Lee (Plenum Publishers, New York), to be published.

5) H. Glaefeke, in Thermally Stimulated Relaxation in Solids, ed. by P. Braunlich (Springer Verlag, Berlin, 1979), pp. 229.

6) R. Chen and Y. Kirsh, Analysis of Thermally Stimulated Processes (Pergamon Press, Oxford, 1981), pp.48-52.

7) M. L. Knotek and P. J. Feibelman, Phys. Rev. Lett. 40, 964 (1978).

8) A. von Engel, in Ionized Gases (Clarendon Press, Oxford, 1955), pp. 147-180.

9) A. M. Howatson, in An Introduction to Gas Discharges (Pergamon Press, Oxford, 1965), pp. 51-83.

10) J. Millman and S. Seely, in Electronics (Maple Press, McGraw-Hill, 1941), pp. 288-299.

11) R. Papoular, in Electrical Phenomena in Gases (Butler and Tanner, American Elsevier, 1965), pp. 100-122.

FIGURE CAPTIONS

Fig. 1. Diagrams of two different breaking mechanisms, three-point bend (top) and tensional (middle), and two different electrode configurations, gaseous (the top two) and surface (bottom).

Fig. 2. The electrical circuit used to measure the current during gaseous breakdown.

Fig. 3. Gaseous breakdown current and applied stress versus time for a quartz sample fractured in a three-point bending apparatus. Note the time interval between the breakdown groups.

Fig. 4. Gaseous breakdown current and applied stress versus time for a sapphire sample fractured in a three-point bending apparatus.

Fig. 5. Gaseous breakdown current and applied stress versus time for an alumina sample fractured in a three-point bending apparatus. When viewed on a faster time scale, the breakdown current pulse was typically 0.4 ms in duration.

Fig. 6. Gaseous breakdown current and applied stress versus time for a boron nitride sample fractured in a three-point bending apparatus.

Fig. 7. Gaseous breakdown current and applied stress versus time for a PZT sample fractured in a three-point bending apparatus.

Fig. 8. Gaseous breakdown current and applied stress, both a function of time, for an alumina-filled epoxy sample that was fractured in tension. Note the time interval between the two breakdown groups.

Fig. 9. A diagram of an alumina-filled epoxy sample showing the different break paths relative to the electrodes and the motion of the sample during fra ture.

Fig. 10. The gaseous breakdown current for two different break paths and applied stress, all as a function of time. The top graph is for a path difference of 0.8 mm and the middle graph is for a 0.3 mm path difference. Both samples were alumina-filled epoxy.

AD-A144 149 FRACTO-EMISSION FROM POLYMERS(U) WASHINGTON STATE UNIV 2/2
PULLMAN DEPT OF PHYSICS J T DICKINSON 15 JUL 84
N00014-80-C-0213

UNCLASSIFIED F/G 11/9 NL

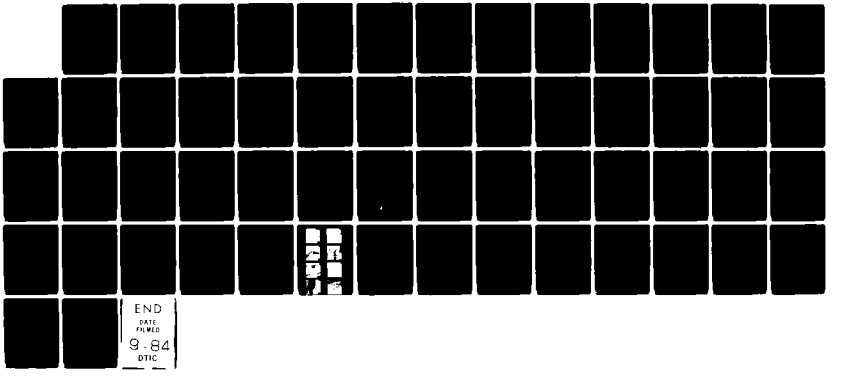

END
DATE FILMED
9-84
DTIC

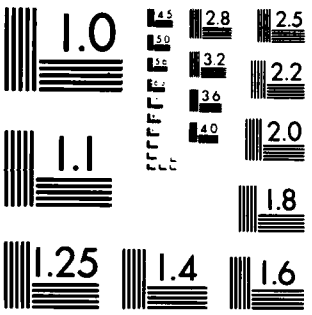

Fig. 11. Gaseous breakdown current and applied stress versus time for tape being peeled from PMMA.

Fig. 12. Gaseous breakdown current and applied stress versus time for a BR sample fractured in tension. The long time interval was attributed to the long time interval for complete failure.

Fig. 13. The breakdown current and applied stress versus time for the surface breakdown experiment. Note the small "bump" in the current before breakdown but after complete failure.

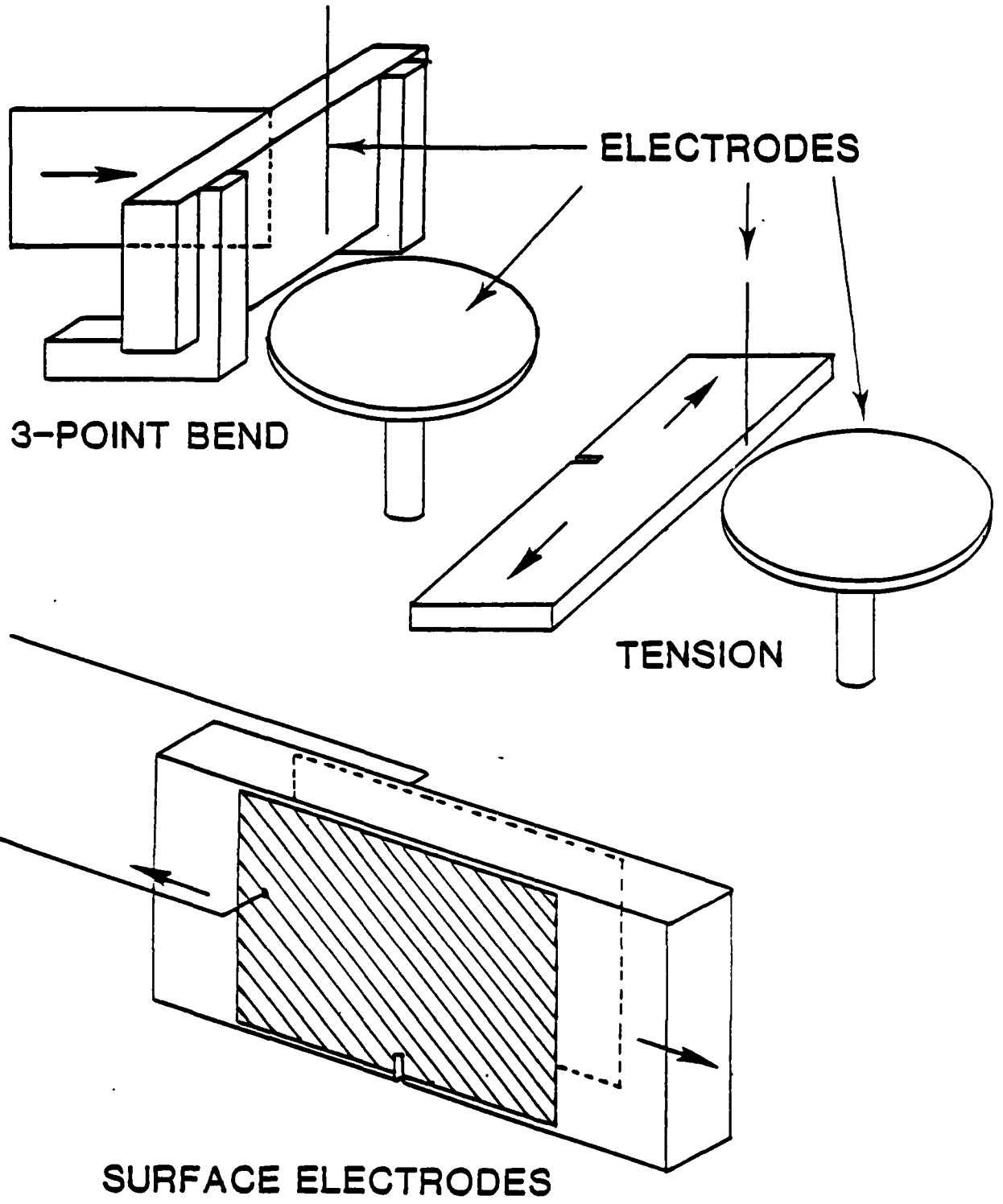

Fig. 1

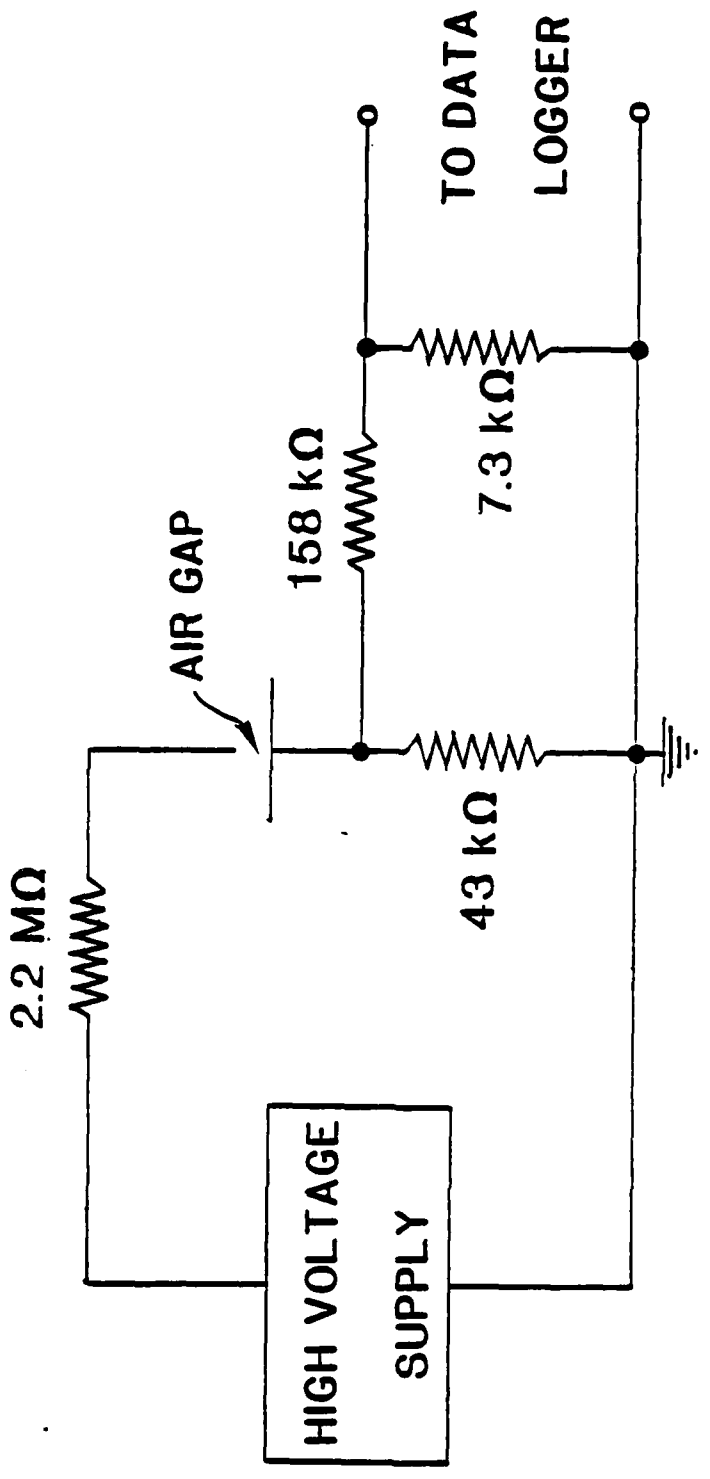
TO DATA
LOGGER
7.3 kΩ
158 kΩ
AIR GAP
43 kΩ
2.2 MΩ
HIGH VOLTAGE
SUPPLY

g. 2

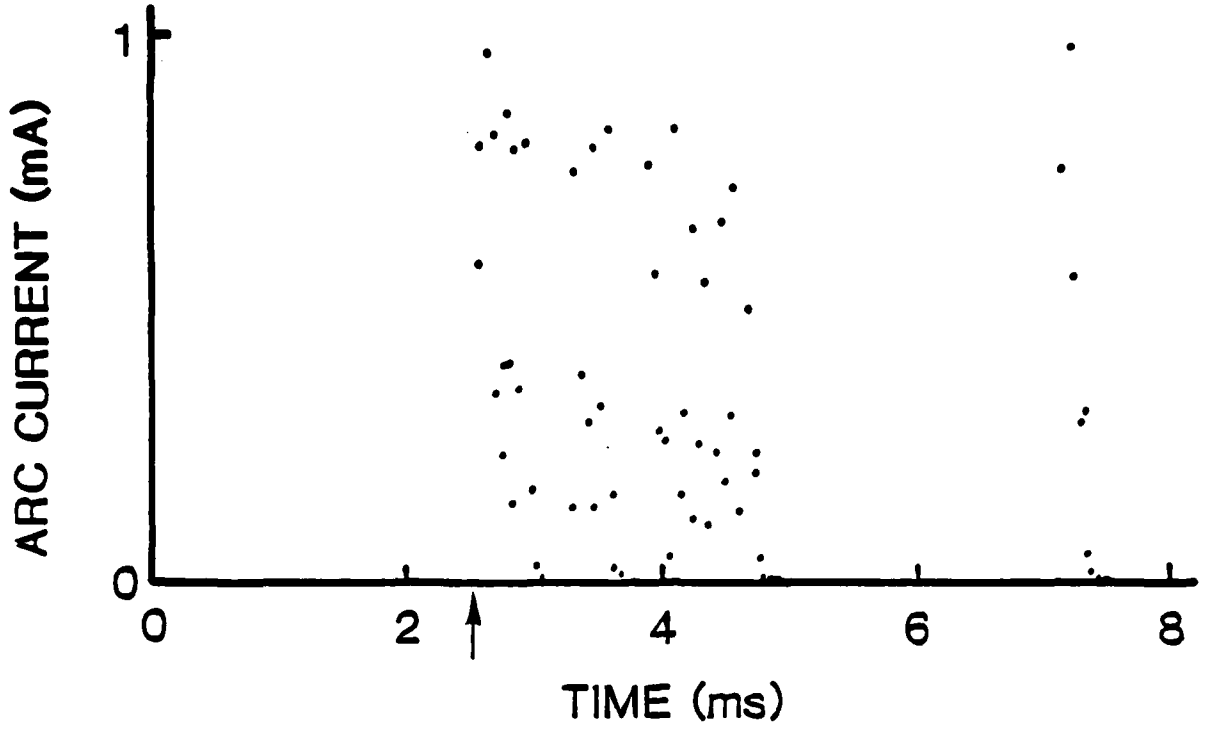
ARC CURRENT (mA)
1
0
0
2
4
6
8
TIME (ms)

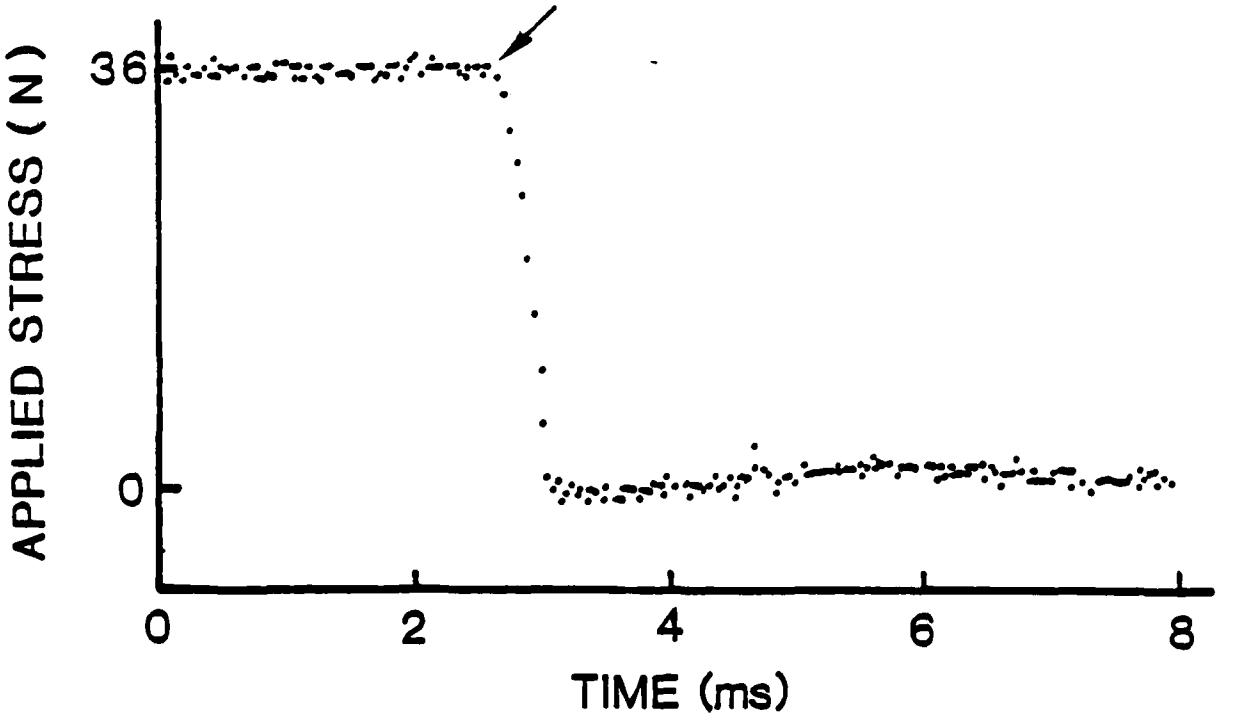
APPLIED STRESS (N)
36
0
0
2
4
6
8
TIME (ms)

Fig. 3

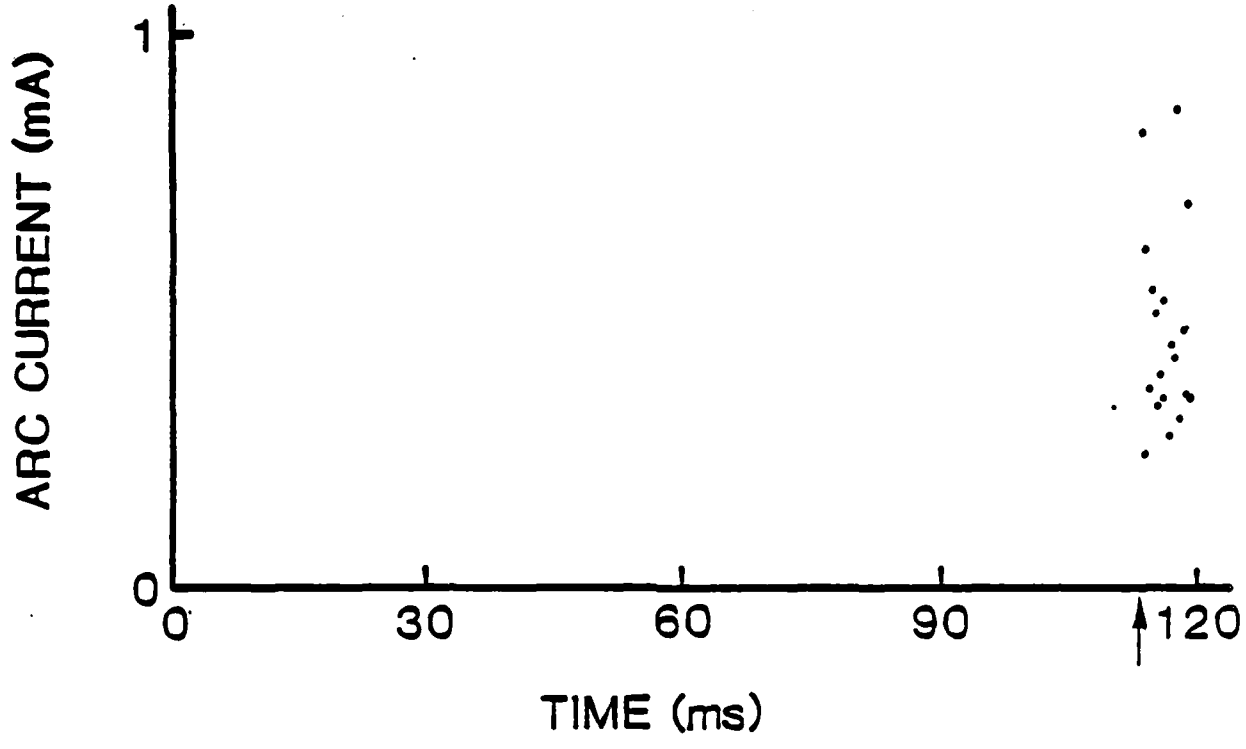
ARC CURRENT (mA)
1
0
0
30
60
90
120
TIME (ms)

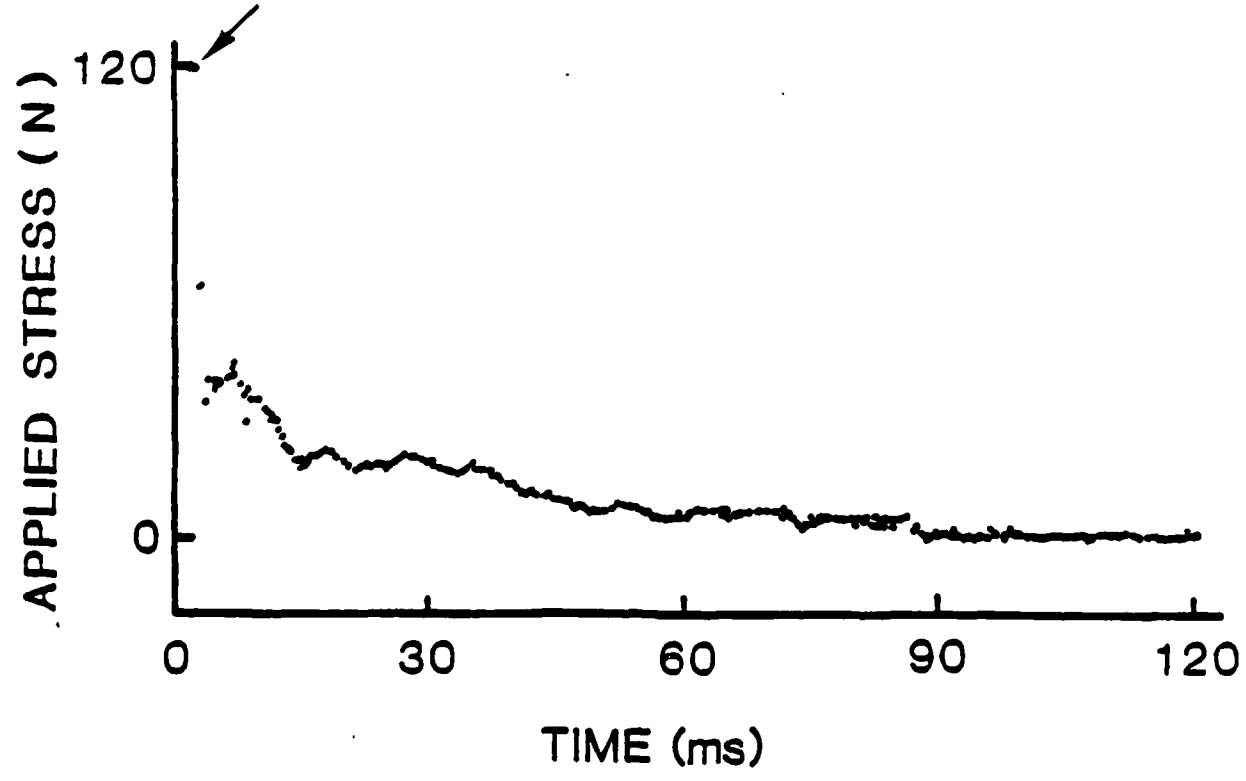
APPLIED STRESS (N)
120
0
0
30
60
90
120
TIME (ms)

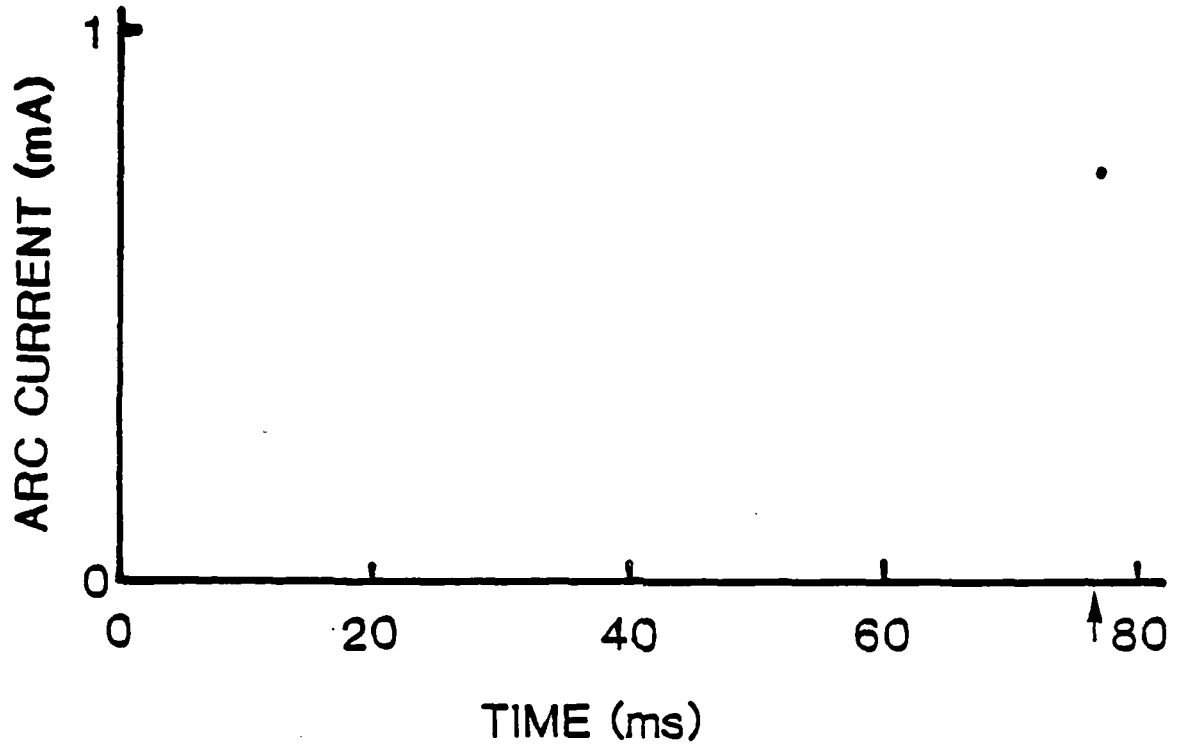
ARC CURRENT (mA)
1
0
0
20
40
60
80
TIME (ms)

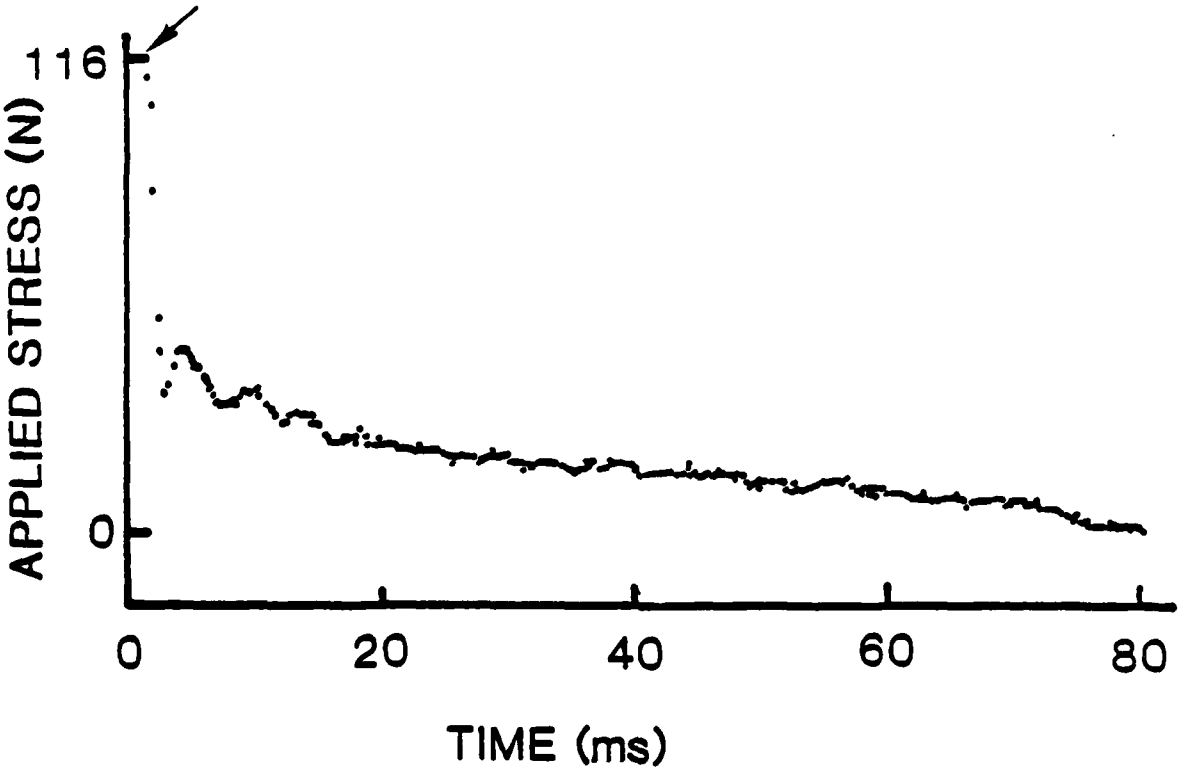
APPLIED STRESS (N)
116
0
0
20
40
60
80
TIME (ms)

Fig 5

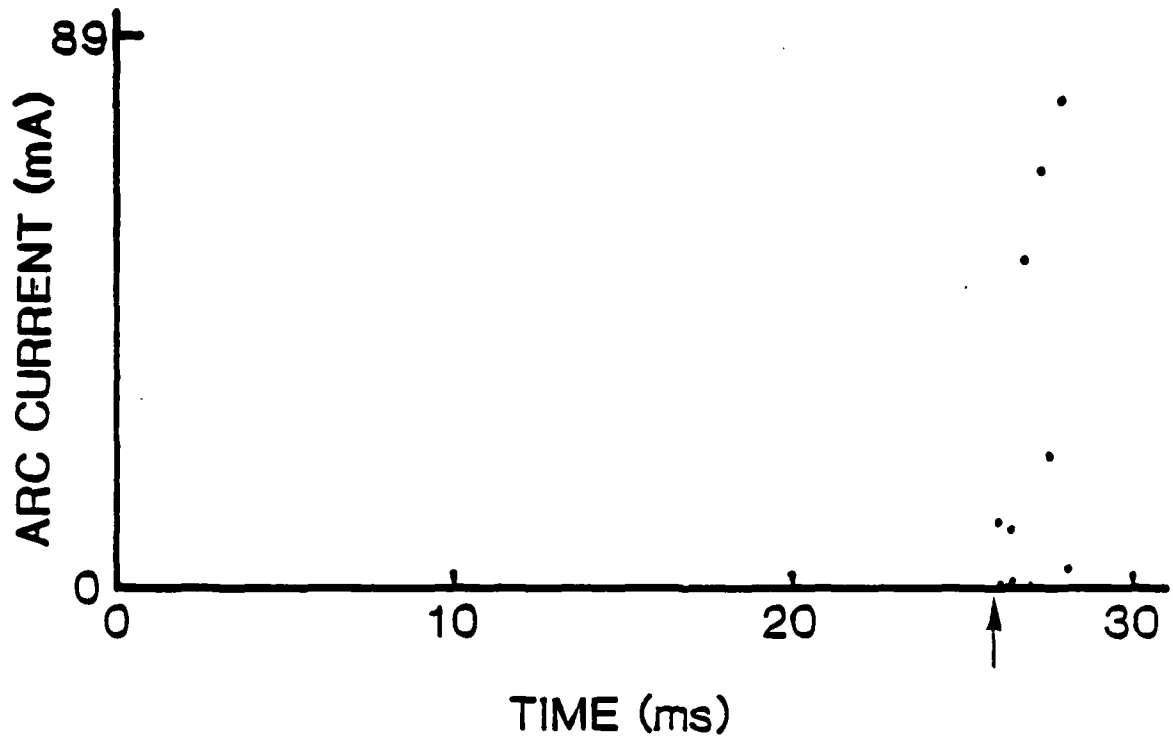
89
ARC CURRENT (mA)
0
0
10
20
30
TIME (ms)

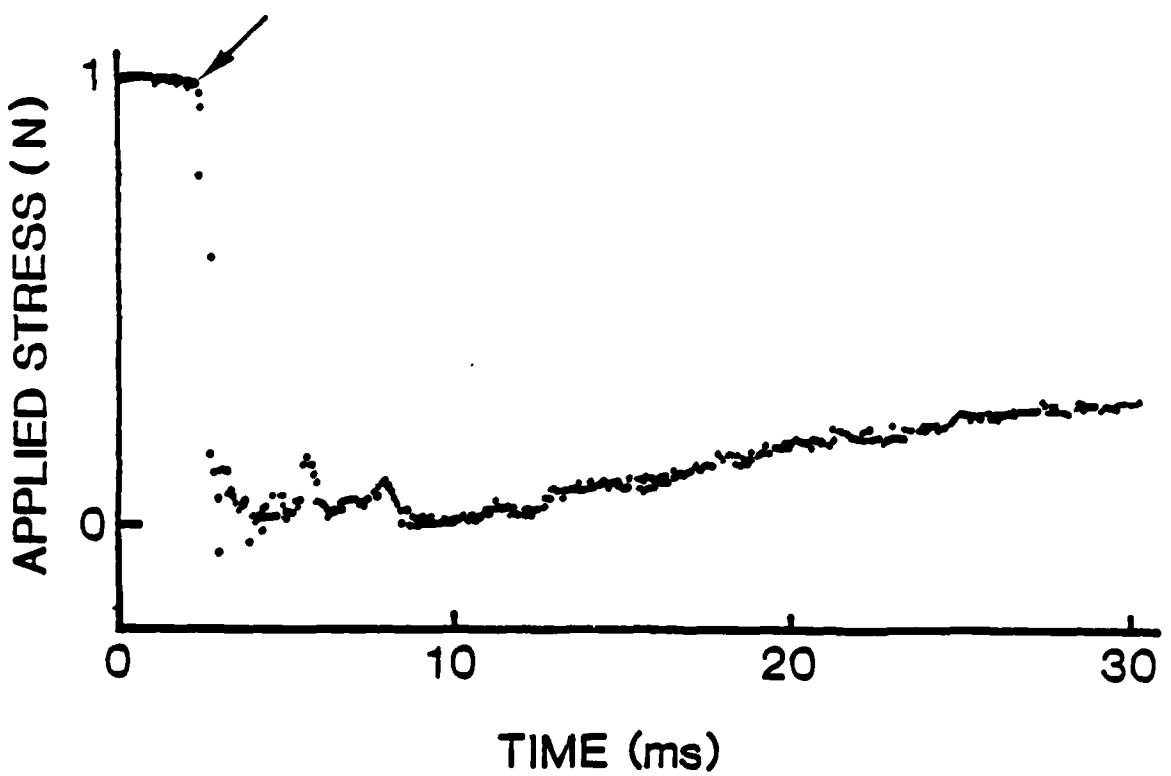
1
APPLIED STRESS (N)
0
0
10
20
30
TIME (ms)

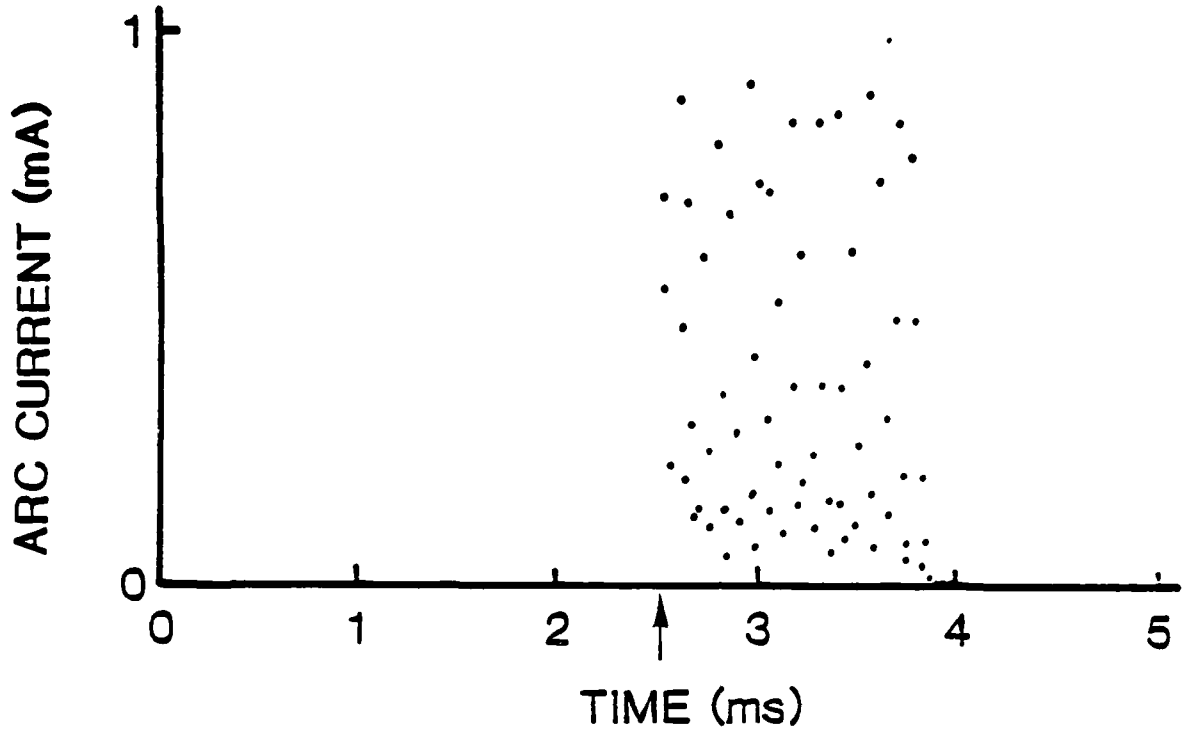
ARC CURRENT (mA)
1
0
0
1
2
3
4
5
TIME (ms)

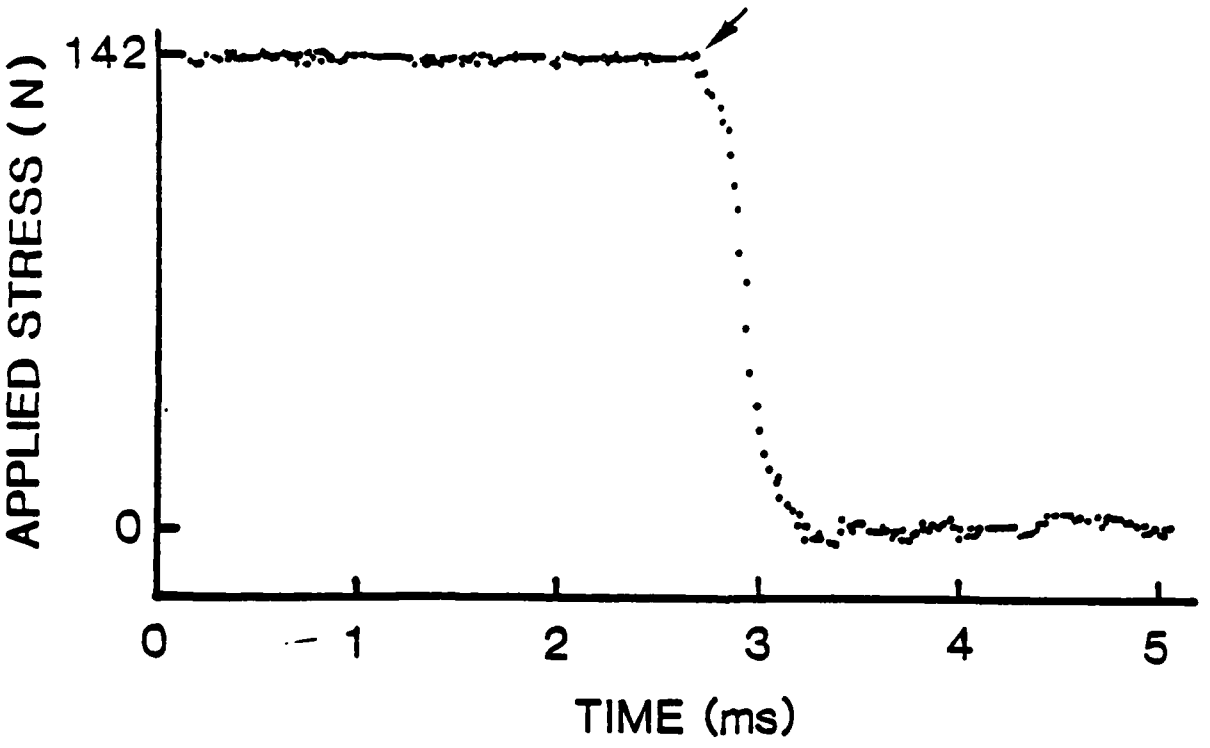
APPLIED STRESS (N)
142
0
0
1
2
3
4
5
TIME (ms)

Fig. 7

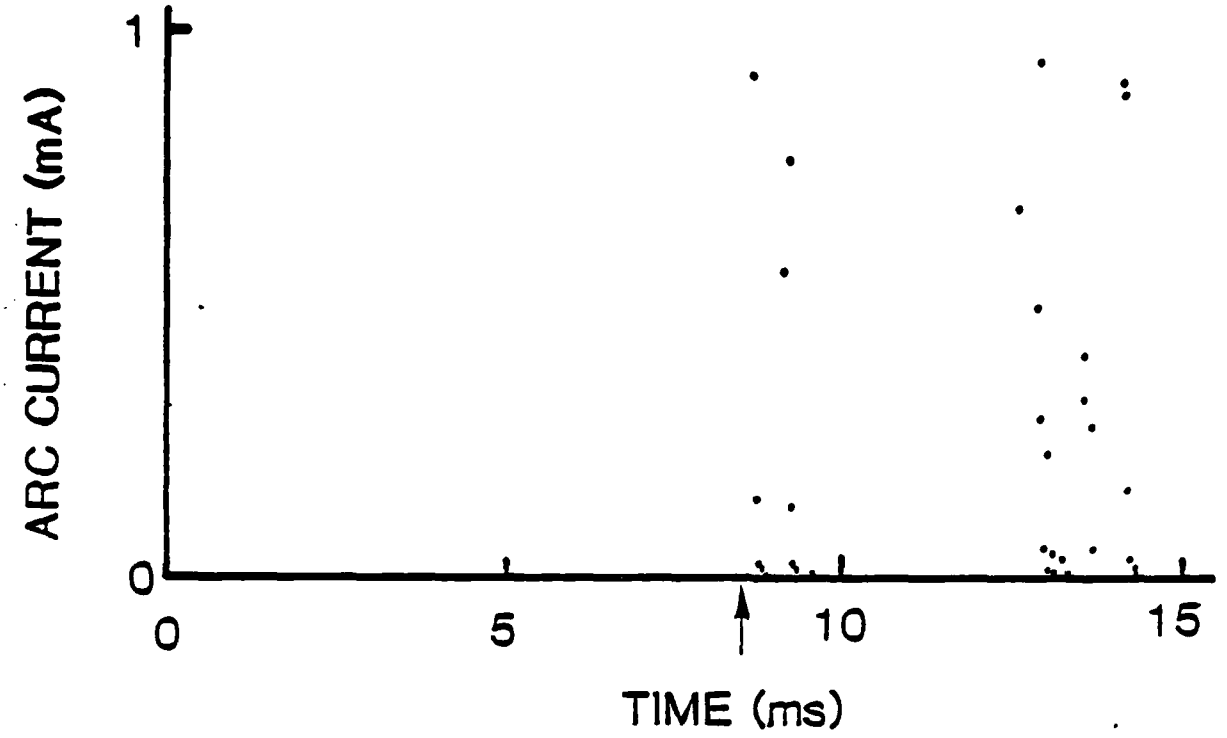
ARC CURRENT (mA)
1
0
0
5
10
15
TIME (ms)

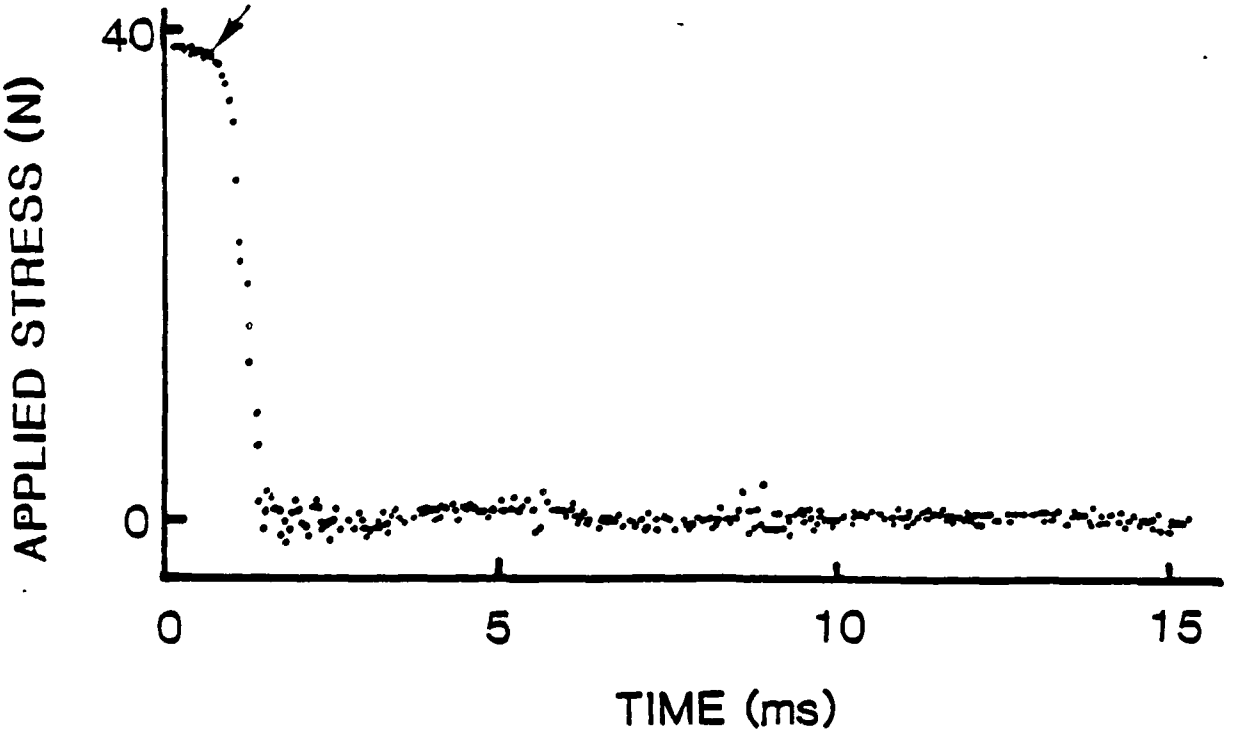
APPLIED STRESS (N)
40
0
0
5
10
15
TIME (ms)

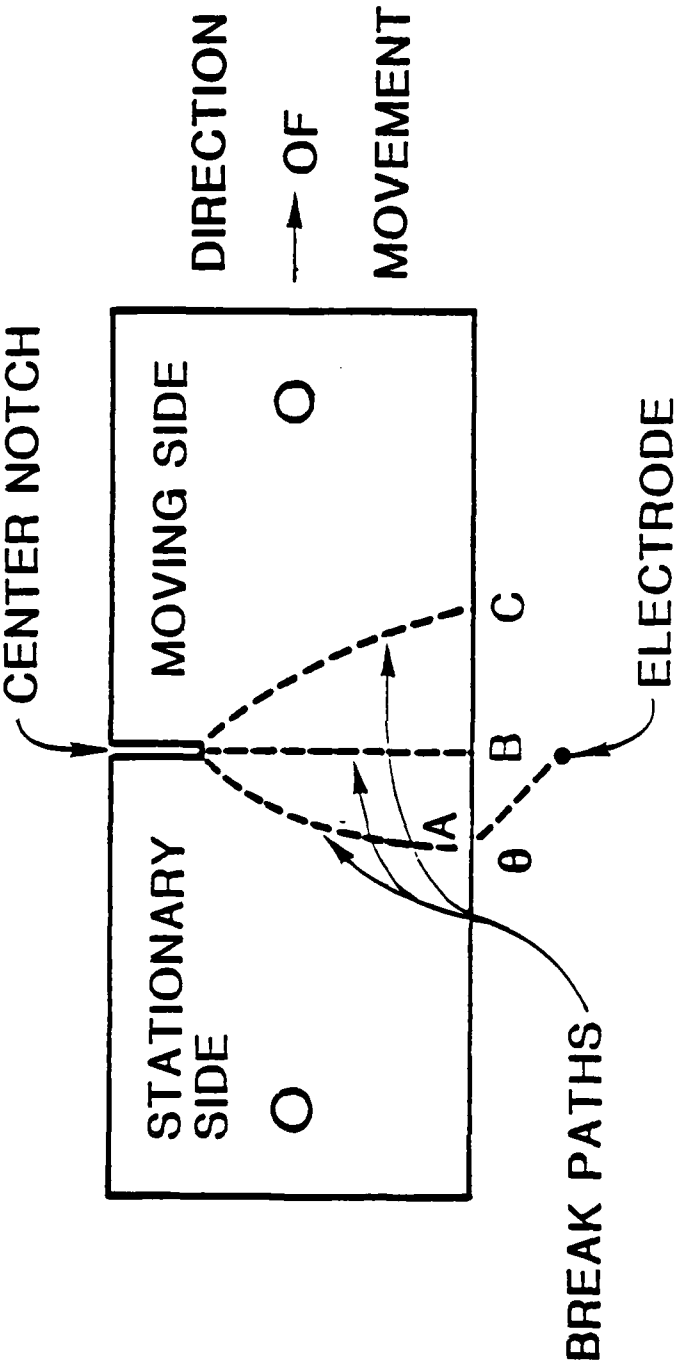
DIRECTION
OF
MOVEMENT
CENTER NOTCH
MOVING SIDE
STATIONARY
SIDE
A
B
C
θ
ELECTRODE
BREAK PATHS

Fig. 9

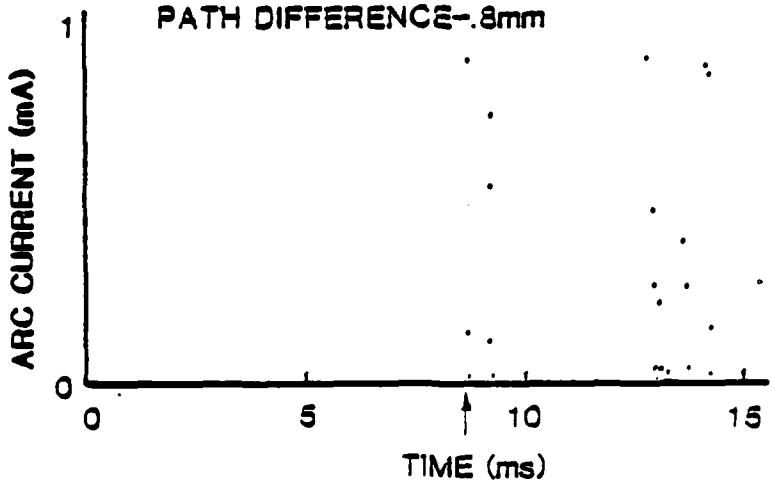
PATH DIFFERENCE-.8mm
ARC CURRENT (mA)
1
0
0
5
10
15
TIME (ms)

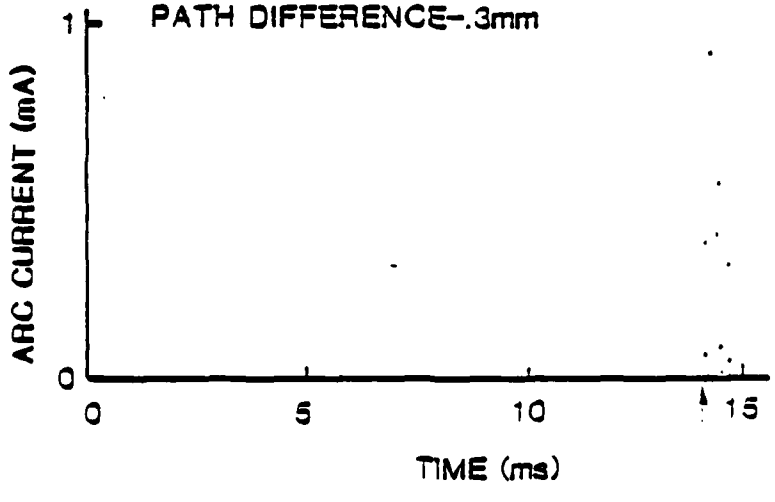
PATH DIFFERENCE-.3mm
ARC CURRENT (mA)
1
0
0
5
10
15
TIME (ms)

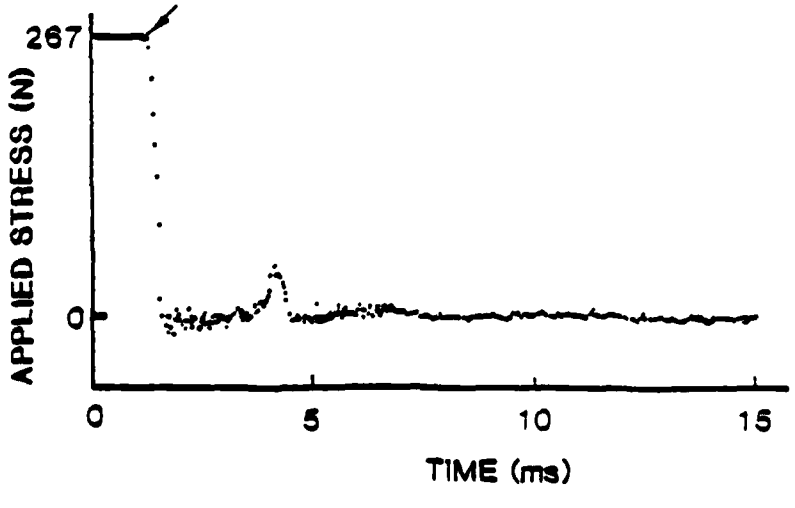
APPLIED STRESS (N)
267
0
0
5
10
15
TIME (ms)

Fig. 10

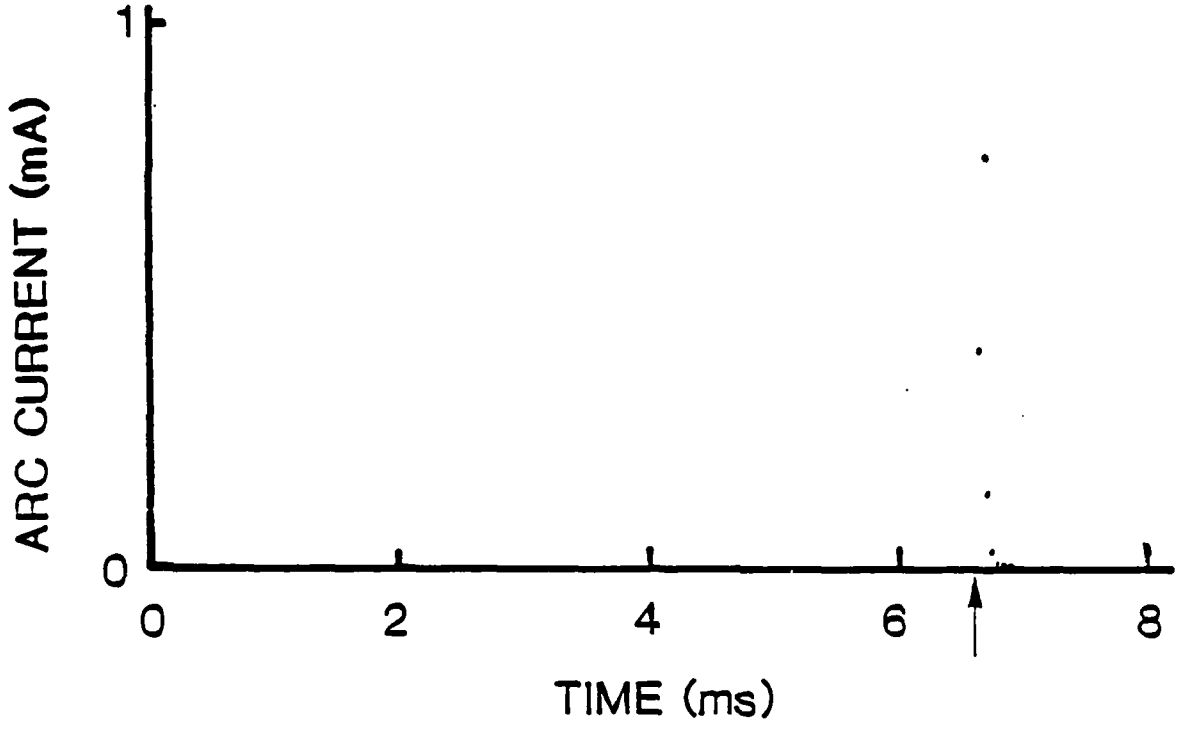
ARC CURRENT (mA)
1
0
0
2
4
6
8
TIME (ms)

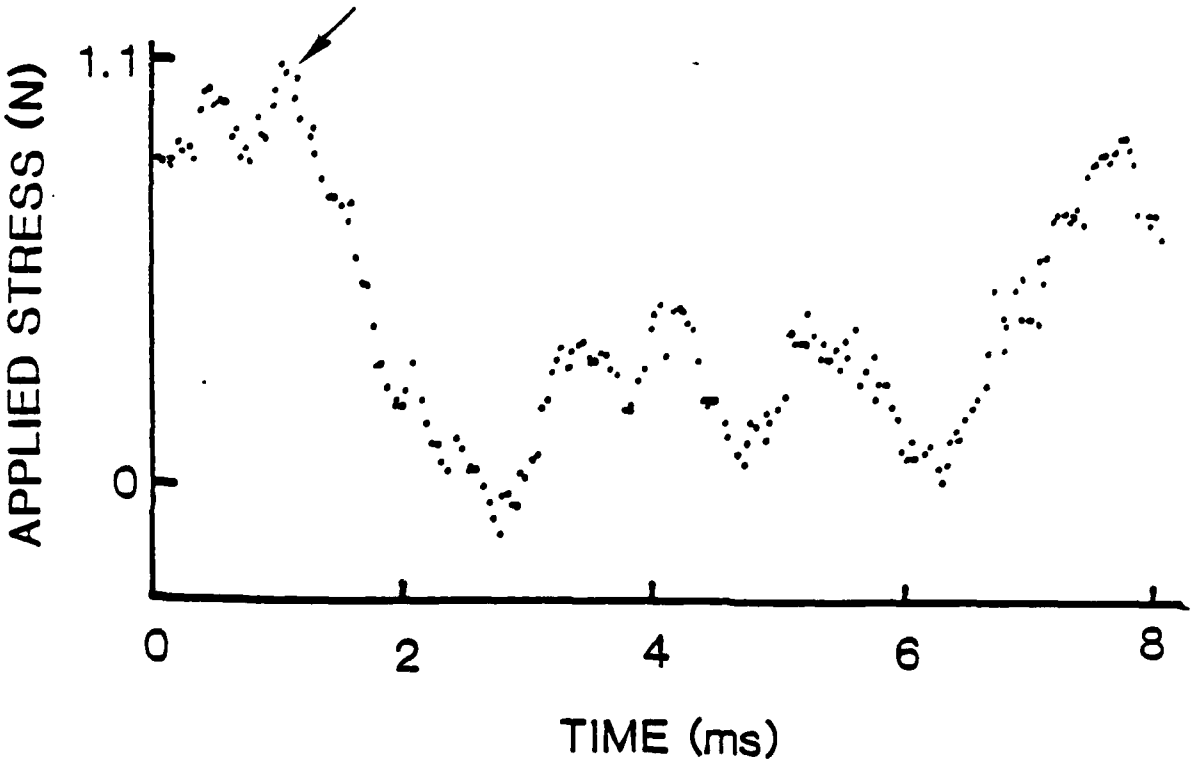
APPLIED STRESS (N)
1.1
0
0
2
4
6
8
TIME (ms)

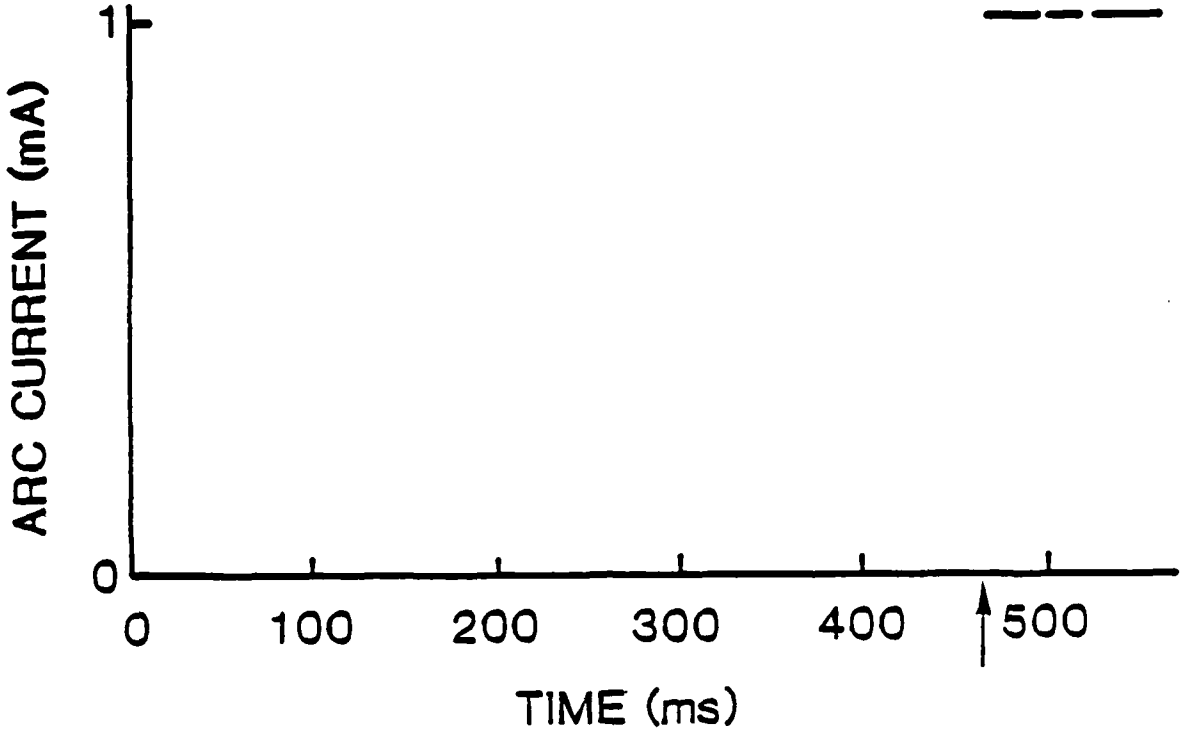
1
0
ARC CURRENT (mA)
0
100
200
300
400
500
TIME (ms)

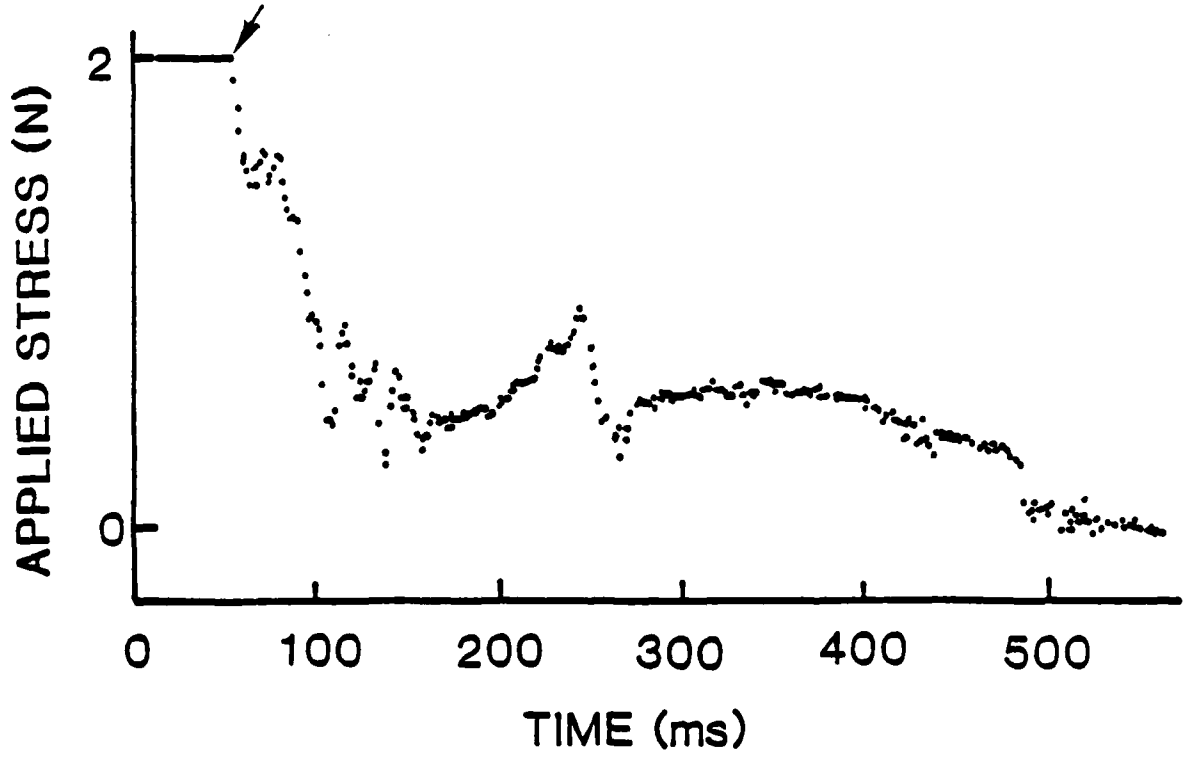
2
0
APPLIED STRESS (N)
0
100
200
300
400
500
TIME (ms)

Fig. 12

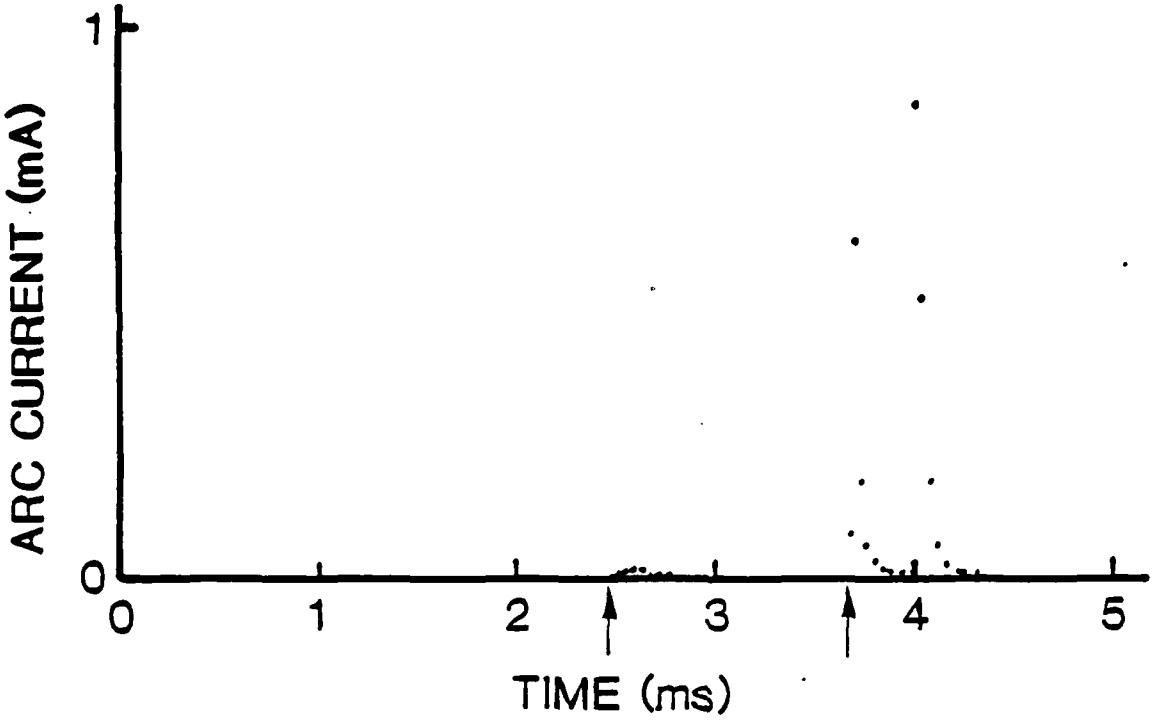
ARC CURRENT (mA)
1
0
0
1
2
3
4
5
TIME (ms)

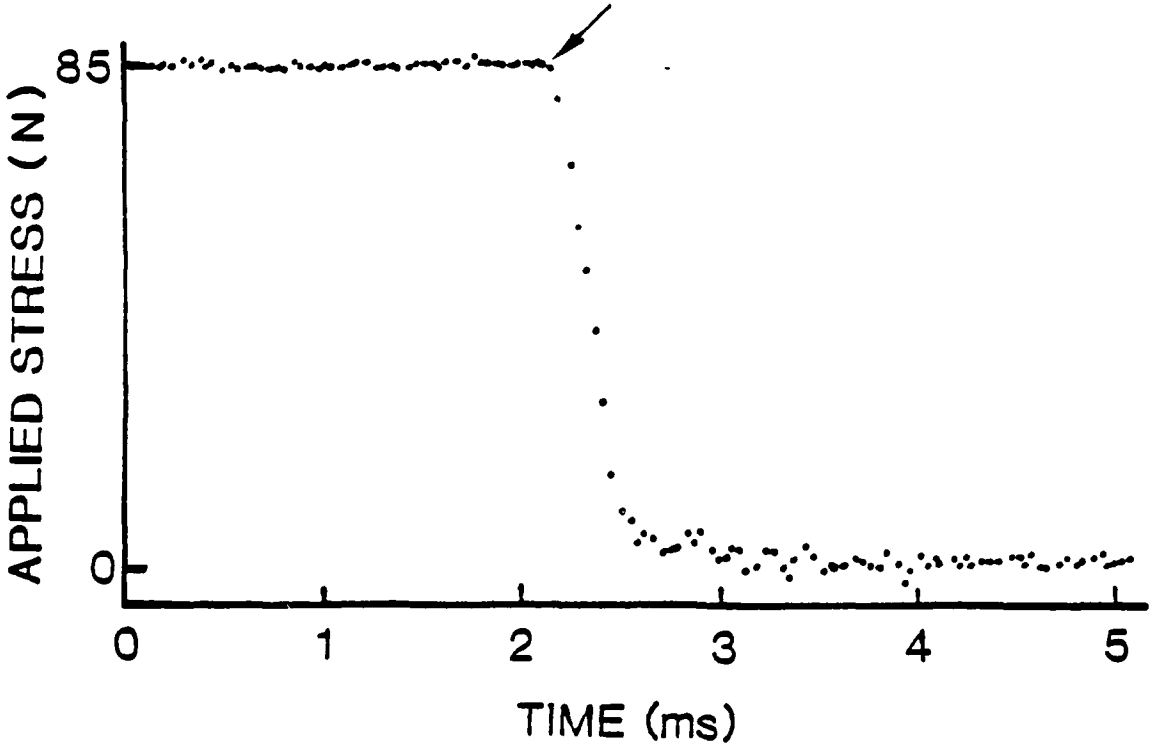
APPLIED STRESS (N)
85
0
0
1
2
3
4
5
TIME (ms)

Fig. 13

VI. ELECTRON BEAM INDUCED FRACTURE OF POLYMERS

J. T. Dickinson, M. H. Miles, L. C. Jensen, and M. L. Klakken
Department of Physics
Washington State University
Pullman, WA 99164-2814

ABSTRACT

When a notched, highly plastic material is stressed, the notch opens into a wide crack-tip, exposing the region of high stress concentration. We explore for the first time the consequences of electron bombardment of the tip of such a stressed crack in polymers under vacuum. We present evidence of induced crack growth at stresses normally below observable crack growth and electron current densities where thermal heating of the zone near the crack tip is minimal. Deflection of the electron beam on and off the sample while making simultaneous measurements of electron current, gas pressure, and sample load provide information on the phenomena involved. Experiments on bombardment of un-notched polymers under stress are also described. Descriptions of the fracture surfaces created by combinations of electron bombardment and stress are given.

I. INTRODUCTION

When a polymer is bombarded by high energy electrons, energy is deposited in the material due to the inelastic collisions that occur. These events cause ionization, broken bonds, and vibrational excitations of the molecules. The chemical effects that can generally result from these events include additional polymerization, cross-linking, and branching of the polymer, all of which tend to increase the strength of the material in the region of bombardment. Likewise, bond scissions, molecular dissociation (via electronic excitations), electron stimulated desorption of ions and neutral species (again, via electronic excitations), as well as thermal degradation and gas evolution (due to a temperature rise in the material being bombarded) can occur, all of which tend to "weaken" the material.

In this paper we wish to explore for the first time the simple question: What happens when we apply simultaneously a combination of stress and electron bombardment at the tip of a crack in a polymer? The primary motivation for such an experiment is to examine the consequences of fracture in a high energy environment. Situations such as stressed materials exposed to radiation, combustion of rocket propellents, and materials exposed to plasma environments are all of interest. Secondly, we propose that by the use of e^- beam excitation of the crack tip we may further our understanding of the physics of fracture by selective bond breaking and/or activated stress-

dependent chemistry. Finally, we eventually hope to attempt various electron spectroscopies, e.g. electron energy loss spectroscopy, on stressed molecules to provide useful information about fracture and therefore view this work as preliminary.

Models of fracture of polymeric solids and elastomers have been reviewed by Andrews[1] and Gent.[2] The continuum fracture of a characteristic energy for tearing[3] and the strain concentration at a scission[4] have been developed by Thomas and coworkers. The continuum and molecular theories of fracture[1] seem compatible in that the different initial assumptions both appear capable of adequately describing the experimental results. However, as fracture investigations become more sophisticated, it is expected that molecular understanding will become increasingly more important.

In this paper we concentrate primarily on the mechanical response of the material. The polymers included here are unfilled polyisoprene, a 50-50 co-polymer of 3,3,bis(azidomethyl)oxetane and tetrahydroturan (BAMO/THF)--a model energetic binder for rocket propellent, and polyethylene.

II. EXPERIMENTAL

Rectangular test specimens of several polymeric materials were mounted in a vacuum system equipped for straining materials in tension. Figure 1a shows a schematic diagram of the apparatus. Two sample orientations were studied, shown in

Fig 1b and 1c. The usual test involved a notched sample mounted horizontally with the notch facing the electron beam (Fig. 1b). The materials chosen deformed to yield open, U-shaped cracks, allowing convenient e^- beam bombardment in the region of high stress.

The samples were subjected to a constant strain rate of 10^{-1} % /s. A load cell (placed in the vacuum) was used to monitor the force applied to the sample. Most of the tests were carried out at a pressure of 10^{-5} Pa. An electron gun was mounted so that the electrons could strike the sample at or near the focal point. The spot size was approximately 3 mm in diameter. The electron beam could be deflected either manually or in a sweeping fashion with appropriate voltages applied to deflection plates. The kinetic energy of the incident electrons was 1.5 keV. Electron currents generally were between 10-20 uA. In most experiments we minimized the time the beam was actually on the sample to avoid build-up of surface charge which would tend to reduce the actual current bombarding the polymer surface.

Some of the samples were in the form of unnotched thin sheets and were mounted vertically, with the e^- beam striking the rectangular face with normal incidence (Fig 1c). In this latter mode, the influence of uniaxial tension on the time required for the e^- beam to penetrate through the specimen was examined. The response of the sample was generally like fracture; furthermore, any displacement of the e^- beam on the sample promoted crack growth in that direction.

In some of our experiments we measured the current striking a collector mounted behind the sample. Thus, if the sample partially or completely blocked the e^- beam, the time at which the e^- beam came on, off, or penetrated through the sample could be determined. We also frequently measured the rise in pressure in the vacuum system by means of an ionization gauge. The appropriate signals from the various transducers were all digitized simultaneously with 0.1 s time resolution using a LeCroy Data Acquisition System and stored on disk for later analysis and plotting.

The samples were cut from sheets of polymers. The polyisoprene (PI), provided by H. M. Leeper, Alza Corporation, were replicate plaques of Goodyear Natsyn 2200 cross-linked with Hercules Di-Cup R. Following a 20 minute cure at 165 C, the plaques were extracted at boiling with acetone. Sample cross-sections were 1 mm x 15 mm with a single edge notch of 1 mm. These samples would generally rupture at 6-12 N of applied force with a strain of about 300%.

The BAMO/THF samples provided by P. Majewski and Y. Gupta, Washington State University, consisted of BAMO/THF reacted with tolylene-2,6 diisocyanide, and cross-linked with 1-1-1 tris(hydroxymethyl)ethane using dibutyl tin dilaurate as a catalyst. Curing took place at 60 C for several days. The BAMO/THF sample cross-sections were 3 mm x 12 mm and were notched to a depth of 1 mm. These samples would tend to fail at an applied force of 5-12 N.

The polyethylene (PE) samples were from commercial sheets

of linear, high density polyethylene (U. S. Industrial Chemicals LR 20175); the density was 0.95 g/cm^3 and a characteristic melt index of 0.1. Sample cross-sections were 50 um x 10 mm.

Fracture surfaces of all materials were prepared for Scanning Electron Microscopy (SEM) by careful cutting and mounting of sections of the sample. Gold coatings 70 A thick were sputtered onto the specimens before examination in the microscope.

III. RESULTS

Figure 2a shows the applied load vs. time to a PI sample, where the sample was elongated relatively rapidly to a load of 7 N, followed by a constant strain rate of 0.007 mm/s (started at the diagonal arrow). At the vertical arrows, the electron beam (10 uA) passed over the notched crack-tip (we called this our "pit and the pendulum" experiment). The response to the passing e^- beam was a dramatic jump of the crack with an accompanying drop in force. On a time scale of seconds, the response appeared to be instantaneous. Earlier experiments on unstressed PI or PI stressed into the elastic region only showed no effect of cutting or visible damage to the PI sample at these beam currents. The last drop in load corresponds to the final rupture of the specimen. Figure 2b shows a typical load vs. time curve for an unbombarded notched sample strained in the same manner as above. Note the longer time scale. The time and therefore the extension at failure is considerably

longer.

Similar data for BAMO/THF is shown in Fig 3a, where the e^- beam current was 10 uA. In this case, the sample was prestrained relatively quickly, allowed to relax for approximately 20 s, then strained at a constant strain rate of 0.007 mm/s (starting at the diagonal arrow). The vertical arrows indicate when the e^- beam swept across the crack-tip. Again, the polymer showed rapid response to the e^- beam. For comparison, Fig 3b shows a typical load curve for the BAMO/THF samples without electron bombardment. 10 uA bombardment of the unstressed material for times of a few seconds showed no evidence of damaging the polymer. Much longer times and higher beam currents led to clear evidence of decomposition of the material, e.g. incandescence and a large increase in total gas pressure in the vacuum system.

Similar results for notched high density PE are shown in Fig. 4. Prior to the application of the e^- beam the sample showed definite signs of crazing in the region of the notch. The vertical arrows in Fig. 4a indicate the times the e^- beam (approximately 14 uA) started hitting the notch. (It should be noted that because of the thin width (50 um) of the PE, a good portion of the e^- beam did not strike the sample.) The resulting decreases in load are again due to crack growth. For comparison, we provide a load curve for an unbombarded, notched sample where the same elongation yielded no failure. (Due to a change in load cells we notched the sample to a greater depth to prevent overloading the cell--thus the maximum load is

somewhat smaller than would be obtained for a sample identical to the one bombarded with the e^- beam.)

To determine more carefully the time required for the stressed material to respond to the application of the e^- beam, we measured simultaneously the e^- current to the collector behind the sample (inverted so that the spike upward represents current hitting the sample) and the change in load at 0.1 s intervals. We also measured the change in total pressure in the vacuum system. Electronic and mechanical response times were approximately on the same time scale. Figure 5 shows typical results, in this case for PI, where the beam swept across the sample four times. The vertical lines on the three graphs indicate the times that the beam was on the sample. The small rise in pressure is exactly in synchronization with the e^- beam striking the polymer. Usually within 0.1 s the load cell indicated a response (i.e. crack growth) to the e^- beam as it came onto the crack tip. This rapid response plus the small accompanying increase in gas pressure are not consistent with any significant heating of the polymer.

In calculations of the rise in temperature due to absorption of the electron beam in time periods of a few seconds, we considered an infinite half space material with heat supplied at the surface at a constant rate, following a development given by Jaeger[5]. Worst case calculations showed temperature increases of only 5-8 C for the appropriate current densities and exposure times. These results indicate that the resulting crack growth is not due to an increase in the

temperature of the polymer. Alternative mechanisms would involve direct bond breaking of molecules in tension.

Similar results for BAMO/THF at 10 uA beam current are shown in Fig. 6. Here we show only the load curve when we are sweeping the e^- beam across the notch (the vertical line) so that the large number of steps due to crack growth can be seen. As in the case of PI, we note that the pressure follows the e^- beam bombardment precisely and returns to the baseline as soon as the beam is removed. The pressure rise during bombardment tended to be higher for BAMO/THF, partly due to the larger sample thickness (3 mm), which means more of the e^- beam is hitting the polymer surface.

Nevertheless, the BAMO/THF does appear to be more sensitive to bombardment in terms of release of gas. However, these changes in pressure are much smaller than that obtained at higher beam currents. Fig. 7a shows the pressure changes accompanying electron beam bombardment of BAMO/THF at a current of 140 uA. The initial, slow rise in pressure was accompanied by the gradual increase in red incandescence in the vicinity of the bombardment. During the large pressure bursts seen in Fig. 7a, the incandescence was observed to flash brightly. The BAMO/THF, which decomposes energetically, i.e., exothermally, was apparently stimulated by the e-beam to decompose in an auto-catalytic fashion. The observed fluctuations may be due to rapid changes in surface temperature due to the expulsion of gases, similar to the effect called ablative photodecomposition proposed by R. Srinivasan.[6]

The rise in pressure due to the combination of e-beam and stress is comparable to that produced by fracture alone. Fig. 7b shows such a rise in total pressure for a fracture of a notched BAMO/THF specimen stressed relatively quickly. The rise in pressure occurs primarily during crack growth, reaching a peak at final rupture of the sample (where the crack tends to move the fastest). The long tail which lasts several seconds seen in Fig. 7b is completely missing in any of the pressure peaks of Fig. 6 (due to e^- beam induced fracture). We hypothesize that in the case of fracture induced by stress alone, the higher plastic work occurring at the crack tip raises the temperature sufficiently to cause diffusion and desorption of gases from the polymer. Thus, the tail of the neutral emission curve represents the combined effects of cooling after fracture and the depletion of the available gases near the fracture surfaces. In the case of the e^-beam induced fracture, the lack of a tail on the pressure spikes during bombardment suggests the fracture is relatively "cool".

Another mode of e^- beam induced fracture involves the sample arrangement of Fig. 1c where an unnotched sample is stressed and the e-beam is allowed to strike the sample side-on. Of interest here was the ability of the e^- beam to initiate a crack and thereby penetrate the sample. Thus, at t=0 the e^-beam is quickly applied to the center of the elongated sample (so the collected current rapidly drops) and then as the e^-beam penetrates through to the other side due to opening of a crack, the current hitting the sample drops (so

the collected current rises). Un-notched samples of PI, initially of 1 mm thickness were strained to approximately 200 % elongation. Fig. 8 show the change in total pressure, collector current (essentially the inverse of the current to the sample), and applied load for such a PI sample with an e^- beam current of 150 uA. The time to penetrate through this particular PI sample was 22 s. In this particular sample, as soon as the e^- beam penetrated through the sample, the sample immediately failed. This happened approximately half the time. In terms of the time to penetrate through the material, usually higher currents penetrated faster, lower currents penetrated slower. In general, higher currents were necessary to induce this type of fracture in PI primarily due to severe charging problems at normal incidence. The e^- beam showed immediate defocusing which means that the effective current density hitting the sample was considerably reduced. Application of the e^- beam to unstressed samples of PI for times of several seconds led to no noticeable damage and no penetration.

Similar results are shown in Fig. 9 for a 50 um sheet of PE where the sample was pre-stressed, allowed to relax for 15 seconds, and then hit with the e^- beam. Prior to application of the e^- beam, there was extensive crazing over the entire sample. In 1.7 s the e^- beam had initiated a crack through the sample, resulting in a rise in the collector current. Likewise the accompanying pressure change was quite small and began decreasing as soon as penetration started and the opening in the sample widened. In this particular case, the PE sample did

not fail after penetration of the e^- beam. When a current of similar magnitude bombarded a similar PE sample without stress, penetration did not occur, although several hundred seconds of exposure sometimes produced a visible darkening of the polymer, presumably due to carbon formation.

The resulting surfaces of e^- beam induced fracture compared to fracture surfaces produced by stress only are quite different. Fig. 10 shows the comparison for each of the materials. The direction of bombardment in these photographs is horizontal. Included are the surfaces of another polymer we've just begun to study, an elastomer, polybutadiene. In each case one sees significant differences in the fracture surfaces. In the case of the elastomers, there are a large number of ridges or rows, spaced less than a micron apart, generally aligned parallel to the crack tip (i.e. in Fig 1b, these rows would tend to be vertical on the fracture surface). For PE, the e^- beam induced fracture surface does not show quite the same regular pattern, but still is bumpy compared to the surface produced by stress alone. Bombardment of an ordinary fracture surface produced by stress alone does produce a similar pattern provided the bombardment is at glancing incidence, although the combination of stress and e^- beam exaggerates the roughness considerably. It should be noted that the spacing of the ridges and valleys on the elastomers are not the same for different materials.

IV. DISCUSSION

The basic characteristics of the electron beam induced fracture which we can describe at this point are the following:

1) The polymers must be elongated beyond their yield point, i.e., into the plastic deformation region, to observe crack growth under bombardment. However, no evidence of crack growth occurs before the e^- beam is applied, i.e. we are below the initial stress concentration.
2) The current densities necessary to obtain noticeable crack growth below critical stress levels were on the order of 100 uA/cm^2.
3) The higher the stress, the more evident the response to the e^- beam. At high stress, the time of response is < 0.1 s.
4) The calculated heating effect of the e^- beam on this time scale is negligible.
5) The change in gas pressure due to evolution of gases from e^- beam bombardment of the polymer is considerably smaller compared to that obtained at higher currents and follows the e^- beam current to the sample precisely with no evidence of a "cooling curve".
6) Samples of un-notched PI and PE also respond to e^- beam bombardment when stressed.
7) The fracture surfaces show features (rows/ridges or "bumps") on the e^- beam induced fracture completely

missing from the unbombarded fracture surface. These features seem to be primarily due to bombardment of the fracture surface at glancing incidence.

These results suggest that the phenomenon of e^- beam induced fracture is at least not dominated by thermal effects, but appear to be a direct consequence of electronic interactions; i.e., direct scissions of load bearing molecular chains by these electron collisions which in turn leads to crack propagation.

A 10 uA electron beam deposits 0.02 J/s into a volume estimated to be 10^{-6} cm^2. Assuming a G factor of unity for main chain bond scissions, we estimate a chain scission rate of 10^{15} bonds/s. A density of load bearing chains of $10^{14}/cm^3$ corresponds to 10^{16} main chain bonds in our radiation volume. Hence it appears that every tenth bond is broken every second. At zero stress the electron induced scissions tend to quickly react to reform the original bond or produce a crosslink. However, when the load bearing chains in the crack tip region are under sufficient tension, electron induced bond scissions would tend to lead to separation of the newly created chain ends thereby suppressing reattachment and thereby favoring crack growth. Since only a small portion of our electron beam bombarded the crack tip region, it seems that the irreversibility of breaking these stressed bonds is extremely high.

Although the work reported here should be regarded as tentative, the prospect for performed controlled direct

electron rupture of bonds appears promising and should lead to improved understanding of fracture in elastomers and polymeric materials. Furthermore, the unique type of fracture surfaces due to combinations of stress and electron bombardment may lead to practical applications, e.g. preparation of surfaces for adhesive bonding. Finally, we mention that we are currently investigating the e^- beam induced fracture of single fibers of polymers and seeing similar results.

V. ACKNOWLEDGEMENTS

The authors would like to thank H. M. Leeper, Alza Corporation, for providing the PI samples, Y. Gupta and P. Majewski, Washington State University, for providing the BAMO/THF samples, and A. N. Gent, University of Akron Institute of Polymer Science for the BR samples. This work was supported by the Office of Naval Research, contract N00014-80-C-0213 and Sandia National Laboratories.

V. REFERENCES

1. E. H. Andrews, Polymer Science (A.D. Jenkins ed.) Vol.1, Ch.9 American-Elsevier, New York (1972)

2. A. N. Gent, Science and Technology of Rubber (F. R. Eirich ed.), Ch.1Ø Academic Press, New York (1978)

3. R. S. Rivlin and A. G. Thomas, J. Poly. Sci. 1Ø, 291 (1953).

4. A. G. Thomas, J. Poly. Sci. 18, 177 (1955).

5. J. C. Jaeger, Australian Journal of Scientific Research 5, 1 (1952).

6. R. Srinivasan and V. Mayne-Banton, Appl. Phys. Lett. 41, 576 (1982).

Figure Captions

Figure 1. (a) Schematic diagram of apparatus for electron beam assisted fracture investigations. (b) Horizontal sample with an edge notch facing the electron beam. (c) Vertical sample with electron beam normal to the rectangular face.

Figure 2. (a) Response of load (vs time) to passing the electron beam across a stressed crack tip in polyisoprene. The sudden decrease in load is due to crack growth. (b) Load vs time for a notched, unbombarded polyisoprene sample.
Diagonal arrow indicates when strain rate was reduced. Vertical arrows show when the e^- beam was incident on the crack tip.

Figure 3. (a) Response of load (vs time) to passing the electron beam across a stressed crack tip in BAMO/THF. (b) Load vs time for a notched, unbombarded BAMO/THF sample. Diagonal arrows indicate when strain rate was changed. Vertical arrows show when the e^- beam was incident on the crack tip.

Figure 4. (a) Load vs time for a notched polyethylene sample with periodic bombardment of crack tip with an electron beam. (b) Load vs time for a more deeply notched, unbombarded polyethylene sample (measured with a different load cell).

Figure 5. Response of notched polyisoprene to periodic electron bombardment. (a) Electron beam current to the collector (inverted to represent current to the sample) behind the sample vs time, (b) sample load vs time, and (c) change in total pressure in the vacuum chamber vs time.

Figure 6. Response of notched BAMO/THF to periodic electron bombardment of the crack tip. (a) Electron beam current to the collector (inverted to represent current to the sample) vs time, (b)\sample load vs time, and (c) change in total pressure in the vacuum chamber vs time.

Figure 7. (a) Change in total pressure vs time during electron bombardment of BAMO/THF with a current of 140 uA. Arrows indicate when the e^- beam was placed on and off the sample. (b) Change in total pressure vs time accompanying the fracture of BAMO/THF without electron bombardment. The rapid rise in pressure was during crack growth.

Figure 8. Response of unnotched polyisoprene under stress to

electron bombardment normal to the surface. Shown are the change in total pressure vs time, collector current (the collector is immediately behind the sample) vs time, and sample load vs time.

Figure 9. Response of unnotched polyethylene under stress to electron bombardment normal to the surface. Shown are the change in total pressure in the vacuum system, the current to a collector immediately behind the sample, and the sample load vs time.

Figure 10. Scanning electron micrographs of fracture surfaces: (a) and (a') polyisoprene without and with electron beam, (b) and (b') polybutadiene without and with electron beam, (c) and (c') BAMO/THF without and with electron beam, (d) and (d') polyethylene without and with electron beam. In each bombarded sample the direction of the e beam was horizontal.

(a)

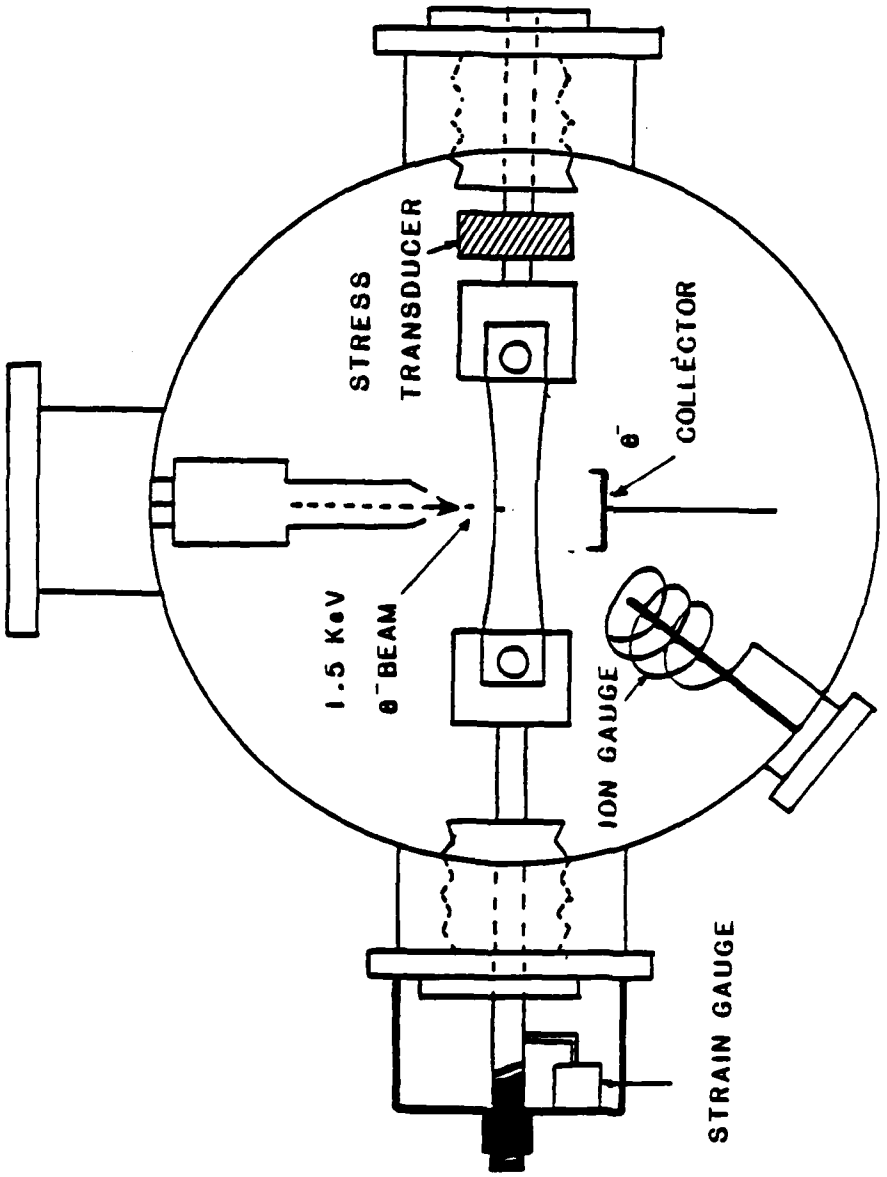
STRESS
TRANSDUCER
COLLECTOR
e⁻
1.5 KeV
e⁻BEAM
ION GAUGE
STRAIN GAUGE

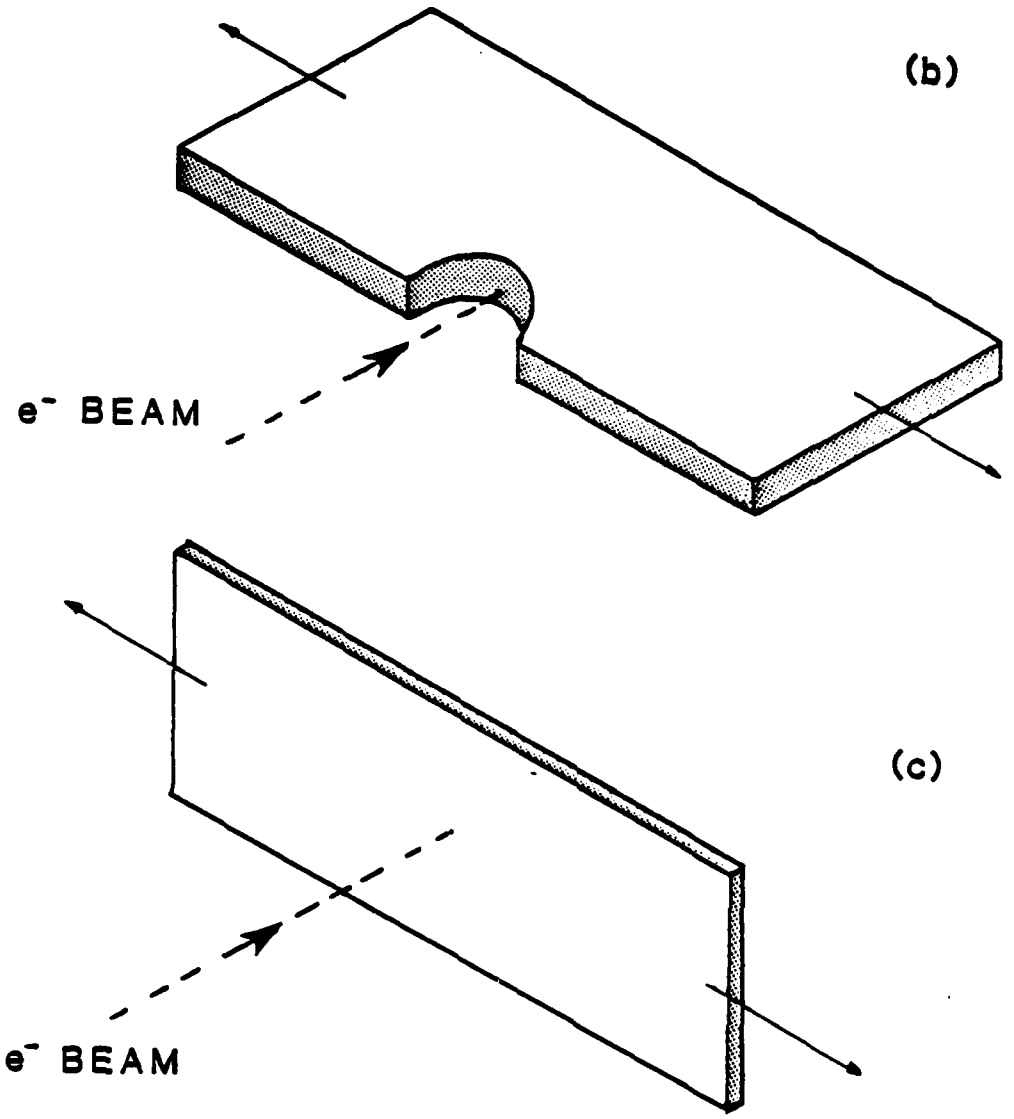
(b)
e⁻ BEAM
(c)
e⁻ BEAM

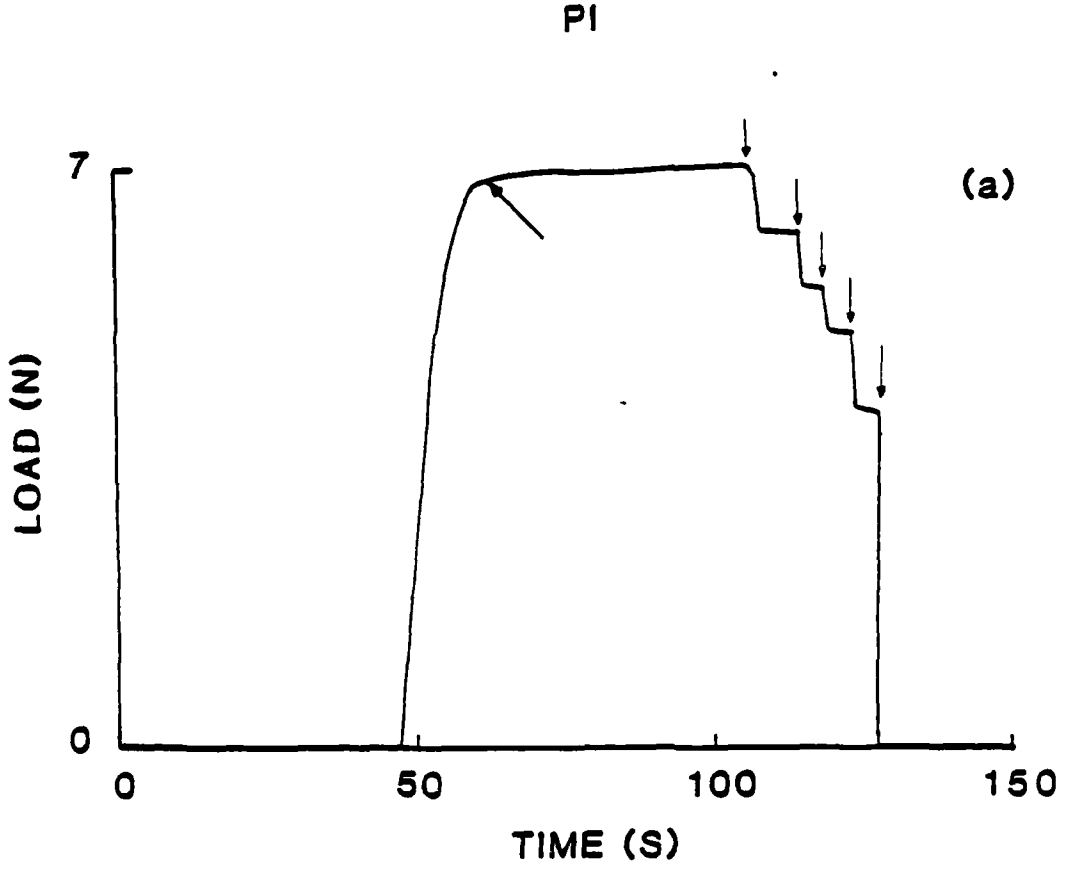

Fig. 2a

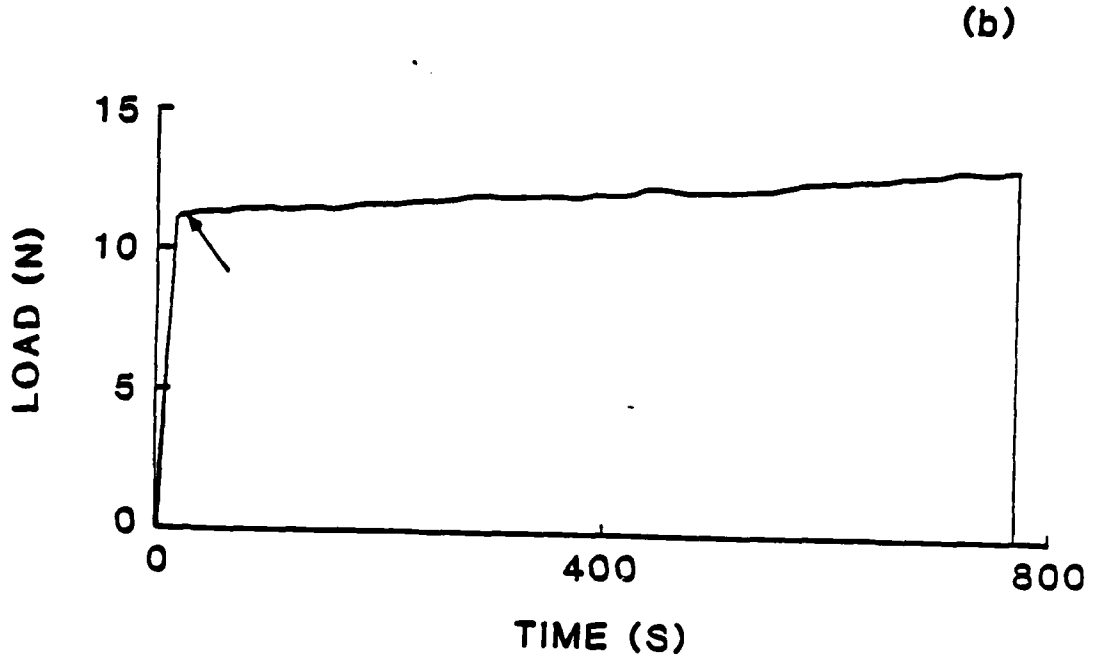
(b)
15
10
5
0
LOAD (N)
0
400
800
TIME (S)

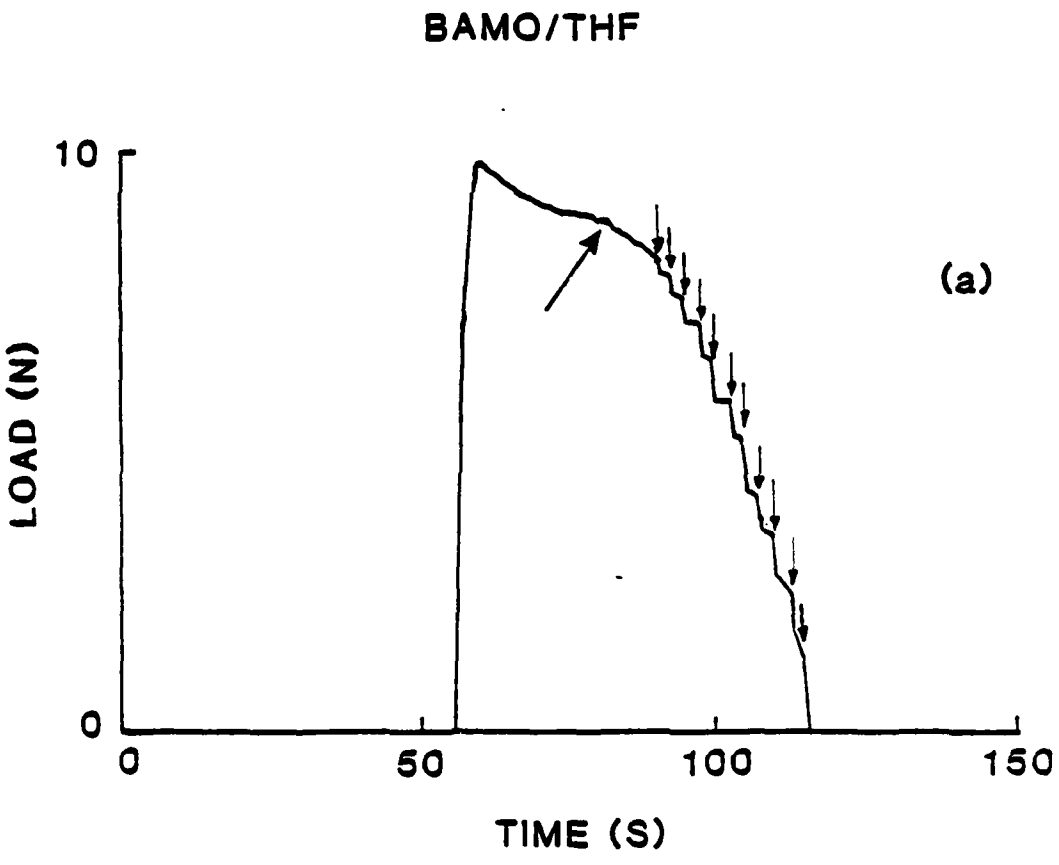

Fig 3.1

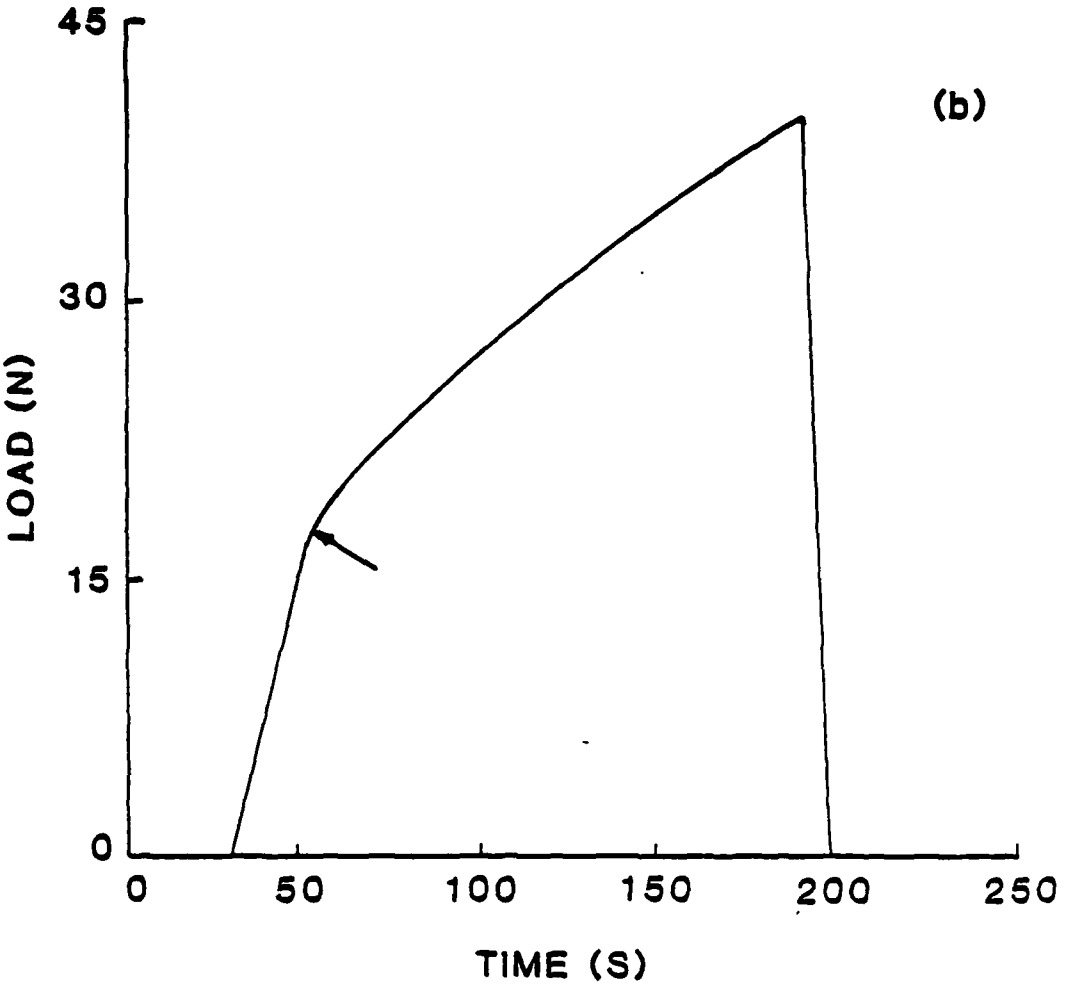

Fig 30

PE

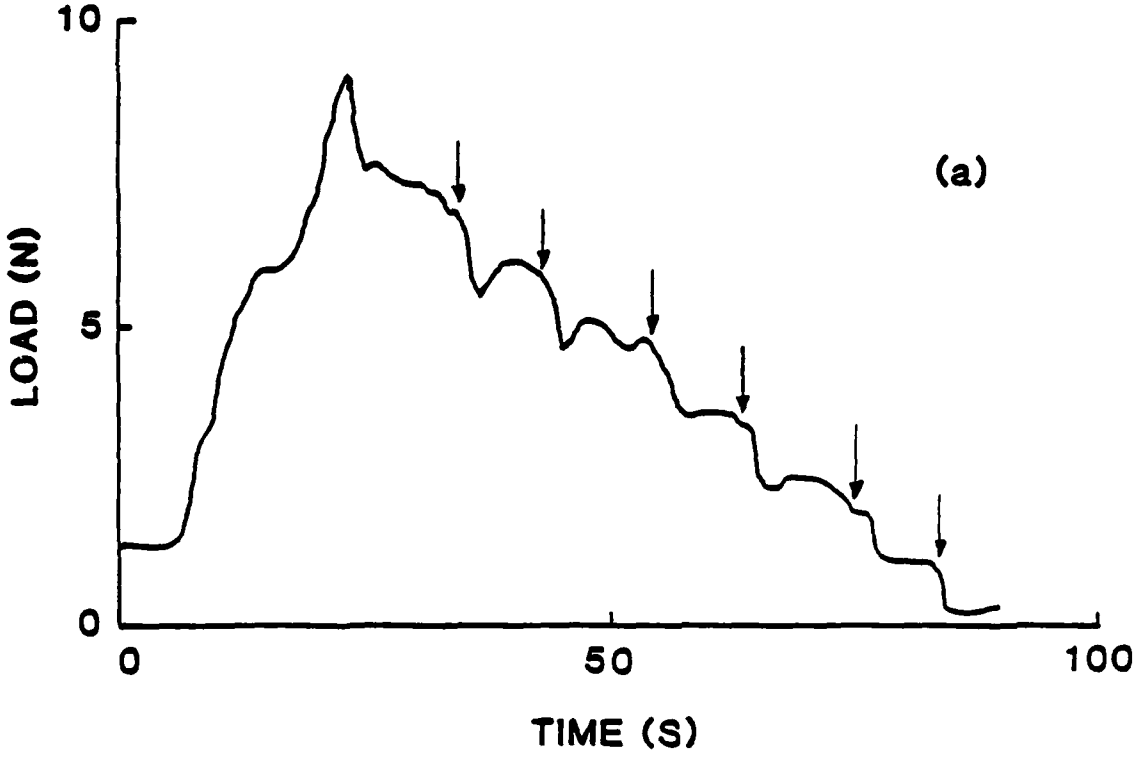

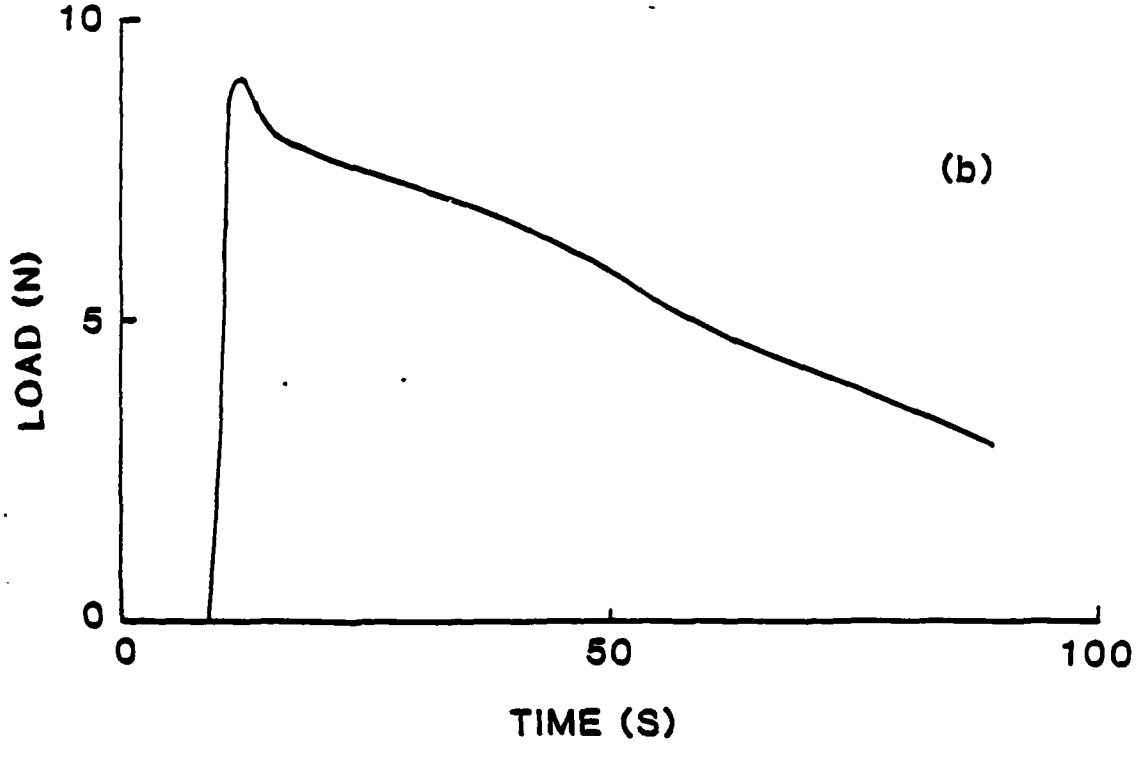

Fig. 4

ELECTRON BOMBARDMENT

ASSISTED FRACTURE OF PI

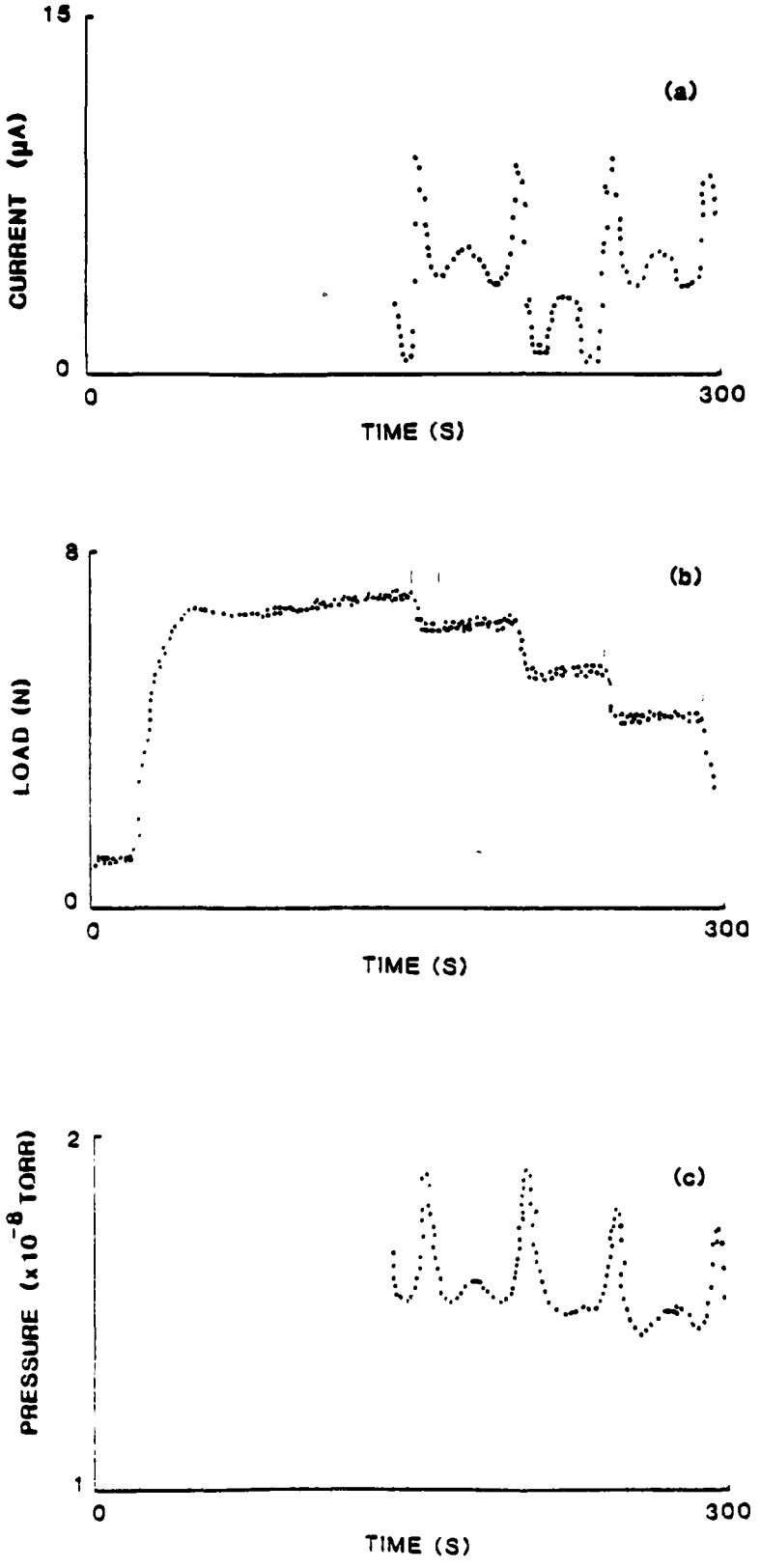

Fig 5

ELECTRON BOMBARDMENT

ASSISTED FRACTURE OF BAMO/THF

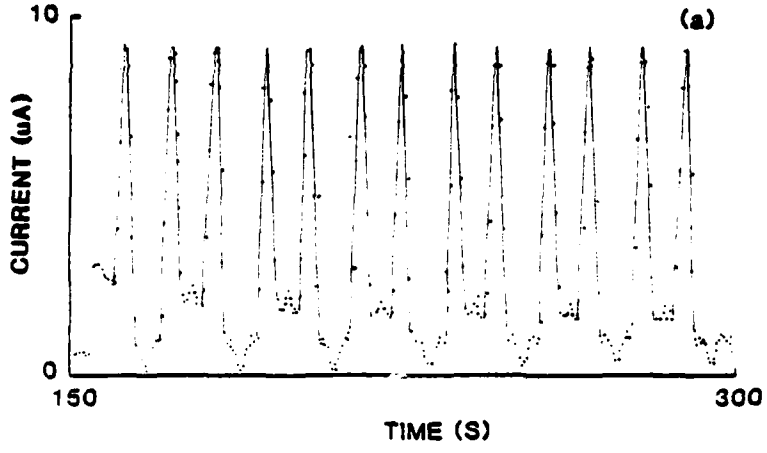

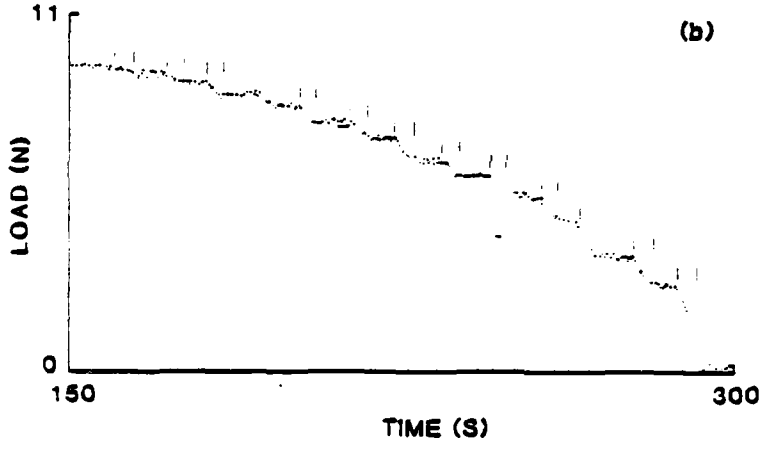

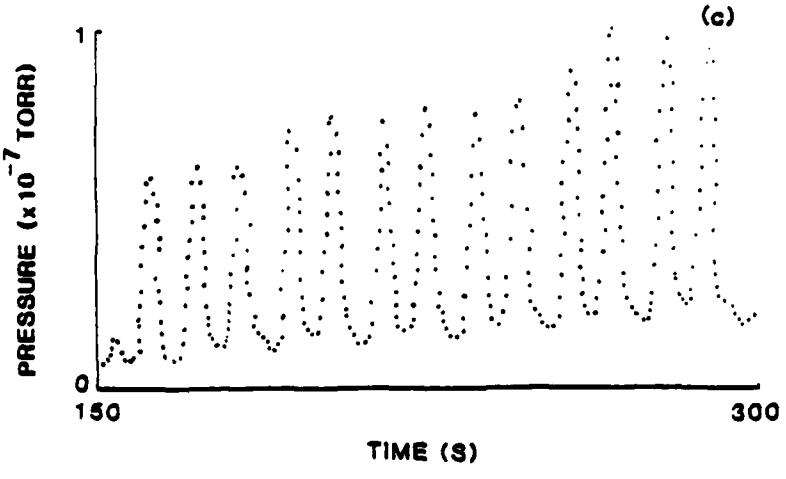

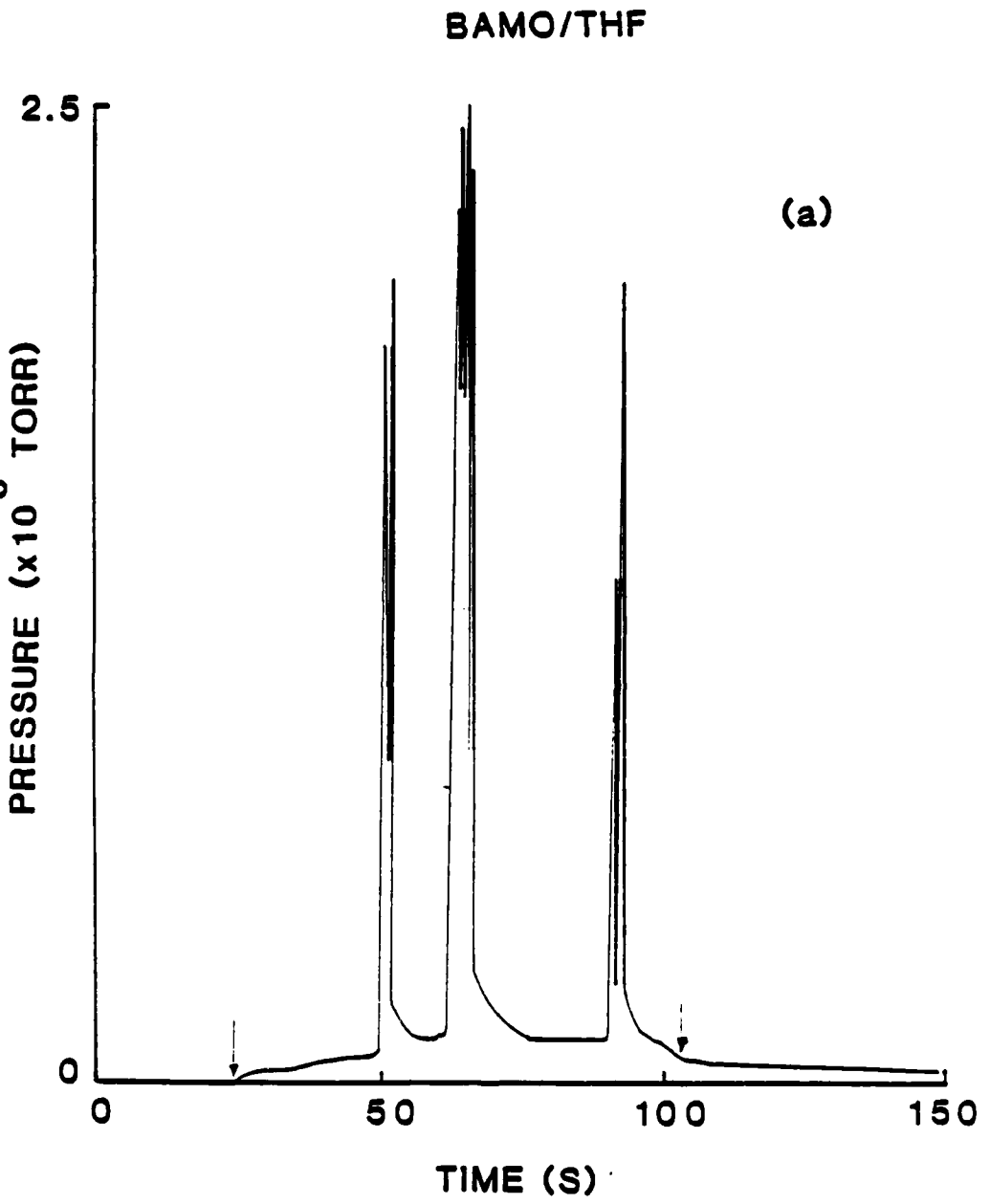
BAMO/THF
2.5
(a)
PRESSURE (x10^{-6} TORR)
0
0
50
100
150
TIME (S)

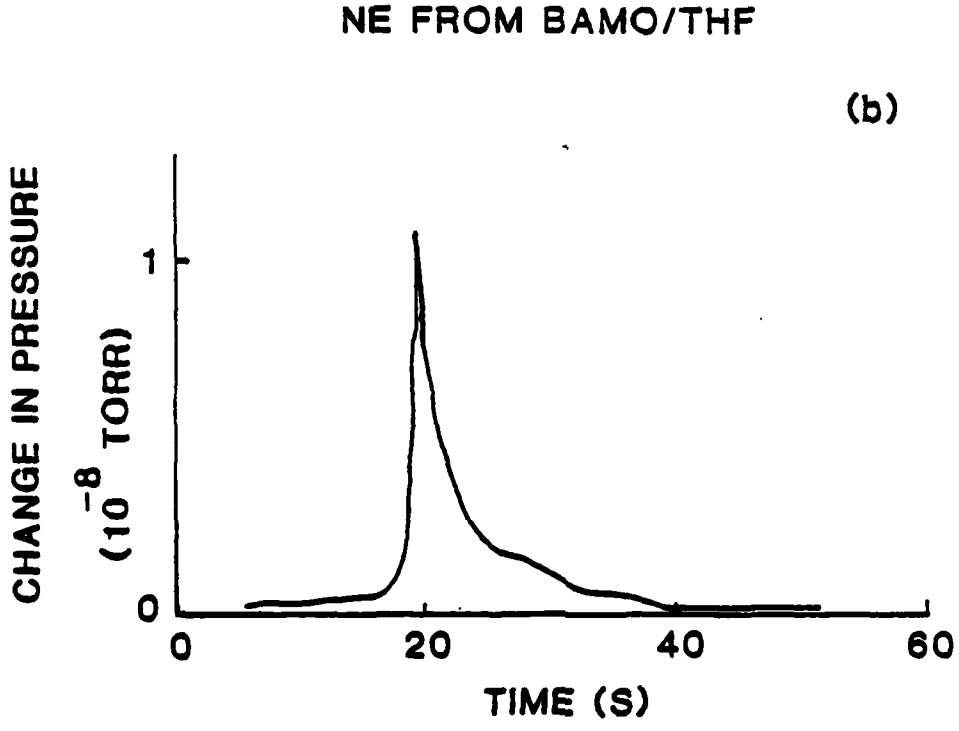
NE FROM BAMO/THF
(b)
CHANGE IN PRESSURE
(10^{-8} TORR)
1
0
0
20
40
60
TIME (S)

Fig. 7b

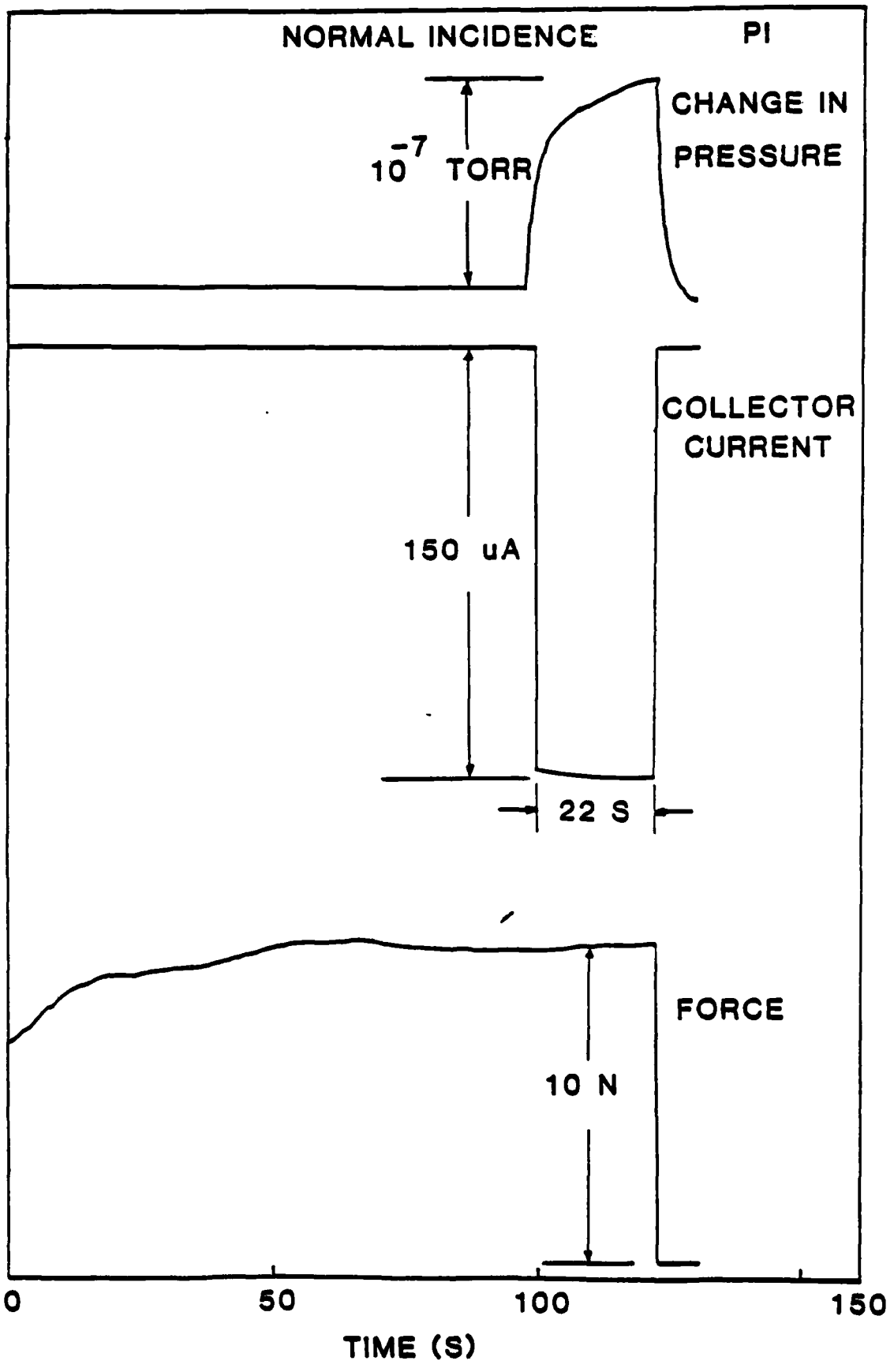
NORMAL INCIDENCE
PI
10^{-7} TORR
CHANGE IN PRESSURE
150 uA
COLLECTOR CURRENT
22 S
FORCE
10 N
0
50
100
150
TIME (S)

Fig 8

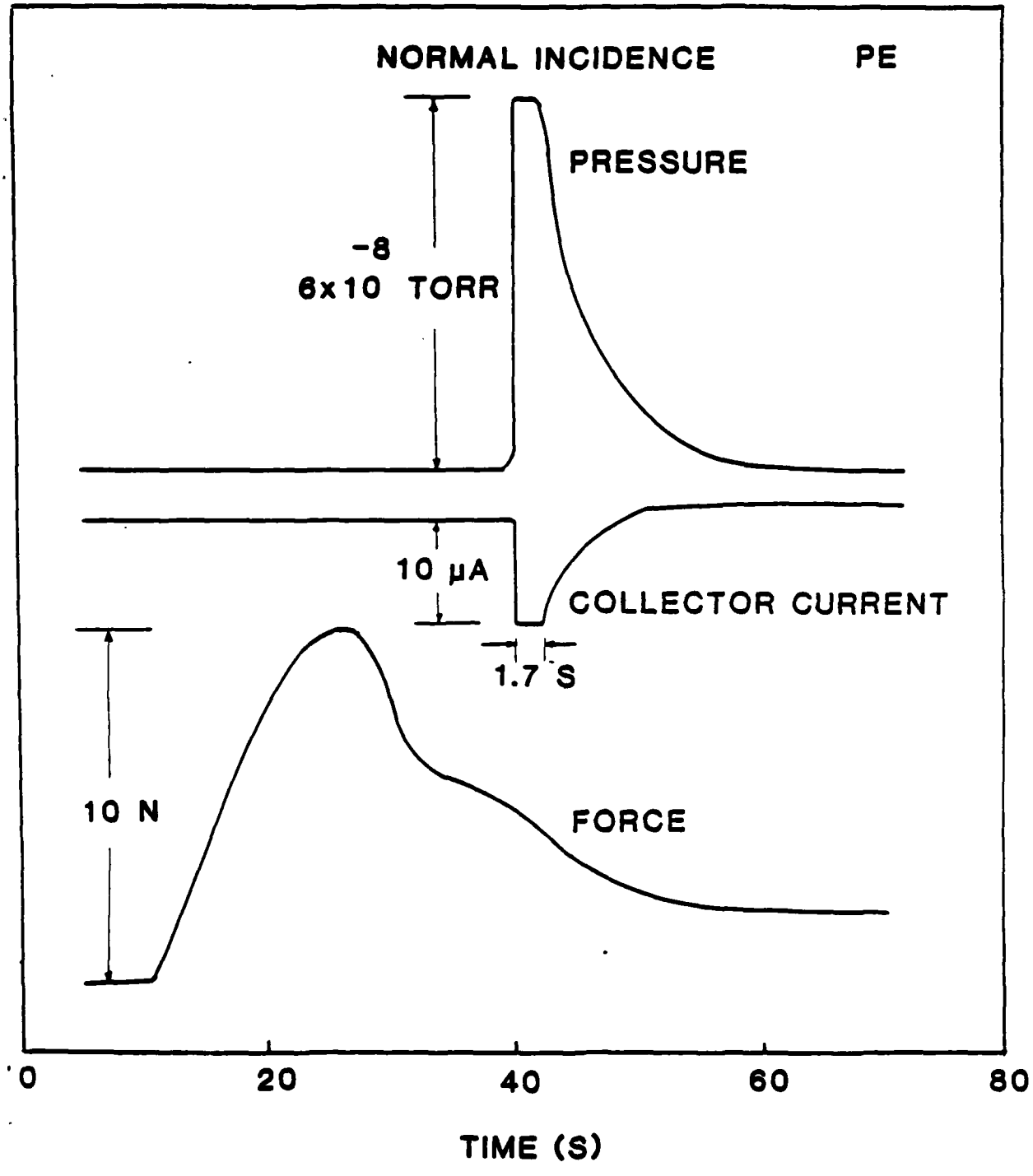
NORMAL INCIDENCE
PE
PRESSURE
-8
6x10 TORR
10 μA
COLLECTOR CURRENT
1.7 S
10 N
FORCE
0
20
40
60
80
TIME (S)

Fig. 1

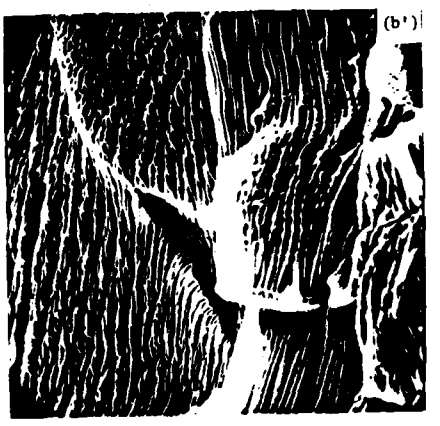

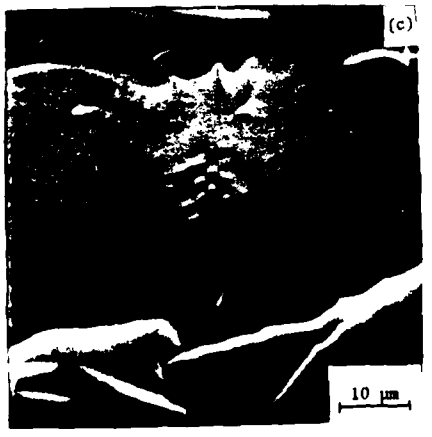

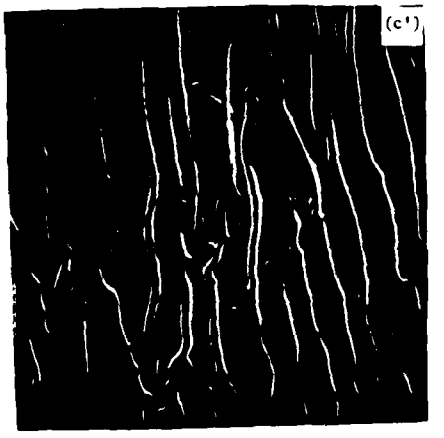

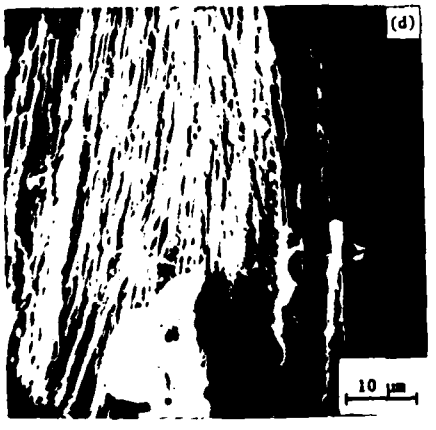

VII. CONCLUSIONS

In this year we have continued to make considerable progress in our understanding of the emission of electrons, positive ions, and photons during and following the fracture of polymers, inorganic crystals, and organic crystals. The concepts of charge separation, gas desorption, a gaseous discharge, and particle bombardment of the fracture surfaces followed by subsequent relaxation processes continue to provide the foundation for making predictions and suggest a qualitative model which agrees with experimental data for the decay curves observed in the EE, PIE, and phE signals.

Also, we have shown that cleavage type fracture of PETN produced no detectable FE, whereas compressional loading (both slow and impact loading) yielded FE. In particular, during impact loading there was evidence of a microdischarge as well as enhanced EE and PIE. We suspect that the shear effects and frictional grinding of crystals at high rates plays an important role in this enchanced emission.

In addition, we predicted and verified that when strong FE emitters are fractured in the vicinity of a voltage gap, electrical breakdown can be induced due to the emission of charged particles into the space near the gap.

Finally, we have explored on a preliminary basis the consequences of simultaneous application of stress and an electron beam to a notched crack in a polymer. Here we see

crack growth induced by the electron bombardment. It is shown that the effect does not appear to be thermal, but due to direct bond scissions in the polymer under stress.

VIII. FRACTO-EMISSION TALKS AND PAPERS PRESENTED

1. "Fracto-Emission", Sandia Laboratories, July, 1984.
2. "Fracto-Emission: A New Way to Investigate Fracture", Dupont, Wilmington, DE, July, 1983.
3. "Fracto-Emission Accompanying Adhesive Failure," Third International Symposium on Adhesion, Washington State University, September, 1983.
4. "Fracto-Emission and Fracture Surfaces", Pacific Conference on Chemistry and Spectroscopy, Pasadena, CA, October, 1983.
5. "Fracto-Emission from Filled and Unfilled Polymers", ONR, Arlington, VA, October, 1983.
6. "Fracto-Emission: The Role of Charge Separation", American Vacuum Society Conference, Baltimore, MD, October, 1983.
7. "Particles From Fracture," McDonnell-Douglas Research Labs, St. Louis, MO, March, 1984.
8. "Fracto-Emission: A New Means of Studying Fracture," U. of Idaho Physics Department, April, 1984.
9. J. T. Dickinson, "Electron Beam Induced Fracture of Polymers," American Physical Society, Detroit, MI, March 1984.
10. J. T. Dickinson, "Charge Separation and Fracto-Emission from Polybutadiene," American Physical Society, Detroit, MI, March 1984.
11. J. T. Dickinson, "Fracto-Emission from Ferro-electric Ceramics," American Physical Society, Detroit, MI, March 1984.

12. "Fracto-Emission," IBM Research Laboratories, San Jose, CA, April 1984.

13. J. T. Dickinson, "Mechanisms for the Emission of Electrons and Positive Ions During the Fracture of Brittle Materials," American Ceramics Society, Pittsburgh, PA, May 1984.

14. J. T. Dickinson, "Electromagnetic Radiation and Induced Electrical Breakdown from the Fracture of Ceramics," American Ceramics Society, Pittsburgh, PA, May 1984.

15. J. T. Dickinson, "Measurements of the Mass-to-Charge Ratio of Positive Ions from the Fracture of Glass," American Ceramics Society, Pittsburgh, PA, May 1984.

DISTRIBUTION LIST

	No. Copies	No. Copies
Dr. S. Sheffield Sandia Laboratories Division 2513 P.O. Box 5800 Albuquerque, NM 87185	1	
Dr. M. Farber Space Sciences, Inc. 135 Maple Avenue Monrovia, CA 91016	1	
Dr. Y. M. Gupta SRI International 333 Ravenswood AVenue Menlo Park, CA 94025	1	
Mr. M. Hill SRI International 333 Ravenswood Avenue Menlo Park, CA 94025	1	
Professor Richard A. Schapery Texas A&M Univ. Dept of Civil Engineering College Station, TX 77843	1	
Dr. Stephen Swanson Univ. of Utah Dept. of Mech. & Industrial Engineering MEB 3008 Salt Lake City, UT 84112	1	
Mr. J. D. Byrd Thiokol Corp. Huntsville Huntsville Div. Huntsville, AL 35807	1	
Professor G. D. Duvall Washington State University Dept. of Physics Pullman, WA 99163	1	
Prof. T. Dickinson Washington State University Dept. of Physics Pullman, WA 99163	1	

DISTRIBUTION LIST

	No. Copies
Dr. Ingo W. May Army Ballistic Research Labs ARRADCOM Code DRDAR-BLI Aberdeen Proving Ground, MD 21005	1
Professor N.W. Tschoegl California Institute of Tech Dept. of Chemical Engineering Pasadena, CA 91125	1
Professor M.D. Nicol University of California Dept. of Chemistry 405 Hilgard Avenue Los Angeles, CA 90024	1
Professor A. G. Evans University of California Berkeley, CA 94720	1
Professor T. Litovitz Catholic Univ. of America Physics Department 520 Michigan Ave., N.E. Washington, D.C. 20017	1
Professor W. G. Knauss Graduate Aeronautical Lab California Institute of Tech. Pasadena, CA 91125	1
Professor Edward Price Georgia Institute of Tech. School of Aerospace Engin. Atlanta, Georgia 30332	1
Dr. Kenneth O. Hartman Hercules Aerospace Division Hercules Incorporated P.O. Box 210 Cumberland, MD 21502	1
Dr. Thor L. Smith IBM Research Lab 042.282 San Jose, CA 95193	1
Dr. J. P. Marshall Dept. 52-35, Bldg. 204/2 Lockheed Missile & Space Co. 3251 Hanover Street Palo Alto, CA 94304	1
Ms. Joan L. Janney Los Alamos National Lab Mail Stop 920 Los Alamos, NM 87545	1
Dr. J. M. Walsh Los Alamos Scientific Lab Los Alamos, NM 87545	1
Professor R. W. Armstrong Univ. of Maryland Department of Mechanical Eng. College Park, MD 20742	1
Prof. Richard A. Reinhardt Naval Postgraduate School Physics & Chemistry Dept. Monterey, CA 93940	1
Dr. R. Bernecker Naval Surface Weapons Center Code R13 White Oak, Silver Spring, MD 20910	1
Dr. M. J. Kamlet Naval Surface Weapons Center Code R11 White Oak, Silver Spring, MD 20910	1
Professor J. D. Achenbach Northwestern University Dept. of Civil Engineering Evanston, IL 60201	1
Dr. N. L. Basdekas Office of Naval Research Mechanics Program, Code 432 Arlington, VA 22217	1
Professor Kenneth Kuo Pennsylvania State Univ. Dept. of Mechanical Engineering University Park, PA 16802	1

DISTRIBUTION LIST

	No. Copies
Dr. J.F. Kincaid Strategic Systems Project Office Department of the Navy Room 901 Washington, D.C. 20376	1
Strategic Systems Project Office Propulsion Unit Code SP2731 Department of the Navy Washington, D.C. 20376	1
Mr. E.L. Throckmorton Strategic Systems Project Office Department of the Navy Room 1048 Washington, D.C. 20376	1
Dr. D.A. Flanigan Thiokol Huntsville Division Huntsville, Alabama 35807	1
Mr. G.F. Mangum Thiokol Corporation Huntsville Division Huntsville, Alabama 35807	1
Mr. E.S. Sutton Thiokol Corporation Elkton Division P.O. Box 241 Elkton, MD 21921	1
Dr. G. Thompson Thiokol Wasatch Division MS 240 P.O. Box 524 Brigham City, UT 84302	1
Dr. T.F. Davidson Technical Director Thiokol Corporation Government Systems Group P.O. Box 9258 Ogden, Utah 84409	1
Dr. C.W. Vriesen Thiokol Elkton Division P.O. Box 241 Elkton, MD 21921	1
Dr. J.C. Hinshaw Thiokol Wasatch Division P.O. Box 524 Brigham City, Utan 83402	1
U.S. Army Research Office Chemical & Biological Sciences Division P.O. Box 12211 Research Triangle Park NC 27709	1
Dr. R.F. Walker USA ARRADCOM DRDAR-LCE Dover, NJ 07801	1
Dr. T. Sinden Munitions Directorate Propellants and Explosives Defence Equipment Staff British Embassy 3100 Massachusetts Ave. Washington, D.C. 20008	1
LTC B. Loving AFROL/LK Edwards AFB, CA 93523	1
Professor Alan N. Gent Institute of Polymer Science University of Akron Akron, OH 44325	1
Mr. J. M. Frankle Army Ballistic Research Labs ARRADCOM Code DRDAR-BLI Aberdeen Proving Ground, MD 21005	1

DISTRIBUTION LIST

	No. Copies
Mr. J. Murrin Naval Sea Systems Command Code 62R2 Washington, D.C. 20362	1
Dr. D.J. Pastine Naval Surface Weapons Cneter Code R04 White Oak Silver Spring, MD 20910	1
Mr. L. Roslund Naval Surface Weapons Center Code R122 White Oak, Silver Spring MD 20910	1
Mr. M. Stosz Naval Surface Weapons Center Code R121 White Oak Silver Spring, MD 20910	1
Dr. E. Zimmet Naval Surface Weapons Center Code R13 White Oak Silver Spring, MD 20910	1
Dr. D. R. Derr Naval Weapons Center Code 388 China Lake, CA 93555	1
Mr. Lee N. Gilbert Naval Weapons Center Code 3205 China Lake, CA 93555	1
Dr. E. Martin Naval Weapons Center Code 3858 China Lake, CA 93555	1
Mr. R. McCarten Naval Weapons Center Code 3272 China Lake, CA 93555	1
Dr. A. Nielsen Naval Weapons Center Code 385 China Lake, CA 93555	1
Dr. R. Reed, Jr. Naval Weapons Center Code 388 China Lake, CA 93555	1
Dr. L. Smith Naval Weapons Center Code 3205 China Lake, CA 93555	1
Dr. B. Douda Naval Weapons Support Center Code 5042 Crane, Indiana 47522	1
Dr. A. Faulstich Chief of Naval Technology MAT Code 0716 Washington, D.C. 20360	1
LCDR J. Walker Chief of Naval Material Office of Naval Technology MAT, Code 0712 Washington, D.C. 20360	1
Mr. Joe McCartney Naval Ocean Systems Center San Diego, CA 92152	1
Dr. S. Yamamoto Marine Sciences Division Naval Ocean Systems Center San Diego, CA 91232	1
Dr. G. Bosmajian Applied Chemistry Division Naval Ship Research & Develoopment Center Annapolis, MD 21401	1
Dr. H. Shuey Rohn and Haas Company Huntsville, Alabama 35801	1

DISTRIBUTION LIST

	No. Copies
Mr. R. Brown Naval Air Systems Command Code 330 Washington, D.C. 20361	1
Dr. H. Rosenwasser Naval Air Systems Command AIR-310C Washington, D.C. 20360	1
Mr. B. Sobers Naval Air Systems Command Code 03P25 Washington, D.C. 20360	1
Dr. L.R. Rothstein Assistant Director Naval Explosives Dev. Engineering Dept. Naval Weapons Station Yorktown, VA 23691	1
Dr. Lionel Dickinson Naval Explosive Ordnance Disposal Tech. Center Code 0 Indian Head, MD 20640	1
Mr. C.L. Adams Naval Ordnance Station Code PM4 Indian Head, MD 20640	1
Mr. S. Mitchell Naval Ordnance Station Code 5253 Indian Head, MD 20640	1
Dr. William Tolles Dean of Research Naval Postgraduate School Monterey, CA 93940	1
Naval Research Lab. Code 6100 Washington, D.C. 20375	1
Dr. J. Schnur Naval Research Lab. Code 6510 Washington, D.C. 20375	1
Mr. R. Beauregard Naval Sea Systems Command SEA 64E Washington, D.C. 20362	1
Mr. G. Edwards Naval Sea Systems Command Code 62R3 Washington, D.C. 20362	1
Mr. John Boyle Materials Branch Naval Ship Engineering Center Philadelphia, PA 19112	1
Dr. H.G. Adolph Naval Surface Weapons Center Code R11 White Oak Silver Spring, MD 20910	1
Dr. T.D. Austin Naval Surface Weapons Center Code R16 Indian Head, MD 20640	1
Dr. T. Hall Code R-11 Naval Surface Weapons Center White Oak Laboratory Silver Spring, MD 20910	1
Mr. G.L. Mackenzie Naval Surface Weapons Center Code R101 Indian Head, MD 20640	1
Dr. K.F. Mueller Naval Surface Weapons Center Code R11 White Oak Silver Spring, MD 20910	1

DISTRIBUTION LIST

	No. Copies
Dr. R.G. Rhoades Commander Army Missile Command DRSMI-R Redstone Arsenal, AL 35898	1
Dr. W.D. Stephens Atlantic Research Corp. Pine Ridge Plant 7511 Wellington Rd. Gainesville, VA 22065	1
Dr. A.W. Barrows Ballistic Research Laboratory USA ARRADCOM DRDAR-BLP Aberdeen Proving Ground, MD 21005	1
Dr. C.M. Frey Chemical Systems Division P.O. Box 358 Sunnyvale, CA 94086	1
Professor F. Rodriguez Cornell University School of Chemical Engineering Olin Hall, Ithaca, N.Y. 14853	1
Defense Technical Information Center DTIC-DDA-2 Cameron Station Alexandria, VA 22314	12
Dr. Rocco C. Musso Hercules Aerospace Division Hercules Incorporated Alleghany Ballistic Lab P.O. Box 210 Washington, D.C. 21502	1
Dr. Ronald L. Simmons Hercules Inc. Eglin AFATL/DLDL Eglin AFB, FL 32542	1
Dr. E.H. Debutts Hercules Inc. Baccus Works P.O. Box 98 Magna, UT 84044	1
Dr. James H. Thacher Hercules Inc. Magna Baccus Works P.O. Box 98 Magna, UT 84044	1
Mr. Theordore M. Gilliland Johns Hopkins University APL Chemical Propulsion Info. Agency Johns Hopkins Road Laurel, MD 20810	1
Dr. R. McGuire Lawrence Livermore Laboratory University of California Code L-324 Livermore, CA 94550	1
Dr. Jack Linsk Lockheed Missiles & Space Co. P.O. Box 504 Code Org. 83-10, Bldg. 154 Sunnyvale, CA 94088	1
Dr. B.G. Craig Los Alamos National Lab P.O. Box 1663 NSP/DOD, MS-245 Los Alamos, NM 87545	1
Dr. R.L. Rabie WX-2, MS-952 Los Alamos National Lab. P.O. Box 1663 Los Alamos NM 37545	1
Dr. R. Rogers WX-2 Los Alamos Scientific Lab. P.O. Box 1663 Los Alamos, NM 87545	1

DISTRIBUTION LIST

	No. Copies
Dr. L.V. Schmidt Assistant Secretary of the Navy (R,E, and S) Room 5E 731 Pentagon Washington, D.C. 20350	1
Dr. A.L. Slafkosky Scientific Advisor Commandant of the Marine Corps Code RD-1 Washington, D.C. 20380	1
Dr. Richard S. Miller Office of Naval Research Code 413 Arlington, VA 22217	10
Mr. David Siegel Office of Naval Research Code 260 Arlington, VA 22217	1
Dr. R.J. Marcus Office of Naval Research Western Office 1030 East Green Street Pasadena, CA 91106	1
Dr. Larry Peebles Office of Naval Research East Central Regional Office 666 Summer Street, Bldg. 114-D Boston, MA 02210	1
Dr. Phillip A. Miller Office of Naval Research San Francisco Area Office One Hallidie Plaza, Suite 601 San Francisco, CA 94102	1
Mr. Otto K. Heiney AFATL - DLDL Elgin AFB, FL 32542	1
Mr. R. Geisler ATTN: MKP/MS24 AFRPL Edwards AFB, CA 93523	1
Dr. F. Roberto Code AFRPL MKPA Edwards AFB, CA 93523	1
Dr L.H. Caveny Air Force Office of Scientific Research Directorate of Aerospace Sciences Bolling Air Force Base Washington, D.C. 20332	1
Mr. Donald L. Ball Air Force Office of Scientific Research Directorate of Chemical Sciences Bolling Air Force Base Washington, D.C. 20332	1
Dr. John S. Wilkes, Jr. FJSRL/NC USAF Academy, CO 80840	1
Dr. R.L. Lou Aerojet Strategic Propulsion Co. P.O. Box 15699C Sacramento, CA 95813	1
Dr. V.J. Keenan Anal-Syn Lab Inc. P.O. Box 547 Paoli, PA 19301	1
Dr. Philip Howe Army Ballistic Research Labs ARRADCOM Code DRDAR-BLT Aberdeen Proving Ground, MD 21005	1
Mr. L.A. Watermeier Army Ballistic Research Labs ARRADCOM Code DRDAR-BLI Aberdeen Proving Ground, MD 21005	1
Dr. W.W. Wharton Attn: DRSMI-RKL Commander U.S. Army Missile Command Redstone Arsenal, AL 35898	1